The Key Laboratory of Weak Light Nonlinear Photonics,
Ministry of Education

Annual Report 2018

南开大学弱光非线性光子学

教育部重点实验室

Annual Report 2018

The Key Laboratory of Weak Light Nonlinear Photonics,
Ministry of Education

南开大学弱光非线性光子学

教育部重点实验室

▼ 应任梦昕副教授邀请，英国帝国理工大学物理系博士后李毅博士访问弱光非线性光子学教育部重点实验室，并为师生作了题为“纳米光子学的非线性研究以及单分子检测应用”的学术报告。（2018.1.2）

▼ 在南开大学观摩第十届物理学术竞赛的台湾师范大学师生一行 20 余人，参观弱光非线性光子学教育部重点实验室并进行师生交流。（2018.5.15）

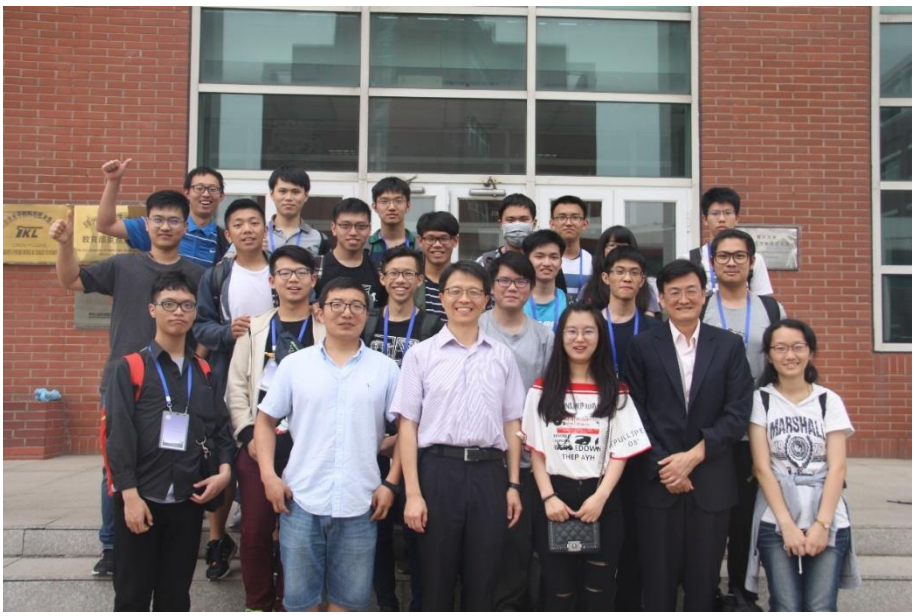

▼ 天津市高校物理有关专业大三本科生 80 余人，来到弱光非线性光子学教育部重点实验室进行参观学习交流。（2018.5.27）

▼ 弱光非线性光子学教育部重点实验室外聘专家美国阿拉巴马农工大学物理系 Nickolai V.Kukhtarev 教授和 Tatiana Kukhtareva 教授来重点实验室进行科研和指导研究生工作。（2018.7.3-8.1）

▼ 河南师范大学物理与材料科学学院师生共 23 人，来到弱光非线性光子学教育部重点实验室进行参观学习交流。（2018.7.9）

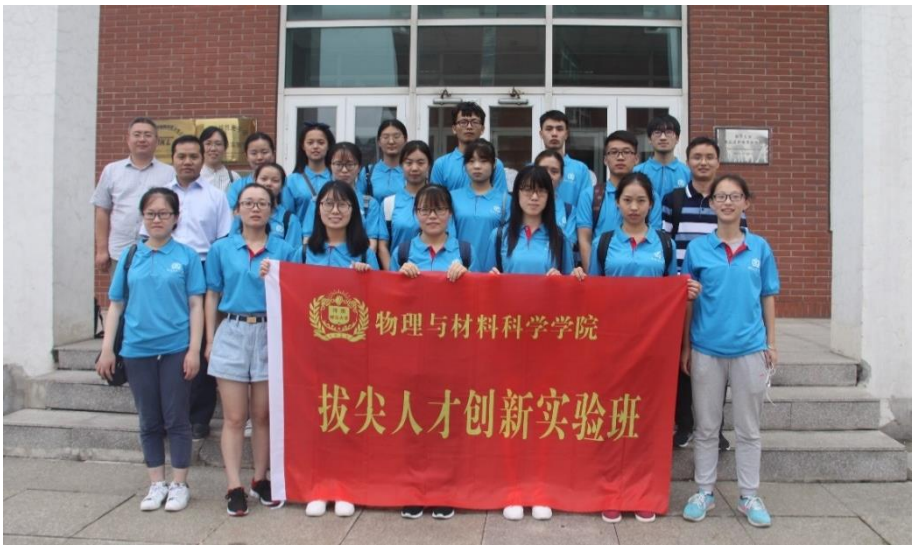

▼ 为充分展示物理魅力和南开物理特色，增进高校间优秀大学生的交流与联系，吸纳优秀物理学本科生来我院进一步学习深造，物理科学学院和泰达应用物理研究院于 2018 年 7 月 15 日至 7 月 18 日举办“2018 年南开大学‘我爱物理’优秀大学生夏令营”。来自全国 60 多所高校的百余名优秀本科生参加了本次夏令营活动，7 月 16 日，夏令营营员来到弱光非线性光子学教育部重点实验室，分组依次进行参观学习。

（2018.7.16）

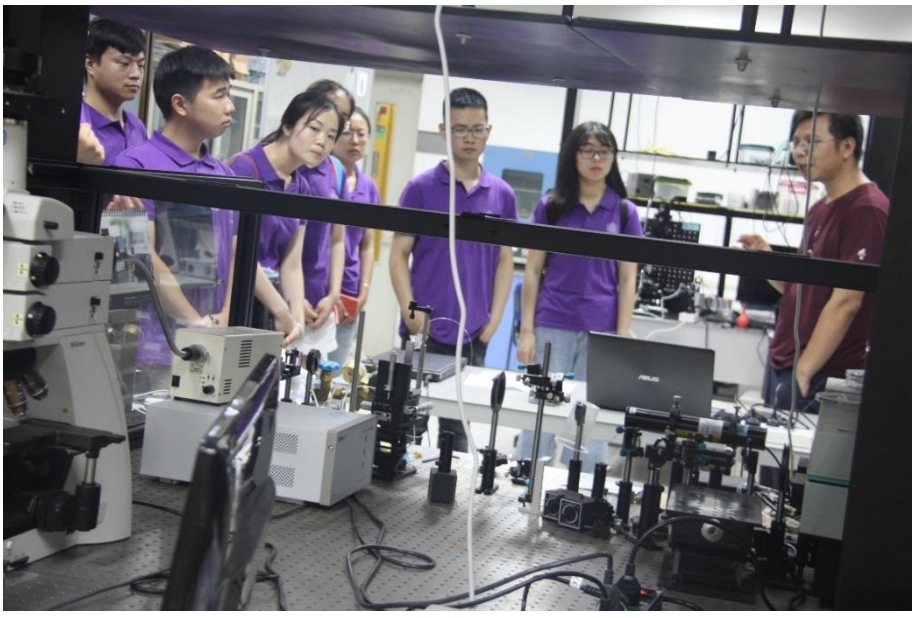

▼ 陈志刚教授课题组邀请克罗地亚萨格勒布大学的 Hrvoje Buljan 教授来弱光非线性光子学教育部重点实验室进行访问交流，并为师生作题为“Engineering Weyl fermions and anyons; engineering synthetic magnetic fields and dimensions in photonic lattices”的学术报告。（2018.9.7）

▼ 为增加实验室安全知识，提高实验室安全意识，吴强教授和潘雷霆副教授为即将进入重点实验室进行科研实验的学生分别做光学、电学、生物和化学等方面的实验室安全知识讲座，并安排学生进行相关实验室安全知识学习。（2019.9.25）

- 任梦昕副教授邀请《Nanophotonics》杂志的编辑 Dennis Couwenberg 来重点实验室访问交流，并为师生作题为“A publishing editor's view and insights on how to get your research published in the journal Nanophotonics”的学术报告。（2018.10.8）

- 弱光非线性光子学教育部重点实验室外聘专家奥地利维也纳大学 Romano Rupp 教授来重点实验室进行科研和指导研究生工作，并为研究生授课。（2018.10.12-11.15）

- 弱光非线性光子学教育部重点实验室外聘专家乌克兰国家科学院 Andrey Ilyin 研究员来重点实验室进行研究工作，并指导研究生的科研实验；工作期间 Ilyin 研究员为重点实验室师生作了题为“A view on LC’s prospects for holography applications”的学术报告。（2018.10.19-11.30）

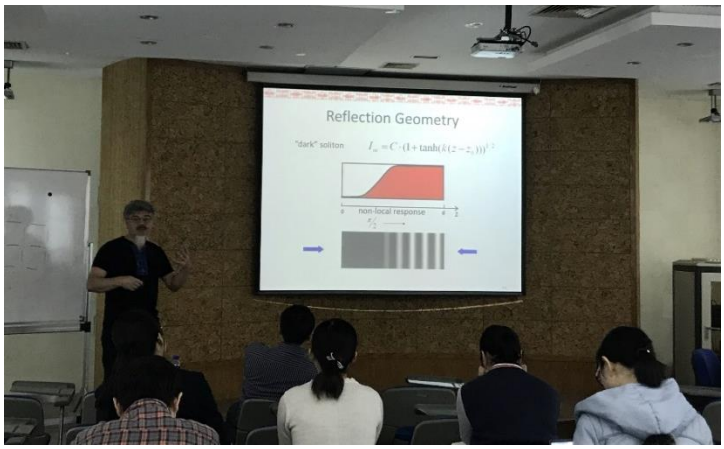

▼ 为培养本科~~生~~新生的科研兴趣，增强科研素养，物理科学学院组织全体本科新生参观了弱光非线性光子学教育部重点实验室。（2018.11.3）

▼ 弱光非线性光子学教育部重点实验室特聘教授，卢布雅尔娜大学&斯特藩研究所教授 Irena Drevenšek-Olenik 来重点实验室进行教学和科研工作，并为师生作题为“Magnetically tunable diffractive optical elements based on ferromagnetic liquid crystals”的学术报告。（2018.11.6-11.15）

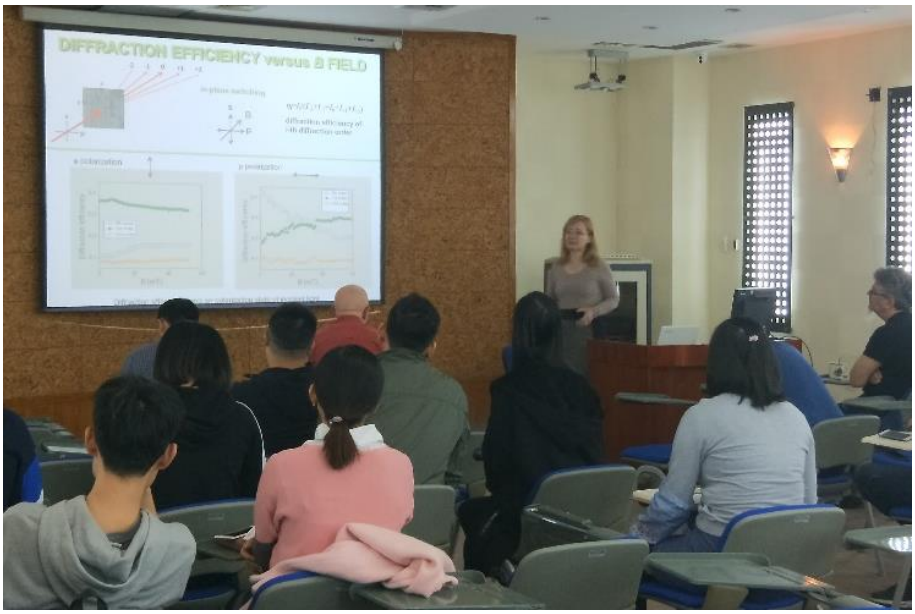

目　录/Contents

人员结构/Organization

实验室主任/Director

张国权　教　授

实验室副主任/Deputy Directors

刘智波　教　授

李勇男　教　授

学术秘书/Academical Secretary

禹宣伊　副教授

研究方向负责人/Research Group Leaders

弱光非线性及量子相干光学	许京军　教　授
非线性物理与光子技术	田建国　教　授
非线性光子学材料及先进制备技术	孔勇发　教　授
光场调控及其应用	王慧田　教　授
光谱表征及传感技术	宋　峰　教　授

学术委员会/Academic Committee

主　任/Chairman

李树深　院　士　（中国科学院半导体研究所）

委　员/ Committee Members

薛其坤　院　士	（清华大学）
孙昌璞　院　士	（中国工程物理研究院北京计算科学研究中心）
龚旗煌　院　士	（北京大学）
陆　卫　研究员	（中国科学院上海技术物理研究所）
资　剑　教　授	（复旦大学）
申德振　研究员	（中国科学院长春光学精密机械与物理研究所）
曾和平　教　授	（华东师范大学）
童利民　教　授	（浙江大学）
王雪华　教　授	（中山大学）
陈　峰　教　授	（山东大学）
田建国　教　授	（南开大学）
王慧田　教　授	（南开大学）
许京军　教　授	（南开大学）
张国权　教　授	（南开大学）

外籍学术顾问委员

Yuri Kivshar	院　士	澳大利亚国立大学
D. Kip	教　授	德国 Clausthal 工业大学
L. Hessenlink	教　授	美国斯坦福大学物理系
R. A. Rupp	教　授	奥地利维也纳大学实验物理所
T. Volk	教　授	俄罗斯国家晶体研究所
Y. Tomita	教　授	日本电气通信大学
K. A. Nelson	教　授	美国麻省理工学院

杰出人才/Intelligent Staff

教育部“长江奖励计划”特聘教授

许京军（1999）　王慧田（1999）　陈志刚（2006）

国家杰出青年基金获得者

许京军（1998）　田建国（2001）　王慧田（2003）　李宝会（2009）

教育部“优秀青年教师资助计划”入选者

张国权（2002）　宋　峰（2003）

教育部“跨世纪优秀人才培养计划”入选者

许京军（1998）　田建国（2000）　孙　骞（2001）　孔勇发（2002）

教育部“新世纪优秀人才支持计划”入选者

张国权（2004）　宋　峰（2004）　臧维平（2005）　李宝会（2005）
孙甲明（2007）　张心正（2008）　刘智波（2009）　陈　璟（2009）
顾　兵（2010）　楼慈波（2010）　张天浩（2011）　武　莉（2011）
周向锋（2012）　陈树琪（2013）　孙　军（2013）

首批新世纪百千万人才工程国家级人选

田建国（2004）

国家海外青年学者合作研究基金获得者

陈志刚（2005）

“天津市授衔专家”称号获得者

许京军（2005）　田建国（2005）

天津市杰出青年科学基金获得者

陈树琪（2018）　周向锋（2018）

教育部“长江学者和创新团队发展计划”创新团队基金资助

弱光非线性光子学重点实验室人员名录/Name List

研究人员/Scientific Staff（52 人）

许京军　王慧田　田建国　陈志刚　张国权　孔勇发　孙　骞　宋　智　宋　峰　臧维平
李宝会　姚江宏　赵丽娟　曹亚安　张天浩　李玉栋　徐晓轩　张心正　周文远　邢晓东
禹宣伊　余　华　吴　强　孙同庆　武　莉　高　峰　刘智波　李祖斌　薄　方　齐继伟
叶　青　潘雷霆　蔡　卫　陈树琪　宋道红　孙　军　陈　璟　李勇男　刘宏德　王　斌
皮　彪　任梦昕　涂成厚　周向锋　胡　毅　鄢小卿　程　化　杨　帆　郑大怀　张玲（兼）
刘士国（兼）　Romano A. Rupp

技术人员/Technical Staff（4 人）

陈绍林　张　玲　刘士国　兀　伟

行政人员/Administrative Staff（3 人）

刘　烨　李　威　唐柏权

博士生/Ph.D Students（120 人）

常朋发　陈慧敏　陈少楠　戴　凡　杜成林　冯　源　付钰婷　高博峰　高少华　高晓光
高晓莉　高晓梅　高旭珍　龚圣超　郭宇翱　韩小芳　韩迎东　韩中兴　郝永鑫　郝振中
何新玲　胡鸟俊　黄　松　黄凯程　黄凯旋　黄双印　贾子熙　江晓洁　姜小强　姜一凡
蒋鹏翀　焦跃健　进晓荣　巨丹丹　孔腾飞　李　丽　李　智　李登辉　李瀚博　李利明
李萍萍　李青霄　李文灿　李小宽　李占成　李致力　栗亚楠　刘　慧　刘　瑞　刘　洋
刘汉雄　刘甲琛　刘建基　刘诗可　刘文玮　刘秀英　刘志瑶　卢　瑶　吕家琪　马吉娜
马军军　马增红　裴雨苗　齐文荣　钱月照　邱文娟　任杨阳　商继芳　宋永兵　苏宝旺
王　超　王　聪　王　丹　王　珂　王海平　王日德　王维维　王云龙　王兆远　王周祥
文虹镜　翁晓基　吴　婧　吴佳坪　伍　浩　夏士齐　谢　飞　谢博阳　邢福临　熊　浩
徐鹏伟　徐晓丹　薛丽云　颜　赛　杨　渤　杨建宇　杨亚俊　张　莉　张　路　张　妮
张　琦　张　娅　张冠林　张景雪　张明偲　张旭光　张雪静　张跃变　赵　侨　赵宏阳
赵梦丹　赵文娟　郑玲飞　钟　阳　周爱华　朱梦红　诸　玲　兰子鉴　Adnan Khan
Saeed Shahzad

硕士生/M.S. Students（211 人）

安炳旭　安亚文　白江波　薄莹雷　边达民　曹　翰　曹　雷　曹博弢　车　颖　陈桂林
陈国行　陈嘉鑫　陈烈裕　仇玉洁　崔芮铭　戴芷轩　董　瑞　董海阳　董皓天　董艳艳
樊　江　范洪鸣　范友静　冯　源　符显辉　高宁慧　葛天昊　耿　娟　弓　楠　龚子涵
郭　埠　郭　敏　郭浩玮　郭丽娟　郭丽英　郭琴琴　韩小芳　韩晓彤　郝慧文　郝泽霖
何慧霞　侯晶钰　胡　月　胡　祯　胡慧敏　胡梦媛　胡志婵　化梦梦　黄　荣　黄露露
黄宁宁　黄少蕾　回振海　霍唱福　贾　笛　贾龙飞　贾鹏博　靳建宁　井志平　康倩倩
康倩倩　雷思弘　李　玲　李　强　李　珊　李　羽　李彩芬　李德康　李瀚博　李记伟
李金泽　李三兵　李晓荣　李晓婷　李星业　李逸凡　李志轩　栗星星　梁　菁　梁丹丹
梁朋辉　刘　磊　刘　旭　刘　艳　刘冬雪　刘继宗　刘锦锦　刘俊芳　刘丽娜　刘时康
刘秀英　刘雪刚　刘雪婷　刘瑶瑶　娄宗帅　陆一平　栾　敏　罗　强　吕雪峰　马进勇
马梦琳　马姝琼　马文锦　玛地娜　茼诗洁　孟生轲　苗　慧　牟　雪　裴维维　皮泽坤
钱豆豆　强美娟　曲　达　桑　旭　邵　震　申子媛　石家榕　石召君　石召君　时金蒙
史德坤　宋　筱　宋少清　宋晓鹏　宋祎杰　孙若轩　孙文倩　台玉可　田倩倩　汪海军
王　欢　王　敏　王　楠　王　强　王　瑞　王　晓　王丹阳　王佳艺　王倩倩　王烁琳
王苏云　王谢地　王新格　王旭英　王雪晴　王艳娥　王艺驰　王俞萱　王子范　蔚莹琪
吴佳琦　武　兵　谢俊芳　谢语晨　徐阳阳　许恩泽　许海洁　荀　爽　闫　娜　颜　森

颜欣龙　燕文超　杨　超　杨　晨　杨　贺　杨　硕　杨慧梅　杨江涛　杨朋真　杨鹏宇
杨夏夏　姚　森　殷子杭　于　洪　于　溪　于殿强　余莹凤　翟艳子　詹晶谚　詹亦飞
张　灯　张　迪　张　利　张　盼　张　平　张　茹　张　月　张春妹　张海涵　张弘智
张洪爽　张嘉伟　张倩南　张亚卿　张玉娇　张煜晨　张月颖　赵　艺　赵大平　赵晓敏
赵雅丽　郑晓晨　郑秀燕　郑忠忠　周　超　周冬旭　周天寒　周娅玲　朱砚涵　祝冬兰
祝志茂

承担主要课题/Projects under Researching

序号	项 目 名 称	项 目 来 源	起止时间	负责人
1	新型线性和非线性人工微结构及器件 2016YFA0301102	科技部重点专项	2016.06-2021.05	田建国
2	具有拓扑特性的空间光场产生、调控及与微结构相互作用 2017YFA0303800	国家重点研发计划	2017.07-2022.06	陈志刚
3	激光器工程化与清洗应用中的关键技术 2017YFB0405105	国家重点研发计划	2017.07-2020.12	宋 峰
4	具有拓扑特性的光量子态与量子效应 2017YFA0303803	国家重点研发计划	2017.07-2022.06	许京军
5	西部典型缺水地区农村供水排水一体化技术及应用示范 2016YFC0400700	国家重点研发计划（子任务）	2016.07-2020.12	徐晓轩
6	单光子时间分辨成像光谱仪研发与应用任务一：单光子时间分辨成像光谱仪整机性能评估、标定与调试 2013YQ030595	国家重大科学仪器设备开发专项	2013.10-2018.09	田建国
7	高通量高分辨病理切片扫描 31527801	国家重大科研仪器研制项目	2016.01-2020.12	周文远
8	人工微结构中的光/声拓扑性质研究 2017YFA0305100	国家重点研发计划青年项目（子任务）	2017.01-2021.12	任梦昕
9	内窥型 OCT 设备环状模体研制及关键参数计量检测方法的研究 2016YFF0201005	国家重点研发计划（子课题）	2016.07-2020.12	叶 青
10	光场的超衍射、超聚束效应及其应用 91750204	国家自然科学基金重大研究计划重点项目	2018.01-2021.12	张国权

序号	项 目 名 称	项 目 来 源	起止时间	负责人
11	空域分形光场的调控、新效应及其潜在应用 11534006	国家自然科学基金重点项目	2016.01-2020.12	王慧田
12	铌酸锂晶体微腔中的非线性过程与调控研究 11734009	国家自然科学基金重点项目（子任务）	2018.01-2022.12	薄 方 程 亚
13	数字双光子干涉、聚焦及其应用 61475077	国家自然科学基金面上项目	2015.01-2018.12	张国权
14	折射率显微镜技术及其应用研究 61475078	国家自然科学基金面上项目	2015.01-2018.12	叶 青
15	超快激光超饱和掺杂微观机制及材料物性研究 11574158	国家自然科学基金面上项目	2016.01-2019.12	姚江宏
16	对向双光驱动回音廊模光机械参量调控的研究 11574161	国家自然科学基金面上项目	2016.01-2019.12	高 峰
17	基于光刻技术的小胶质细胞间通讯特性及机制的研究 11574165	国家自然科学基金面上项目	2016.01-2019.12	潘雷霆
18	基于微纳光学角动量模式的光场调控及应用 11574162	国家自然科学基金面上项目	2016.01-2019.12	陈 璟
19	溶剂退火过程中嵌段共聚物薄膜形态的分子模拟研究 21574071	国家自然科学基金面上项目	2016.01-2019.12	李宝会
20	少层超表面高效调控光学特性和新型光场研究 11574163	国家自然科学基金面上项目	2016.01-2019.12	程 化
21	稀土体相掺杂氟化物纳米晶的制备、性能优化及应用研究 11574164	国家自然科学基金面上项目	2016.01-2019.12	赵丽娟

序号	项 目 名 称	项 目 来 源	起止时间	负责人
22	整形脉冲对光纤中色散波产生的优化与调控研究 61575098	国家自然科学基金面上项目	2016.01-2019.12	胡 毅
23	名义纯及高掺镁铌酸锂晶体 1.06μm 激光损伤的研究 61575099	国家自然科学基金面上项目	2016.01-2019.12	孙 军
24	低维硼的结构预测及性质研究 11674176	国家自然科学基金面上项目	2017.01-2020.12	周向锋
25	稀土包覆金属纳米核壳结构掺杂液晶的发光调控 11674183	国家自然科学基金面上项目	2017.01-2020.12	宋 峰
26	基于铌酸锂微盘腔的窄带宽可调谐宣布式单光子源 11674181	国家自然科学基金面上项目	2017.01-2020.12	薄 方
27	基于铌酸锂芯片的量子光源 11674184	国家自然科学基金面上项目	2017.01-2020.12	李勇男
28	聚合物手性液晶无序微纳复合材料中的光子局域化及随机激射研究 11674182	国家自然科学基金面上项目	2017.01-2020.12	张心正
29	抗光损伤铌酸锂晶体与体光生伏打效应的研究 11674179	国家自然科学基金面上项目	2017.01-2020.12	孔勇发
30	光诱导蜂窝型光子晶格中与赝自旋相关涡旋现象的研究 11674180	国家自然科学基金面上项目	2017.01-2020.12	宋道红
31	基于光折变表面波的切趾啁啾波导阵列研究 61675101	国家自然科学基金面上项目	2017.1- 2020.12	张天浩
32	基于二维材料折射率传感的新型光热成像和光声成像研究 11774184	国家自然科学基金面上项目	2018.01-2021.12	刘智波

序号	项 目 名 称	项 目 来 源	起止时间	负责人
33	基于飞秒直写介电微纳结构的光场调控及应用研究 11774183	国家自然科学基金面上项目	2018.01-2021.12	涂成厚
34	基于微纳共振复合材料的非线性偏振调控效应及其应用研究 61775106	国家自然科学基金面上项目	2018.01-2021.12	任梦昕
35	锂基中子探测闪烁共晶的设计、制备及性能表征 11775120	国家自然科学基金面上项目	2018.01-2021.12	杨 帆
36	纳米尺度铌酸锂的载流子输运和光电性能研究 11774182	国家自然科学基金面上项目	2018.01-2021.12	张国权
37	嵌段共聚物自组装多孔形态的形成机理研究 21774066	国家自然科学基金面上项目	2018.01-2021.12	李宝会
38	特殊晶场环境下二价锰离子的非常规获得及反常发光的机理研究 11774187	国家自然科学基金面上项目	2018.01-2021.12	武 莉
39	线性和非线性多功能超表面光场调控及应用 11774186	国家自然科学基金面上项目	2018.01-2021.12	程 化
40	紫外波段铝表面等离激元的阴极荧光光谱研究 11774185	国家自然科学基金面上项目	2018.01-2021.12	蔡 卫
41	利用 XRD-XRF 进行铁矿石矿物定量与表征方法的基础研究 U1460201	国家自然科学基金联合基金重点项目	2015.01-2018.12	武 莉
42	非线性无衍射光束的设计与特性研究 11504186	国家自然科学基金青年基金	2016.01-2018.12	胡 毅
43	快响应掺铋铌酸锂晶体及其实时动态全息 3D 显示的研究 61705116	国家自然科学基金青年基金	2018.01-2020.12	郑大怀

序号	项 目 名 称	项 目 来 源	起止时间	负责人
44	不同工艺制备的低掺镁近化学计量比铌酸锂晶体缺陷结构及其对性能的影响研究 61705059	国家自然科学基金青年基金（联合申请）	2018.01-2020.12	孙 军
45	太赫兹声子极化激元与微结构作用的高时间分辨定量成像研究 61705013	国家自然科学基金青年基金（联合申请）	2018.01-2020.12	吴 强
46	全介质手性纳米材料 11711530205	国家自然科学基金中英合作与交流项目	2017.04-2019.03	许京军
47	金属纳米颗粒对稀土掺杂液晶发光调控及其在提高有机太阳能电池效应的应用 11811530075	国家自然科学基金中俄合作与交流项目	2018.01-2019.12	宋 峰
48	JPPT-XXX	国防科工局（军工）	2015.01-2018.12	孙 军
49	微像素形心定位技术-低差频激光干涉光场产生与调控	军委科技委项目	2017.08-2018.08	高 峰
50	液晶取向的微图案化及其在微流控器件中的应用 11-16	科技部政府间合作项目	2016.11-2018.10	张心正
51	硼烯的生长表征及性质	天津市杰出青年科学基金	2017.10-2021.09	周向锋
52	基于少层人工微结构的光场调控物理及其应用 18JCJQJC45700	天津市杰出青年科学基金	2018.10-2021.12	陈树琪
53	水环境智能监测检测技术开发及应用 BHXQKJXM-PT-ZJSHJ-2017003	天津市滨海新区合作共建研发平台科技项目	2017.12-2019.06	孙 骞
54	基于“定制”微纳结构的光场调控研究 16JCZDJC31300	天津市自然科学基金重点项目	2016.04.2019.03	涂成厚
55	紫外光激发的金属纳米结构增强发光的单一基质白光 LED 荧光材料 17JCZDJC37800	天津市自然科学基金重点项目	2017.04-2020.03	宋 峰

序号	项 目 名 称	项 目 来 源	起止时间	负责人
56	层间转角可控二维材料及其光电性能研究 18JCZDJC30400	天津市自然科学基金重点项目	2018.04-2021.03	刘智波
57	基于飞秒光聚合的新型液晶定向技术及其在矢量光场产生中的应用 17JCYBJC16700	天津市自然科学基金面上项目	2017.03-2019.09	张心正
58	深紫外非线性光学磷酸盐功能晶体的设计、生长和构效关系研究 17JCYBJC17800	天津市自然科学基金面上项目	2017.04-2020.03	孙同庆
59	硬 X 射线成像用高分辨碘化铯闪烁屏研制 18JCYBJC17800	天津市自然科学基金面上项目	2018.04-2021.03	杨 帆
60	少层超表面高效调控光学特性和新型光场研究 11574163	天津市自然科学基金青年项目	2016.04-2019.03	程 化
61	基于超分辨成像技术和光刻图案化技术的细胞骨架调控机制的研究 18JCQNJC02000	天津市自然科学基金青年项目	2018.04-2021.03	潘雷霆
62	基于石墨烯等离激元的中红外结构光场研究 18JCQNJC02100	天津市自然科学基金青年项目	2018.04-2021.03	蔡 卫
63	折射率显微镜技术及其应用研究 15JCQNJC02600	天津市应用基础与前沿技术研究计划项目	2015.06-2018.03	叶 青
64	光学级铌酸锂晶体研制 2016254	横向课题	2016.11-2018.12	张 玲 刘士国
65	高温 Nd:YAG 晶体生长的工业研究 2016244	横向课题	2016.11-2019.12	孙 军 郑大怀
66	国家军用标准《铌酸锂电光调 Q 晶体规范》编制 17ZF314	中央军委装备发展部	2018.01-2019.09	孙 军
67	基于微腔的高效率矢量涡旋光场发生器	光学信息技术科学教育部重点实验室开放课题	2016.06-2018.06	薄 方

序号	项 目 名 称	项 目 来 源	起止时间	负责人
68	低差频激光干涉光场产生与调控	中科院光电研究院横向课题	2017.06-2018.06	高 峰
69	新型低维 MoS_2 基催化剂的制备与性能调控 010/BE044121	重点实验室开放基金	2017.09-2018.09	曹亚安
70	等离子激元超表面光学特性调控	南开大学百名青年学科带头人培养计划	2014.12-2018.12	陈树琪
71	红外石墨烯等离激元的激发与调控研究 ZB14007801	南开大学百名青年学科带头人培养计划	2013.12-2019.11	张心正
72	富硼材料的结构预测及物理性质研究	南开大学百名青年学科带头人培养计划	2015.01-2018.12	周向锋
73	利用阴极荧光光谱实现等离激元超分辨的研究	南开大学百名青年学科带头人培养计划	2015.01-2020.12	蔡 卫
74	等离激元耦合体系中非线性旋光效应对光波偏振的调控研究	南开大学百名青年学科带头人培养计划	2016.01-2021.12	任梦昕
75	光子石墨烯中新颖物理现象的研究	南开大学百名青年学科带头人培养计划	2016.01-2019.12	宋道红
76				

仪器设备平台/Facilities

仪器设备名称	规格型号	购置时间
聚焦离子束电子显微镜	nanolab 600i	2014.06
分子速外延生长炉	Compact 21T	2003.12
扫描探针显微镜	Nonoscope Ⅲa	2006.04
激光显微竟拉曼光谱仪	inVia	2009.09
近场扫描光学显微镜系统	MV4000	2009.09
飞秒激光器系统	Legend Elite clsp	2010.03
散射式近场光学显微镜	neaSNOM	2015.04
荧光光谱仪	FSP920	2008.12
研磨抛光系统		2003.12
多轴激光并行直写光刻系统	Microlab 4A-100	2012.04
磁控溅射薄膜沉积系统	KJLC-LAB18	2010.09
激光器工作站	899-29	2005.11
飞秒激光器	VF-T2S	2000.09
时间分辨光谱及瞬态吸收光谱系统		2002.06
飞秒倍频系统		2002.06
显微拉曼光谱仪	MKI2000	1998.01
激光分子束外延系统	LMBE450A	2006.05
钛宝石激光器系统	PRO-FIKXP	2010.03
准分子激光器	COMPexPro205	2009.06
原子力显微镜	MULTZMDE V	2010.03
全自动宽带调谐飞秒激光器	UltraII	2012.12
傅立叶变换红外光谱仪	VERTEX 70	2014.12
连续钛宝石激光器	SolsTis 4000S BRF XF	2015.09
显微弱光探测系统		2008.04
大功率超快激光器	Mai Tai HP	2016.01
显微镜	TI-E	2014.09
服务器	HS21	2009.07
无液氦低温光学恒温器	4106-510	2016.05
超精细多功能无液氦低温光学恒温器	4200-520N	2015.01
皮秒激光器	PY61	2003.12
高脉冲固体激光器	EMPPWER 30-220	2009.01
光谱仪	iHR550	2010.07
倒置显微镜	Axio OpeseverA1	2009.01
纳微结构光耦合测试仪	AP-SA25L003-CM	2014.01
超连续谱光纤激光器	EXR-15	2013.12
高温综合热分析仪	SETSYS Evo	2014.01
氩离子激光器系统	Innova 308C	2007.01
荧光光谱仪	FluoroLog-3	2014.06
氩离子激光器	Inno1a 92-0C-A6	2008.07
纳秒激光器	Panther OPO	2003.12
高级倒置显微镜	TiU	2013.01

仪器设备名称	规格型号	购置时间
光谱型成像椭偏仪	Nanofilm_EP4SE	2017.09
原子力显微镜	MFP-3D Infinity	2017.10
超窄线宽可调谐环形激光器	Matisse 2 DX	2017.11
倒置研究型显微镜	Ti-U	2017.09
高性能计算服务器	X240M5	2017.03
半导体参数测试仪	4200A-SCS	2017.06
倒置研究型显微镜	Ti-E	2017.11
超快激光脉冲整形器	MIIPS-HD	2017.12
超连续谱光纤激光器	EXR-20	2017.06
扫描共聚焦拉曼与多场联用系统	alpha300RAS	2018
X 射线衍射仪	D8 ADVANCE	2018
飞秒激光器	RegA-9000	2018
光学真空镀膜机	STAR-800IR	2018
超连续谱光纤激光器	WL-SC-400-15	2018

注：除开放基金外，所有仪器设备均为有偿使用

研究工作报告/Scientific Report

弱光非线性及量子相干光学/ Weak Light Nonlinear Optics and Quantum Coherent Optics

负责人：许京军

本年度主要围绕石墨烯、金属纳微结构、光子晶格、微腔、光纤等纳微结构体系的非线性光学效应与光场调控及其应用、超分辨成像及其应用等开展研究，取得了一系列阶段性的成果。具体如下：

In this year, we mainly focused on the onlinear photonic properties, optical field manipulation and their applications of graphene, the plasmonics in metalic micro-/nano-structure, photonic lattices, micro-resonators and optical fibers, super-resolution imaging and its applications. The followings are the main chievements.

1. 石墨烯、金属微纳结构的等离激元调控及其应用

氦离子刻蚀石墨烯三角腔的近场成像。石墨烯纳米共振腔在生物传感、光探测器和光调制器等方面具有重要的应用。因此，一种精确、有效的纳米尺度的石墨烯加工手段是目前亟需的。相比于传统的镓离子束刻蚀方式，氦离子束刻蚀方式可以获得更高的精度。我们利用氦离子束加工了一系列的三角形石墨烯共振腔，利用近场等离激元成像方法研究了其面内等离激元模式的响应。研究表明氦离子束能有效的诱导石墨烯等离激元反射边界，并能通过改变离子束剂量实现边界反射的控制。该研究为更精确的石墨烯纳米结构的加工提供了新的参考方案，有望拓展石墨烯等离激元的应用。

Plasmon nanoresonators in graphene have many applications in biosensing, photodetectors and modulators. As a result, an efficient and precise patterning technique for graphene is required. Helium ion lithography (HIL) emerges as a promising tool for direct writing fabrication because it owns improved fabrication precision compared to electron beam lithography and conventional gallium focused ion beam technique. In this paper, utilizing HIL, a set of graphene triangles are patterned and excellent plasmon response is detected. Particularly, the evolution of breathing mode in these structures is unveiled by scattering-type scanning near-field optical microscopy. Besides, the plasmon response of graphene structures can be efficiently tuned by adjusting the irradiated ion dose during the etching process, which can be explained by the phenomenal simulation model. Our work demonstrates that HIL is a feasible way for precise plasmonic nanostructure fabrication, and can be applied to graphene plasmon control at the nanoscale as well.

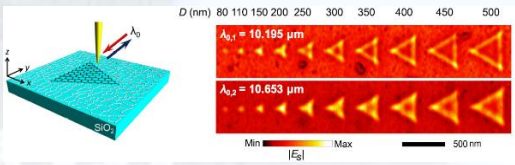

图1. 氦离子刻蚀石墨烯纳米结构的等离就元近场成像。

Fig. 1. Near-field imaging of graphene triangles patterned by helium ion beams.

基于石墨烯氧化反应的石墨烯纳米结构的超衍射激光直写加工。基于石墨烯的光电器件具有宽光谱相应、门电压调谐等优点，受到了人们的广泛关注。而石墨烯纳米结构的加工能力是实现石墨烯光电器件的基石。我们利用飞秒激光诱导石墨烯和二氧化硅的氧化还原反应，成功实现了石墨烯纳米结构的激光直写加工。被破坏石墨烯的加工线宽的分辨率可达到100 nm，远高于红外飞秒光的衍射极限，并且加工线的精度高达± 7 nm。基于此，我们可以高精度的加工不同的石墨烯纳米结构，并在不同结构中激发了

石墨烯等离激元。这种新型石墨烯纳米结构的光学加工方法具有低成本、高效率、无掩模和高精度等优点，将会进一步推动基于石墨烯的光电器件的实用化。

The fabrication ability of graphene nanostructures is the cornerstone of graphene-based devices, which are of particular interest because of their broad optical response and gate-tunable properties. Here, via laser-induced redox reaction of graphene and silica, we fabricate nano-scale graphene structures by femtosecond laser direct writing. The resolution of destructed graphene lines is far beyond the diffraction limit up to 100 nm with a precision as small as ±7 nm. Consequently, graphene nanostructures are fabricated precisely and excellent plasmon responses are detected. This novel fabrication method of graphene nanostructures has the advantages of low costs, high efficiency, maskless and especially high precision, which would pave the way for practical application of graphene-based optical and electronic devices.

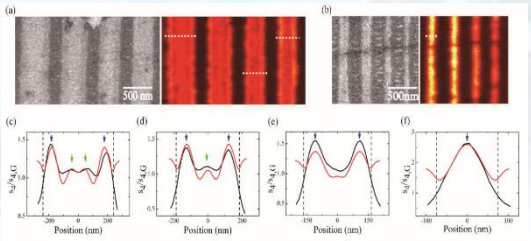

图2. 石墨烯条带的等离激元特性，激发波长为9.588 μm。（a）宽度分别为 480, 430, 370, and 330 nm 的石墨烯条带的 SEM 图和近场图；（b）宽度分别为 150, 140, 80, and 70 nm 的石墨烯条带的 SEM 图和近场图；（c）-（f）图 a 和 b 中沿白色虚线的的近场分布（黑线为实验结果，红线为模拟结果）。

Fig. 2. Plasmonic characteristics of graphene ribbons. The incident wavelengths λ_0 is 9.588 μm. (a) SEM and near-field images of graphene ribbons with widths of 480, 430, 370, and 330 nm. (b) SEM and near-field images of graphene ribbons with widths of 150, 140, 80, and 70 nm. (c)-(f) Experimental (black curves) and simulated (red curves) near-filed profiles perpendicular to graphene ribbons along the white dashed lines from left to right in (a) and (b).

单晶铝脊形光天线的等离激元模式演化与耦合。基于铝的表面等离激元在紫外生物荧光探测、光催化等领域具有重要应用。然而铝表面等离激元存在的较大损耗一直是制约其应用的瓶颈之一。我们利用单晶铝材料，通过离子束加工得到的一字形和十字形脊形纳米天线，通过阴极荧光光谱方法得到了其紫外到可见波段的等离激元模式的演化和耦合。研究表明，基于单晶铝的天线结构具有更低的损耗。一字形的脊形天线的共振可以通过传播等离激元的法布里-帕罗腔共振来解释，而十字形天线的等离激元共振由两个不同的两个传播路径来决定。我们的研究为基于铝的更复杂的光天线设计提供了基础，有望在紫外波段光传感等领域起到应用。

Aluminum (Al) has prominent material and plasmonic properties in the ultraviolet (UV) spectral range. However, the large losses of plasmon antennas with multicrystal Al is the bottleneck for plasmonic applications. Here, the plasmon properties of single-crystal and multicrystal Al nanostructures are compared. In the platform of bulk single-crystal Al, spatially and spectrally resolved cathodoluminescence (CL) spectroscopy is used to excite and image the plasmonic modes of I-shaped and cross-shaped nanoridge antennas. The evolution and coupling of plasmon modes at the nanoscale are clearly observed in these antennas. Plasmon modes for I-shaped antennas can be exactly understood from the standing waves of the propagating plasmons in Al nanoridge waveguides. Moreover, the plasmon response of cross-shaped antennas is determined by the two different standing wave paths. The experimental results agree well with full wave electromagnetic simulations. Our results lay a foundation for the design of more complex and efficient optical antennas with single-crystal Al, which have great potential applications in UV plasmonics, such as fluorescence enhancement or biosensing.

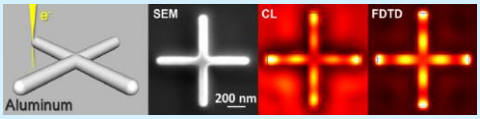

图 3. 基于单晶铝的纳米十字天线的等离激元模式阴极荧光光谱成像。

Fig. 3. Cathodoluminesence image of single aluminum nano-cross antenna.

单晶铝开放等离激元腔的阴极荧光光谱探测。精确的认识和理解表面等离激元腔的等离激元响应、以及其近场在实空间的分布对于表面等离激元效应在辐射控制、生物传感等领域的应用具有决定意义。我们利用阴极荧光光谱成像手段对开放的单晶铝三角腔进行了研究。研究表明，在紫外-可见波段，不同频率的等离激元模式具有截然不同的等离激元场的分布。同时，该腔的模式色散来源于铝/空气界面的传播等离激元，从而能实现较强的电磁场局域。进一步，通过在表面等离激元腔中放置CdZnS/ZnS蓝光量子点，实现了更强的量子点辐射。该研究为紫外波段的量子点辐射特性调控提供了新的思路。

The exact understanding of the plasmon response of aluminum (Al) nanostructures in deep subwavelength is critical for the design of Al based plasmonic applications, such as emission control of quantum dots and surface-enhanced resonance Raman scattering in the ultraviolet (UV) range. Here, the plasmonic properties of open triangle cavities patterned by focused ion beam in a single-crystal bulk Al are explored using cathodoluminescence. The resonant modes are determined by experimental spectra and deep subwavelength real-space mode patterns ranging from the visible to the UV, which agree well with the full-wave electromagnetic simulations. The dispersion relation of the cavity modes is consistent with that at the interface between Al and vacuum, showing a strong electromagnetic field confinement in the cavities. Open Al triangle cavities provide rooms for the interaction between optical emitters and confined electromagnetic fields, paving the way for plasmonic devices for a variety of applications, such as plasmonic light-emitting devices or nanolasers in the UV range.

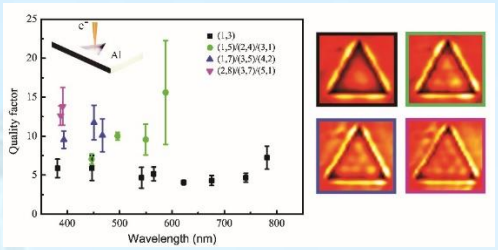

图4. 基于单晶铝的开放等离激元腔的阴极荧光光谱研究。

Fig. 4 Plasmon mode imaging in open triangle single-aluminum cavities by cathodoluminescence.

一维等离激元晶体中的 Zak 相位与拓扑等离激元塔姆态。在周期的金属/介质/金属波导的表面等离激元晶体中，我们理论研究了其能带所具有的Zak相位和可能存在的边界态，提出了在临近的晶体间存在的一种拓扑保护的表面等离激元塔姆态。研究表面该拓扑态不但能实现电磁场的极大增强，并且具有结构缺陷免疫特性，为基于等离激元的拓扑光子学器件的设计提供了新方案。

The Zak phase and topological plasmonic Tamm states in plasmonic crystals based on periodic metal-insulator-metal waveguides are systematically investigated. We reveal that robust topological interfacial states against structural defects exist when the Zak phase between two adjoining plasmonic lattices are different in a common band gap. A kind of efficient admittance-based transfer matrix method is proposed to calculate and optimize the configuration with inverse symmetry. The topologically protected states are favorable for the spatial confinement and enhancement of electromagnetic fields, which open a new avenue for topological photonic applications.

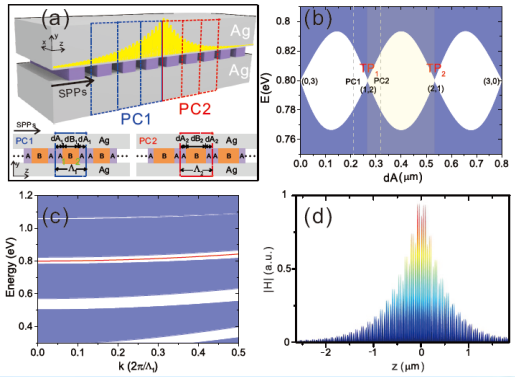

图5. 基于等离激元晶体的拓扑塔姆态。

Fig. 5. The topological protected Tamm state between plasmonic crystals.

基于介质-金属-介质波导的等离激元塔姆态。研究了在周期调制的介质/金属/介质布拉格反射器以及金属界面存在的等离激元塔姆态。通过优化结构设计，计算表明该边界态能实现电场强度的2个量级的增强以及衰减率4个量级的增强。除此之外，由于在介质/金属/介质结构中存在奇模式与偶模式，导致存在基于奇、偶模式的两种不同的等离激元塔姆态。该设计有望用于电磁场聚焦和传感。

Plasmonic Tamm states configuration is proposed for field enhancement in an insulator–metal–insulator (IMI) Bragg reflector by periodic modulation of the dielectrics surrounding the metal core. Finite-difference time domain simulation is carried out for the structure optimization and the dispersion relation of plasmonic Tamm states. In the metal–Bragg reflector interface, 2 orders of magnitude of electromagnetic field intensity enhancement and 4 orders of magnitude of decay rate enhancement are obtained. Besides the field enhancement, there are two plasmonic Tamm states that are related to the even and odd modes in the IMI waveguide. The two plasmonic Tamm states show large difference in the reflection spectra. The proposed structure would provide promising potential for electromagnetic nanofocusing and nanosensing.

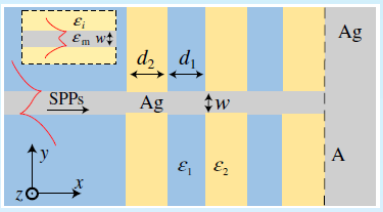

图6. 基于介质/金属/介质波导的等离激元塔姆态结构示意图。

Fig. 6. Side view of the PTSs structure based on IMI waveguides.

表面等离激元与自由电子间轨道角动量的有效转移。理论研究了自由电子与手性倏逝场之间相互作用过程中的角动量转移问题。研究表明极大的轨道角动量能从手性倏逝场转移到自由电子。考虑目前可行的实验条件下，进一步的计算表明该过程具有较高的转移效率。我们的理论研究为利用倏逝场产生高拓扑荷的自由电子提供了新的方法，并为相关实验提供了理论参考依据。

Free electrons can efficiently absorb or emit plasmons excited in a thin conductor, giving rise to multiple energy peaks in the transmitted electron spectra separated by multiples of the plasmon energy. When the plasmons are chiral, this can also give rise to transfer of orbital angular momentum (OAM). Here, we show that large amounts of OAM can be efficiently transferred between chiral plasmons supported by a thin film and free electrons traversing it. Our work supports the use of chiral plasmons sustained by externally illuminated thin films as a way of generating high-vorticity electrons, resulting in a remarkably large fraction of kinetic energy associated with motion along the azimuthal direction, perpendicular to the incident beam.

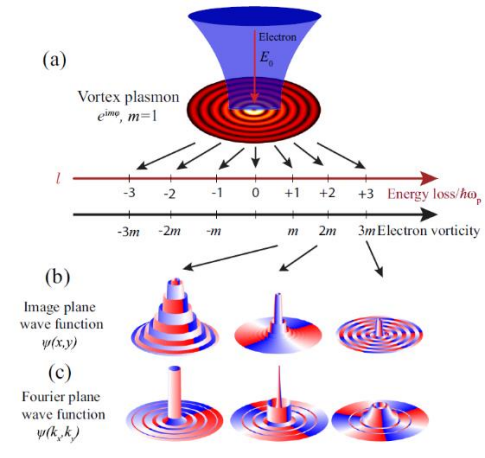

图 7. 手性等离激元场与自由电子之间的轨道角动量转移。

Fig. 7. General description of the interaction between free electrons and chiral plasmons.

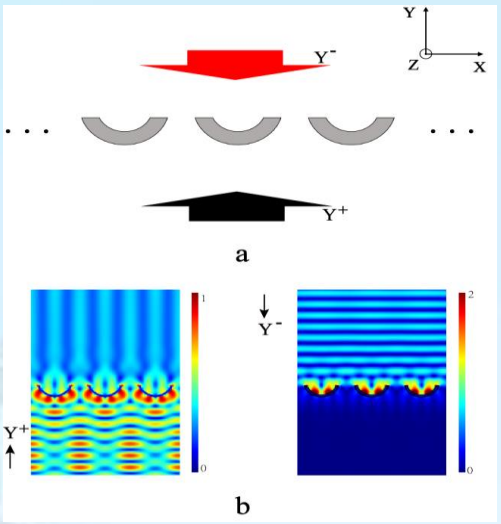

图 8. a. 拱形共振体构成的单层金属光栅示意图；b. 单层金属光栅用于光学传输时电场强度分布图。

Fig. 8. a. Schematic diagram of the single-layer metallic grating (SMG) consisting of cambered resonators (CRs); b. Distributions of electric field intensity $|E|^2$ for upward incident and downward incident conditions.

由金属拱形共振体组成的单层金属光栅由于其结构的非对称性，可以实现光的单向传输。数值模拟结果表明,该单层金属光栅的双向透射率比值可以达到 5000，同时传输方向的透射率高达 39%。单向光学传输特性来源于单层金属光栅在光传输方向上的衍射增强和抑制。衍射强度由拱形共振体表面局域等离子体的电磁辐射的干涉进行调控。该单层金属光栅结构的整体厚度不到 100nm，可用于超集成器件来调控光的传输。

A single-layer metallic grating (SMG) consisting of cambered resonators (CRs) is proposed in this work. Unidirectional optical transmission (UOT) is achieved for the asymmetric structure. Numerical simulation results show that the transmittance contrast ratio of the SMG can reach about 5000 with a high unidirectional transmittance of 39%. UOT results from diffraction enhancement or suppression in transmission direction. Diffraction is manipulated by the interference of electromagnetic radiation from local surface plasmons on CRs. Our single-layer structure has sub-100 nm thickness and can be used in ultracompact optical devices to manipulate light transmission.

我们提出了一种由两个错位的平行的金属光栅组成的复合结构，实现了光学二级管的单向光学传输性能。数值模拟结果表明该结构可以实现双色向光学二极管透射，即光学二极管的单向传输可以在双波带中实现，且这两个波带对应的传输方向相反。在这种结构中，在一层薄电介质材料的两侧分别附有具有不同的光学常数的两个平行的金属光栅。首先被光照射的金属光栅在特定的入射波长下会激发表面等离子体，这个光栅充当透射波带的选择器。另一个光栅通过电磁辐射引导光透射传输出光栅复合结构，它被称为辐射器。入射方向反向后，两光栅的作用互换，表面等离子体会在另一波长处被激发，工作波带发生改变。在双色向光学二极管结构中可以实现超级光学透射，光学隔离对比度可高达 1。此外，通过改变结构参数可以实现对光学二级管工作波带的调制。

An optical diode structure with two dislocated parallel metallic gratings is proposed and investigated numerically. Dichroic optical diode transmission is realized in this structure, i.e., optical diode effect is

observed in two wavebands corresponding to inverse transmission directions. In the structure, two parallel metallic gratings with different grating constants are separated by a dielectric slab in between. The first illuminated grating acts as a selector for exciting surface plasmons at a proper wavelength. The other grating acts as an emitter to realize optical transmission. When the incident direction is reversed, the roles of two gratings exchange and surface plasmons are excited at another wavelength. In dichroic transmission wavebands, the optical diode structure exhibits extraordinary transmission and possesses high optical isolation up to 1. Furthermore, the operating wavebands can be modulated by changing structure parameters.

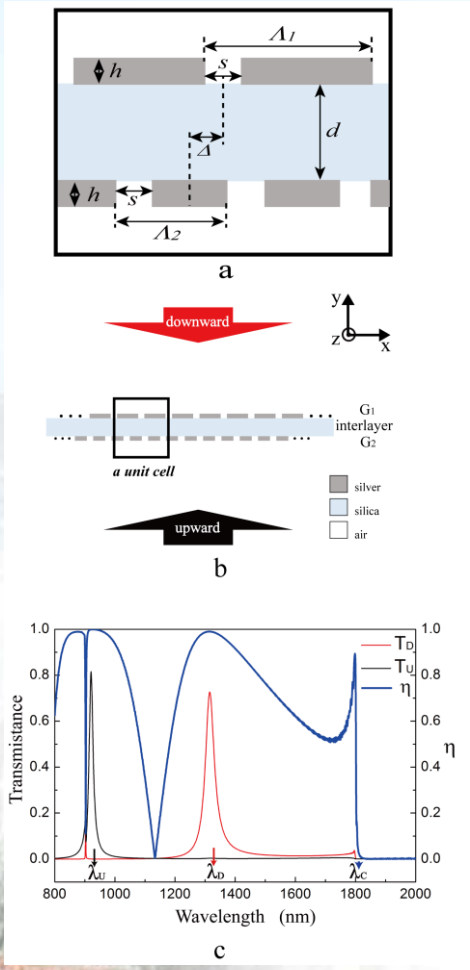

图 9. a. 双金属光栅单胞结构；b. 双金属光栅整体结构示意图；c. 双金属光栅整光栅的透射谱和光学隔离对比度。

Fig. 9. a. Schematic diagram of the unit cell. b. Overall view of the two dislocated parallel metallic gratings. c. Transmission spectra and the isolation contrast ratio of the optical diode structure with d=200nm, s=h=50nm, Λ_1=900nm, Λ_2=600nm and Δ=0nm.

我们详细模拟研究了屏蔽束缚（SB），屏蔽反束缚（SA）以及电荷转移（CTP）等离子共振模式。所有的这些模式都能清晰地出现在消光光谱中。三个模式的强度能够通过调节连接柱的尺寸进行调控。其中 SA 模式的强度可以强于 SB 模式，这是在非连接结构中很难实现的。由于三个模式分别依赖于不同的结构尺寸，所以他们的响应波长可以两两独立调控。我们的研究对等离子共振增强效应的应用具有参考意义。

Screened bonding (SB), screened antibonding (SA) and charge transfer plasmon (CTP) modes in the conductively connected nanorod heterodimer are studied in detail by simulation. All of the SB, SA and CTP modes can be observed in the extinction spectra of the conductively connected nanorod heterodimer. Also, the amplitudes of the three modes can be tuned by changing the radius of the cylinder conductive connection. Even the amplitude of the SA mode can be tuned to be higher than that of the SB mode, which is difficult to achieve in an unconnected nanorod heterodimer. Furthermore, the wavelengths of the three plasmon modes can be adjusted with a high degree of freedom, since the wavelength of the SB mode mainly depends on the length of the longer nanorod, the wavelength of the SA mode mainly depends on the length of the shorter nanorod and the wavelength of the CTP mode mainly depends on the total length of the nanorod heterodimer. Our study will be helpful for the design of plasmon enhancement devices, such as surface enhanced Raman scattering (SERS), plasmon enhanced fluorescence, plasmon rulers and so on.

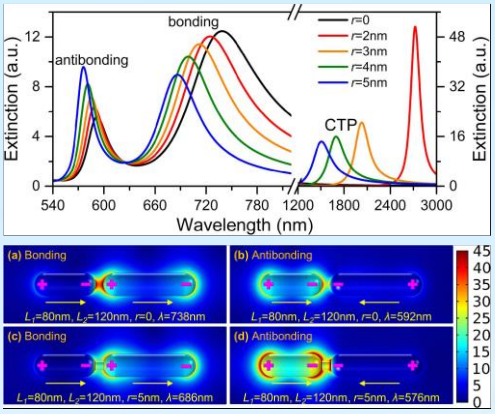

图 10. 不同连接纳米柱尺寸的消光谱以及相应的电场分布。

Fig. 10. The extinction spectra of unconnected (r = 0) and conductively connected nanorod dimer with r increasing from 2 nm to 5 nm. Here, L1 = 80 nm and L2 = 120 nm are fixed. And the electric field intensity distributions of nanorod dimers.

我们实验制作了大面积金属纳米月牙结构，并在实验上和模拟上验证了其具有巨大的赝手性性质。其 CD 系数敏感的依赖于入射角度。根据实验及模拟结果，我们认为其赝手性源于不同角度下，左右圆偏振光对于表面等离子共振模式的激发效率不同。实验上，当入射角为 60 度时，我们获得了最大的 CD 系数，0.37。另外，金属纳米月牙的CD光谱可以通过调节月牙尺寸进行调控。由于我们的赝手性纳米微结构具有 CD 系数大，制作简单，工艺成熟，成本低廉等优势，其具有巨大的应用潜力。

In this work, we demonstrate the strong extrinsic chirality of the larger-area metal nanocrescents by experiments and simulations. Our results show that the metal nanocrescent exhibits giant and tunable circular dichroism (CD) effect, which is intensively dependent on the incident angle of light. We attribute the giant extrinsic chirality of the metal nanocrescent to the excitation efficiencies difference of localized surface plasmon resonance (LSPR) modes for two kinds of circularly polarized light at a non-zero incident angle. In experiment, the largest CD of 0.37 is obtained at the wavelength of 826 nm with the incident angle of 60°. Furthermore, the CD spectra can be tuned flexibly by changing the metal nanocrescent diameter. Benefitting from the simple, low-cost and mature fabrication process, the proposed large-area metal nanocrescents are propitious to application.

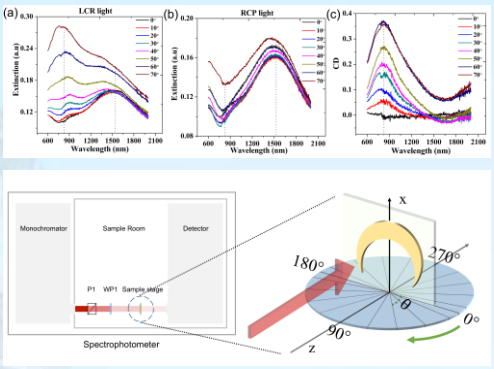

图 11. CD 系数测量实验装置图，测量到的不同角度下的左右旋消光光谱以及 CD 谱。

Fig. 11. Schematic design of the experiment for measuring CD. And the measured extinction and CD spectra of metal nanocrescents with the increase of θ.

基于梯度超构表面的纳米光学分束器。光学分束器是一种广泛使用的基本光学元件，然而传统分束器尺寸大，难于用于微纳集成。我们利用广义斯涅耳定律，在铌酸锂薄膜表面设计了一种反向交叉相位梯度排列的超构表面。实现了向两个传输方向的50:50比例分光。这一分光器的高度为700 nm，单个周期单元的长度和宽度分别为2600 nm和820 nm，易于在微纳光子芯片中进行集成；它对不同入射偏振的透射率差别保持在10%以内，并可通过对结构参数的微调来改变最优工作波段。同时，通过选择性的离子注入等处理，在两个相位梯度方向中改变其中一个方向的结构损耗，能够对分光比例进行改变。这一分光器将能够在小型干涉仪等集成光子学器件中广泛应用。

Beam splitters are essential components in various optical and photonic applications, while present beam splitters based on cubes or plates are normally bulky, which have difficulties to miniature and integrate into compacted photonic devices. Based on various transmission characters of lithium niobate

nanoscale units in different sizes, the phases of the transmitted light have been analyzed. Therefore, a kind of metasurface, whose transmission phase along the sample surface has a constant gradient, has been designed. According to the generalized Snell's law, the transmission direction of the light will be determined by former designed phase gradient value. Thus, the splitting of the incident light into two directions with the ratio of 50:50 can be realized by arranging the structure into opposite gradient directions in each unit cell. This beam splitter achieves a height of 700 nm, and the length and width of a unit cell are 2600 nm and 820 nm, respectively, and can be easily compacted into micro- or nano-photonic circuits. By selectively increasing the losses of part of the structure using the method such as masked ion implantation, various split ratios could also be achieved. This kind of beam splitters can be applicated in fabricating compact photonic devices, such as miniature interferometers, and so on.

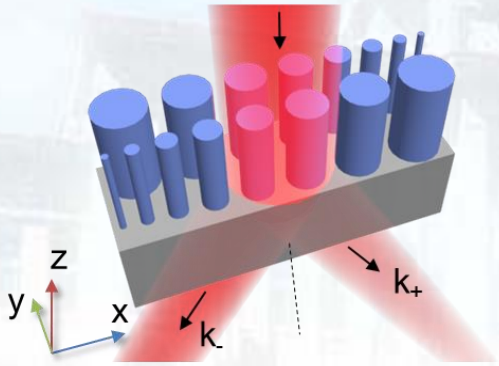

图12. 纳米分光器单元结构示意图。

Fig. 12. Schematic illustration of a unit cell of the nanoscale beam splitter.

基于Pancharatnam Berry可实现超色散异常衍射的超构表面。设计了一种基于Pancharatnam Berry可实现超色散异常衍射的超构表面。相较传统光栅色散仅由光栅晶格的横向倒格矢量贡献，相位梯度超构表面的色散包含了相位梯度所产生的局域倒格矢的贡献，为实现超大色散衍射提供新的调控维度。我们理论上分析了左旋圆偏振光垂直入射到超构表面时的电场分布和远场强度谱线，其在783nm处透射光衍射角大于80°，角色散可实现约0.5°/nm，相比具有相同周期的传统Littrow光栅的角色散大4倍以上。与此同时，衍射效率达到了27%。这明显优于传统光栅近90°时衍射效率接近于零的弊端。此外，超构表面的衍射特性，包括强度和波长，可以通过改变纳米棒的几何参数实现轻松调节。由于超构表面显示出超色散和大偏转角的特性，使得该设计不仅可用于高分辨率光谱仪，还可用于制造具有高NA的平面透镜。

Ultra-dispersive anomalous diffraction from Pancharatnam-Berry metasurfaces are proposed. According to the phase matching condition, the dispersion of the periodic nanorods metasurface introduced with phase gradient is mainly contributed by two parts: the local vector induced by phase gradient and the reciprocal vectors induced by the metasurface subcell lattice. Compared with the traditional grating which only resorts to the transverse reciprocal vectors of the grating lattice, the metasurface is easier to achieve Ultra-dispersive anomalous diffraction. Under normal LCP incidence, the electric field distribution and the far field intensity profiles were analyzed theoretically. The light diffraction angle of more than 80° could be achieved centered at 783 nm. The angular dispersion of about 0.5°/nm can be achieved, which is more than 4 times larger than the conventional Littrow grating with the same period of the metasurface subcell. At the same time, the diffraction efficiency reached 27%, which is significantly better than the conventional grating caused problems of near-zero diffraction efficiency. In addition, Their diffraction properties, including the magnitudes and wavelengths, are easily tunable by varying the geometric parameters of constitutive nanorods. As the metasurface

shows the properties of both the ultra-dispersion and large deflected angle, it would find applications not only in high resolution spectrometers but also in fabricating planar lens with high NA.

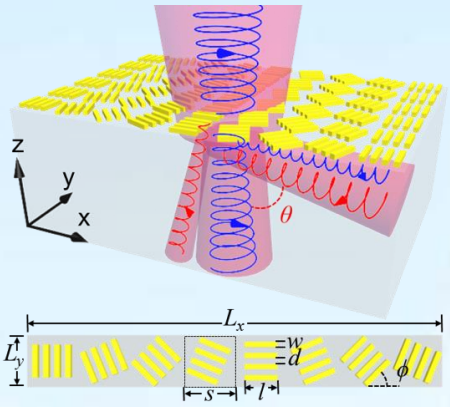

图13. Pancharatnam Berry超表面结构示意图。

Fig. 13. Schematic of Pancharatnam-Berry metasurfaces.

2. 基于微纳结构的光场调控、光学非线性效应及其应用

在自散焦非线性下的周期光子学晶格中，我们从理论和实验上展示了两束非相干光束的空域同向驱动。这两束光分别激发第一布洛赫带的带顶和带底，各自感受正常衍射和反常衍射，在非线性的作用下它们束缚在一起并同向弯曲传输。该行为可类比具有质量反号的两个物体间的相互作用，打破了牛顿第三定律的对称性。除此之外，我们还在动量空间呈现了两束光相互作用后空间频谱的分布与晶体调制度的关系，并分析了加速度逐渐减小的主导因素—激发带顶光束的频谱将先于另一光束的频谱达到饱和。

We experimentally and theoretically demonstrate a spatial diametric drive acceleration of two mutually incoherent optical beams in one dimensional optical lattices under a self-defocusing nonlinearity. The two beams, exciting the modes at the top/bottom edges of the first Bloch band and hence experiencing normal/ anomalous diffraction, can bound together and bend in the same direction during nonlinear propagation, analogous to the interplay between two objects with opposite signs of mass that breaks the Newton's third law. Their spatial spectrum changes associated with the acceleration are analyzed for different lattice modulations. We find that the acceleration limit is determined by the beam exciting the top bandedge that reaches a saturated momentum change prior to the other pairing beam.

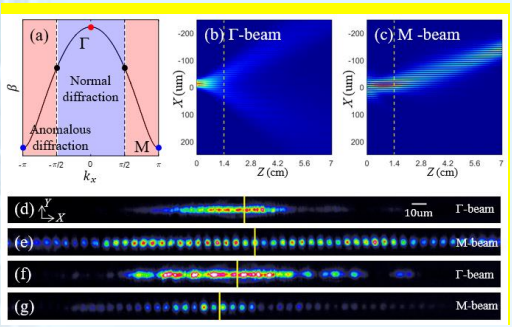

图 14. 空域同向加速驱动的模拟和实验结果。(a) 一维光子晶格的第一布洛赫能带。(b, c)距离为 7 厘米的传输模拟结果，图中黄色虚线表示实验晶体长度。(d-g) 实验结果：Γ和M光束各自的线性出射结果 (d, e)和非线性相互作用后出射结果 (f, g)。

Fig. 14. Simulations and experimental results of the spatial diametric drive acceleration. (a) First Bloch band of the used photonic lattice. (b,c) Numerical simulations of the diametric drive acceleration for a propagation distance of 7 cm, where the yellow dashed vertical lines mark the experimental sample length. (d-g) Experimental results: linear (d,e) and nonlinear (f,g) outputs for Γ-beam or M-beam propagating independently (d,e) or under the cross-phase modulation (f,g).

我们研究了沿圆形轨迹传输的自加速光束对回音廊模式微腔的自由空间耦合，得到了该光束的最佳耦合条件，并被数值模拟验证。与高斯光束相比，我们发现该自加速光束的耦合效率大幅提高（图15a，b），这个优势在使用大数值孔径光学系统或者激发微腔更高阶角向模式的情况下更加明显（图15c）。

We study free-space coupling of optical fields to the whispering-gallery-mode resonators by employing self-accelerating beams orbiting a semicircle. The best coupling

condition is obtained through theoretical analysis, in accord with the numerical results. Comparing with the conventional Gaussian-like beams, much enhanced coupling efficiency is achieved with such self-accelerating beams, particularly when a large numerical aperture of an optical system is used or a higher-order angular mode is considered.

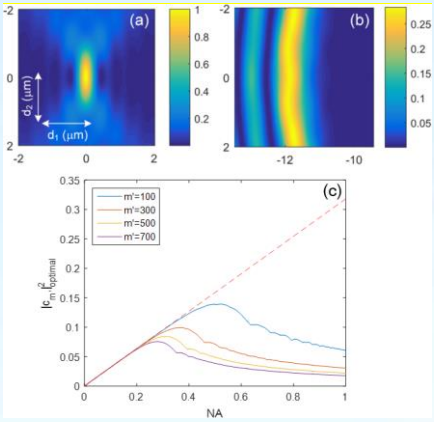

图 15. 自加速光束（a）和高斯光束（b）在不同位置处的耦合效率；（c）自加速光束（虚线）和高斯光束（实线）在不同数值孔径和激发不同模式下耦合效率的比较。

Fig. 15. Analysis of coupling efficiency to the microcavity for accelerating beams (a) and Gaussian-like beams (b) as a function of different beam locations; (c) Optimized coupling efficiency as a function of NA when exciting different cavity modes for accelerating beams (dashed line) and Gaussian-like beams (solid lines).

瓶子光束是一种具有局域空心结构的特殊光束，这种光束广泛应用于粒子捕获与运输。但迄今为止，瓶子光束的产生局限于傍轴领域，傍轴瓶子光束的细长轮廓不利于对单粒子的操控。我们利用突变理论，设计了非傍轴条件下微尺度的瓶子光束，这些光束存在一个无光场分布的微米量级中空结构，并且其内壁形貌可控。图16展示了实验实现的典型的微尺度瓶子光束，其内壁沿球面分布。

Optical bottle beam is a special kind of beam with a local hollow structure, which has been widely used in particle trapping and transporting. However, such bottle beams have thus far been generated in the paraxial regime. As a result, they have an elongated profile not favorable for single-particle manipulation. Here we use catastrophe theory to design the micro-scale bottle beams under the non-paraxial condition. These beams have a micron-scale hollow structure where light fields are absent, and the shape of their inner walls are controllable. Figure 16 shows the typical micro-scale bottle beams with spherical inner walls.

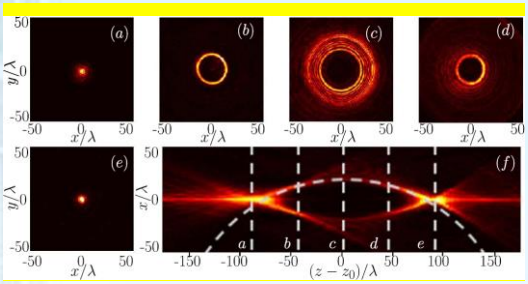

图 16. 内壁沿球面分布的微尺度瓶子光束。(a-e)该光束在(f)中对应位置处的横向光斑分布；(f)纵切面光束传输。

Fig. 16. Micro-scale bottle beam with a spherical inner wall. (a-e) The transverse intensity distribution of the beam at locations marked in (f), where the beam propagation in the longitudinal section is presented.

光子石墨烯是具有狄拉克锥的光学周期结构，为我们提供一个非常便捷的研究与狄拉克点相关物理现象的平台。我们研究了施加梯度场的光诱导光子石墨烯中的布洛赫震荡(BO)和齐纳隧穿(LZT)现象。与通常具有带隙的四方光子晶格中的BO不同，非绝热的光束传输行为对梯度场与狄拉克锥的方向高度敏感。特别的，对称性保持的梯度势场导致近乎完美的LZT和不同能谷之间的相干BO。而对称的梯度势场产生非对称的散射和不完全的LZT，以及由赝自旋不平衡导致的依赖于能谷的涡旋产生。我们的结果清楚的表明，在狄拉克点附近的梯度场并不像通常简单的认为是引入了标量的力，并且LZT的概率是强烈依赖于子晶格的对称性的。我们的结果也说明了各向同性的狄拉克锥在外加的强驱动势场下可以表现为各向异性，这对于操控类石墨烯系统中的子晶格和能谷赝自旋具有有益的借鉴作用。

Photonic graphene, optical anology of graphene, provides a useful platform to study intriguing Dirac physics in optics. We demonstrate intervalley Bloch oscillation (BO) and Landau-Zener tunneling (LZT) in an optically induced honeycomb lattice with a refractive-index gradient. Unlike previously observed BO in a gapped square lattice, we show nonadiabatic beam dynamics that are highly sensitive to the direction of the index gradient and the choice of the Dirac cones. In particular, a symmetry-preserving potential leads to nearly perfect LZT and coherent BO between the inequivalent valleys, whereas a symmetry-breaking potential generates asymmetric scattering, imperfect LZT, and valley-sensitive generation of vortices mediated by a pseudospin imbalance. This clearly indicates that, near the Dirac points, the transverse gradient does not always act as a simple scalar force, as commonly assumed, and the LZT probability is strongly affected by the sublattice symmetry as analyzed from an effective Landau-Zener Hamiltonian. Our results illustrate the anisotropic response of an otherwise isotropic Dirac platform to real-space potentials acting as strong driving fields, which may be useful for manipulation of pseudospin and valley degrees of freedom in graphenelike systems.

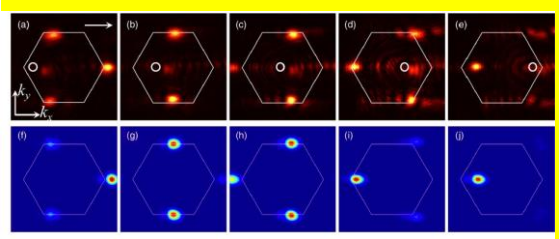

图 17. 光子石墨烯中梯度场下对称布洛赫震荡的实验结果。

Fig. 17. Experimental results of symmetric bloch oscillation in photonic graphene.

飞秒激光拥有极强的峰值功率（10^{12} W量级），这使飞秒激光为金属、半导体、聚合物和电介质等材料的精确加工提供了一种非常高效的工具。与基底材料相互作用时，超短激光（~10^{-15} s）的热效应非常小所以使得热影响区域极小，这让加工变得更加精确。飞秒激光脉冲能量的非线性吸收让加工石英玻璃或者铌酸锂晶体等硬脆材料这一传统中的难题成为可能。铌酸锂是一种多功能的光电材料拥有出色的光学电学性质比如电光效应、声光效应、压电效应、光折变效应以及非线性效应。大多数用于光子集成回路的器件都可以用铌酸锂晶体制备比如光波导、光开关、电光调制器和热释电探测器。在铌酸锂表面加工均匀周期性结构是重要的一步。不过在飞秒激光加工铌酸锂表面微纳结构方面仍然存在一些问题。由于库伦爆炸，在铌酸锂表面只得到了一些底部或边缘有条纹的坑状结构和凹槽结构，这造成材料表面不够均匀。这些问题使宽带隙透明材料表面周期性结构难以加工，这阻碍了微纳器件的制造，包括通讯、探测、生物医药以及微流通道等应用。

A femtosecond (fs) laser with peak power in the range of gigawatts has been proven to be an efficient tool for precise machining of a wide range of materials, including metals, semiconductors, polymers, and dielectrics. When interacting with a substrate material, the ultrashort pulses (~10^{-15} s) cause minimal thermal diffusion and, therefore, produce more precisely machined features with minimal heat-affected zones. Nonlinear absorption of ultrashort pulse laser energy enables precise manufacturing of hard and brittle materials, such as silica glass or LN crystals, which is a challenging task for conventional mechanical manufacturing methods. LN is a multifunctional optoelectronic material with excellent optical and electrical properties, such as the electro-optic effect, acousto-optic effect, pyroelectric effect, piezoelectric effect, photorefractive effect, and nonlinear effect. Most devices used in photonic integrated circuits (PICs) can be prepared with an LN crystal, such as an optical waveguide, optical switch, electro-optical modulator, and

pyroelectric sensor. Achieving a consistent periodic surface microstructure on LN is an important manufacturing step. However, there are still some problems when using a fs laser to prepare micro/ nanostructures on the LN crystal's surface. Because of the coulomb explosion, only craters with some stripes at their edge or bottom and groove structures on the LN crystal's surface can be obtained, which causes an unstable state of the material surface. These problems will lead that periodic micro/nanostructure on wide-bandgap transparent crystals to not be processed, which influences the process of micro/nano photonic devices, including communication and detecting, as well as biomedical microfluid applications.

我们提出通过控制铌酸锂晶体温度抑制库伦爆炸进而得到均匀的飞秒激光诱导表面周期性结构。同时我们研究了激光能流对于样品表面形貌的研究。对于 400-1000 nm 的光，加工后的样品吸收率比纯铌酸锂提高了一个量级。本文所提出的方法为宽带隙晶体微纳结构的加工提供了一个思路，可以被应用到减反纳米光栅的加工以及具有纳米结构的热释电探测器的小型化。

In this paper, we report on the application of a heater to control the temperature of LN crystals, which is designed to inhibit the coulomb explosion to obtain a uniform fs laserinduced periodic surface structure (LIPSS). At the same time, we also studied the effect of laser fluence on the sample morphology. The absorption of a processed sample is one order higher than that of pure LN over the wavelength range 400–1000 nm. This approach is beneficial for fabrication of micro/nanostructures on wide-bandgap crystals, which can be used for fabricating nanogratings with antireflection coatings and miniaturized pyroelectric detectors with nanostructures of PICs.

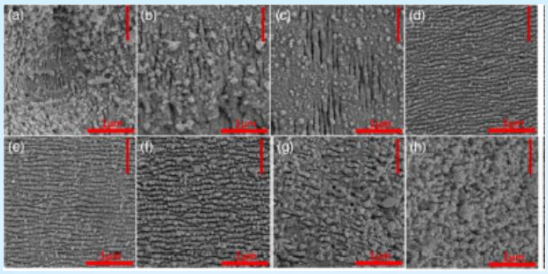

图 18. 在不同温度飞秒激光加工铌酸锂表面 SEM 图：(a) 28°C, (b) 100°C, (c) 200°C, (d) 300°C, (e) 400°C, (f) 500°C, (g) 600°C, (h) 800°C。

Fig. 18. SEM images of a fs laser processed LN surface in N_2 environment with sample temperature of (a) 28°C, (b) 100°C, (c) 200°C, (d) 300°C, (e) 400°C, (f) 500°C, (g) 600°C, (h) 800°C, respectively.

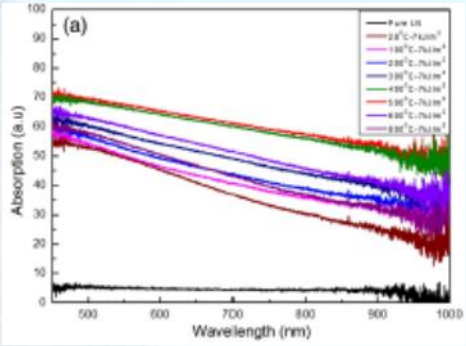

图 19. 飞秒加工样品吸收光谱。

Fig. 19. Absorption spectra of fs laser processed LN.

矩形亚波长波导对于微/纳米光子器件和片上平台的发展是非常重要的。我们利用时间分辨成像系统，研究了 THz 脉冲在矩形亚波长介质波导中的瞬态特性和传播模式。THz 脉冲的动态传输过程被地记录成为一个视频。此外，在亚波长矩形波导中也表现出反常的群速度色散。我们利用有效折射率方法，对矩形亚波长波导中的传输模式进行了理论计算，与实验和模拟结果吻合较好。这项工作为改进和提升集成平台和光子器件的分析和设计提供了机会。

Rectangular subwavelength waveguides are necessary for the development of micro/nanophotonic devices and on-chip platforms. Using a time-resolved imaging system, we studied the transient properties and the propagation modes of THz pulses in

rectangular subwavelength dielectric waveguides. The dynamic process of THz pulses was systematically recorded to a movie. In addition, an anomalous group velocity dispersion was demonstrated in rectangular subwavelength waveguides. By using the effective index method, we theoretically calculated the modes in rectangular subwavelength waveguides, which agree well with the experiments and simulations. This work provides the opportunity to improve the analysis and design of the integrated platforms and photonic devices.

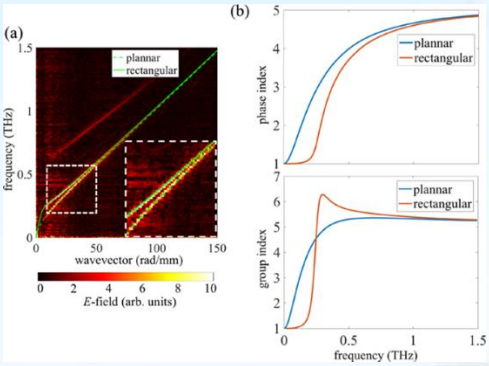

图 20. （a）实验结果。PSW 和 RSW 中 THz 波的色散曲线。蓝色曲线表示理论 PSW 模式，绿色曲线表示 EIM 分析计算的理论 RSW 模式；（b）50 μm PSW 和 50 μm×200 μm RSW 的有效相折射率的理论图。

Fig. 20. (a) Experimental results. The dispersion curves of THz waves in PSW and RSW. The blue curve indicates theoretical PSW mode and the green curve indicates theoretical RSW mode calculated by EIM analysis. (b) Theoretical plots of the effective phase index of 50μm PSW and 50 μm×200 μm RSW.

表面波引起了人们的广泛关注,由于亚波长局域和便于在光子集成电路中操控的特点。它在光信号传输和能量传输中起着重要的作用。近年来，超表面为实现自由传播波与表面波模式之间的转换提供了强有力的方案，但是在太赫兹频段导波与表面波的转化仍然存在缺失，这对于片上光子集成器件的发展是一个瓶颈。

Surface waves (SWs) have attracted a widespread attention due to the characteristic of subwavelength confinement and convenient manipulation in photonic integrated circuits, which can play a significant role in carrying optical signals and energy transfer. Though metasurface provides a powerful tool in realizing the conversion between freely propagating waves and surface modes in recent years, a gulf between guided waves (GWs) and SWs in terahertz (THz) range still exists, which is a bottleneck for on-chip photonic integrated devices.

提出了一种新颖的太赫兹集成平台，通过铌酸锂亚波长波导与超表面天线的耦合，可以实现导波到表面波的转换。利用时间分辨相衬成像技术直接观察了太赫兹的转换过程和传输过程。基于时间演化，通过色散关系分析了表面波的特性。从而证明了表面波是由天线阵列的集体振荡引起的。这项工作将为增强光物质相互作用和太赫兹表面集成器件提供有效方案。

We presented a novel THz integrated platform which could be used for the conversion from GWs to SWs via coupling of a LN subwavelength waveguide and metasurface antennas. The conversion process and transmission of the THz electric field (E-field) were directly observed using time-resolved phase contrast imaging. Based on the temporal evolution, the dispersion relation was extracted and analyzed to demonstrate the characteristics of SWs. We demonstrated that the SWs were induced by the collective oscillation of the antenna array. This work would open a door for strong light-matter interaction and THz surface integrated devices.

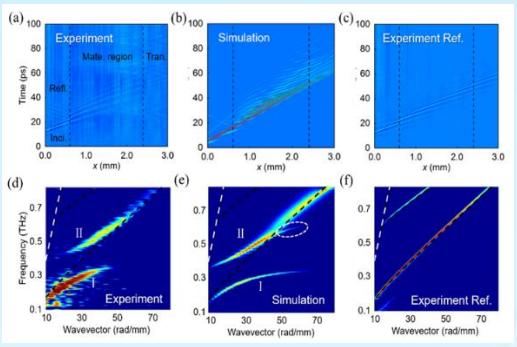

图 21. (a)和(b) 空间-时间演化图；(c)作为对照的空间-时间演化图；(d)-(f)经过对空间-时间图做傅里叶变化得到不同区域的色散曲线。

Fig. 21. (a) and (b) The space-time plots of the hybrid structure with the image intensity showing THz E-field, which suggest the results of SWs propagating in the gap (|y| < 15 μm) from experiment and numerical simulations. (c) The space–time plot of the bare LN subwavelength waveguide as a reference. These plots are divided into three regions: incidence (Inci.) and reflection region (Refl.), metasurface region (Meta. region) and transmitted region (Tran.). (d)-(f) The dispersion curves of excited modes are obtained from experiment and numerical simulation by performing 2D Fourier transform.

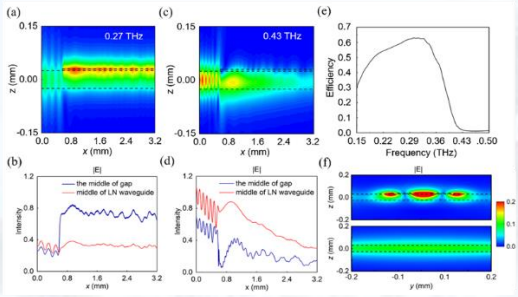

图 22. (a)-(d) 不同频率电场强度分布图；(e)耦合效率图；(f)电场界面分布图。

Fig. 22. (a-b) and (c-d) The E-field intensity maps are recorded in the symmetrical plane (y = 0 plane) of the hybrid structure at f = 0.27 THz and 0.43 THz, respectively. Rectangular dashed frame and two black dashed lines indicate the locations of the antenna array and the LN subwavelength waveguide. The relative intensity |E| is at the center of the gap (blue line) and the middle line (y = 0, z = 0) in the LN waveguide (red line). (e) Simulated coupling efficiency from the mode of stand-alone LN subwavelength waveguide to the SWs. (f) The field confinement in the SWs over the guided mode. The maximal field enhancement of the upper panel is 5 times relative to the lower.

因为超材料可用于实现对电磁特性的控制，可以超出了天然材料的限制，其中可能发生大量令人着迷的物理现象，例如负折射率材料和零折射率材料。尽管负折射率材料和零折射率材料对未来应用具有很大的前景，但它们在物理学中也引起了一些争议，其中之一就是是否违背因果律或超越光速。争议出现的原因是以前的研究人员主要关注稳态研究，但他们忽略了完成负折射建立需要一些时间。有一篇文献在解决争议方面迈出了一大步，其中光子晶体负折射率材料用于研究负折射的瞬时建立，从而解释了负折射的发生没有违反因果律或超越光速。值得注意的是，瞬态分析对于处理材料中的光传播问题是必要的，尤其是在新型负折射率和零折射率材料的情况下。然而，到目前为止，还没有先前的研究涉及零折射的瞬态过程。此外，没有系统的研究比较负，零和正折射的建立过程。

Metamaterial is used to achieve the controls of electromagnetic properties which go beyond the limitations of natural materials, where a large number of fascinating physical phenomena can occur, such as negative-index materials (NIMs) and zero-index materials (ZIMs). Although NIMs and ZIMs have great prospects for future applications, they also cause some controversies in physics, one of which is whether causality and the speed limit c are broken. The reason why the controversy appears is that previous researchers mainly focused on the researches of steady state but they ignored that some time is needed to complete the establishment of negative refraction. A reference takes a good step in solving the controversy, where a specific photonic crystal NIM was used to study the transient establishment of negative refraction, thus explaining the occurrence of negative refraction without causality or speed limit violation. It is noted that transient analysis is necessary for handling the light propagation problems in materials, especially in the case of novel NIM and ZIM. However, so far, there

are no previous study that has dealt with the transient process for zero refraction. Furthermore, no systematic investigation is presented comparing the establishment processes of negative, zero and positive refraction.

我们通过由周期性排列的开环劈裂环和金属线组成的楔形超材料结构定量地展示了负，零和正折射的波前的瞬时建立。三种折射的波前首先沿正折射角通过楔形结构的第二界面传播，然后重新组织，最后分别在一段建立时间后沿有效折射角传播。波前的建立需要时间驳斥了因负折射和零折射而违反因果律或超光速传播的结论。负折射或零折射的建立时间比正折射的建立时间长。对于所有三个折射过程，瞬态建立过程先于稳定传播的建立。此外，在我们的研究中证明了一些具体的特性，包括零折射材料内无限大的波长和均匀的相位，以及负折射率材料中相速度与群速度反平行。

We quantitatively demonstrate transient establishment of wavefronts for negative, zero, and positive refraction through a wedge-shaped metamaterial consisting of periodically arranged split-ring resonators and metallic wires. The wavefronts for the three types of refractions propagate through the second interface of the wedge along positive refraction angles at first, then reorganize, and finally propagate along the effective refraction angles after a period of establishment time respectively. The establishment time of the wavefronts prevents violating causality or superluminal propagation for negative and zero refraction. The establishment time for negative or zero refraction is longer than that for positive refraction. For all three refraction processes, transient establishment processes precede the establishment of steady propagation. Moreover, some detailed characters are proven in our research, including infinite wavelength, uniform phase inside the zero-index material, and the phase velocity being antiparallel to the group velocity in the negative-index material.

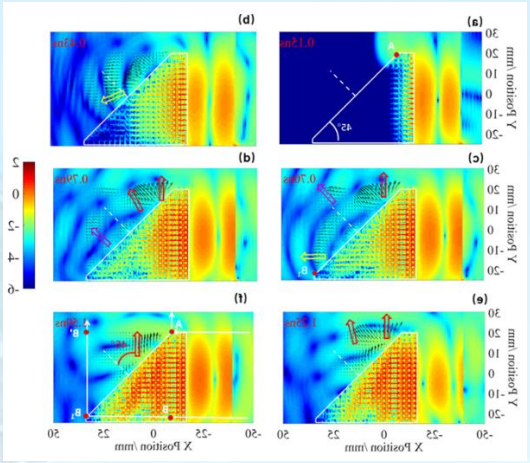

图 23. 负折射过程的电场分布图(电场值取自然对数)，其上加了坡印亭矢量。楔形结构的有效折射率在 10.6GHz 下为 n = -1.04。（a）t = 0.15 ns。（b）t = 0.43 ns。（c）t = 0.70 ns。（d）t = 0.79 ns。（e）t = 1.25 ns。（f）t = 1.50 ns。 楔形结构由白色实线包围，白色虚线是楔形第二界面的法线。 黄色，红色和紫色箭头分别代表正，负和零折射方向。

Fig. 23. Distribution of the electric field (ln(|E|)) overlapped with the Poynting vector for the model. Effective refractive index of the wedge-shaped structure is n = -1.04 at 10.6 GHz. (a) t = 0.15 ns. (b) t = 0.43 ns. (c) t = 0.70 ns. (d) t = 0.79 ns. (e) t = 1.25 ns. (f) t = 1.50 ns. The wedge structure is emphasized by white solid lines, and the white dashed line is the normal of the second interface of the wedge. The yellow, red, and purple arrows represent the positively, negatively and zero-refracted direction, respectively.

基于微纳加工技术，我们成功制备了片上周期极化铌酸锂微盘腔和混沌铌酸锂单晶微腔。上述微腔的品质因子在百万量级。腔中观察到了包括倍频和光学参量振荡效应在内的非线性效应。我们首次发现铌酸锂单晶微腔中的光学参量振荡效应存在多个通道和高温阈值。周期极化铌酸锂晶体微腔的制备使得我们具有利用铌酸锂晶体最大非线性非线性系数的能力。

We successfully fabricate periodically poled lithium niobate (PPLN) microdisk cavities and chaotic lithium niobate microdisk cavities on a chip by using microfabrication

techniques. The quality factor of these microresonators are on the order of one million. Nonlinear effects including second harmonic generation and optical parametric oscillation were investigated in these resonators. Multiple-channel effects and high-temperature threshold were observed in optical parametric oscillation effect in monocrystalline lithium niobate microcavities. The fabrication of PPLN microdisk paves the way to utilize the largest nonlinear coefficient of lithium niobate crystal.

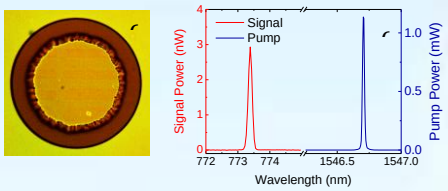

图24.（a）PPLN 微腔的光学显微镜图片；（b）1550nm激光泵浦下的二次谐波信号。

Fig. 24. (a) Optical image of a PPLN disk microcavity with a 40 μm radius. (b) Second harmonic signal observed under a pump in 1550-nm band.

铌酸锂晶体上液晶微滴的电润湿自脉冲和光电/热电能量转换。由连续激光辐照在掺铁铌酸锂晶体上诱导产生的光生电流和电压由于微等离子体放电而展现出准周期的脉冲特性。这种持续将连续输入到周期响应的转变十分有意义，可以作于自激励系统和效仿生物系统中的脉动。微等离子体放电同样可应用于不同场合，如表面处理、杀菌、分解水。我们把向列液晶微滴放在掺铁铌酸锂晶体表面，制作了一个简单的液晶盒，并通过动态电润湿效应将光生伏打电流的自脉冲行为可视化。在同时考虑晶体的光生电流（体光生伏打效应）和热电效应（利用加热-冷却充电）的情况下建立了理论模型。对动态过程的分析发现毫秒量级的的电流脉冲具有非对称线形，上升沿陡峭而下降沿很缓慢。动态电润湿效应调制了反射的干涉图型。由于非线性光生电流效应和微等离子体放电，能量转换效率在更高光强下会得到增强。

Photogalvanic current and voltage photoinduced by CW laser illumination of Fe-doped LN reveals quasi-periodic pulsing due to microplasmas discharges. This transformation of constant external influence into periodic response is interesting as example of self-excited systems, resembling pulsations of biological systems. Microplasmas discharges are also interesting for applications in various fields, such as surface treatment, sterilization, water splitting. We analyze self-pulsing of photogalvanic current visualized by dynamic electrowetting in a simple LC-cell, formed by a nematic LC droplet placed on Fe-doped LN crystal. In modeling contributions from both photogalvanic (bulk photovoltaic) and pyroelectric (charging by heating-cooling) effect are included. The analysis of dynamic regime reveals that a current pulse (in microsecond range) has asymmetric shape with extremely sharp rise with longer decay time. Reflected interference patterned was modulated by the dynamic electro-wetting effect. For high light intensity power conversion efficiency is enhanced due to nonlinear photogalvanic effect and microplasmas discharges.

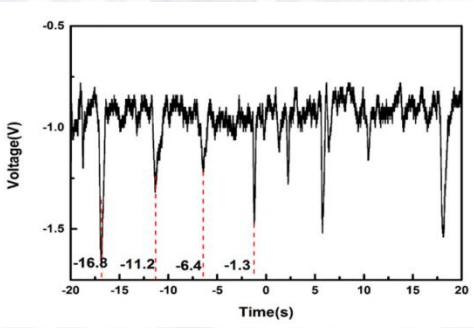

图 25. 连续绿色激光辐照下，从带有液晶微滴的铌酸锂晶体表面反射的脉冲散射光。脉冲周期约为 5 秒。

Fig. 25. Pulsating scattering from LC droplet on LN + green CW laser illumination. Period of Pulsating ~ 5 sec.

1.2微米波段可调谐掺钬ZBLAN光纤激光器。研究了基于Littrow配置1.2微米波段掺钬ZrF_4-BaF_2-LaF_3-AlF_3-NaF光纤连续激光器

的波长调谐特性，波长调节范围为1184–1198 nm，在整个调谐范围内激光的谱线宽度都在0.02 nm左右。泵浦功率为1.97W时，在1192nm获得最大的输出功率81.6mW。波长调节范围受限于光纤波分复用器和耦合器的透过率。利用体光栅的零级衍射使用一个简单光纤激光器结构，可以将激光器的波长调节范围扩展到1177-1201nm。

Wavelength tunability of continuous-wave holmium doped ZrF_4-BaF_2-LaF_3-AlF_3-NaF fiber lasers operating in the 1.2 μm wavelength region was investigated with a Littrow configuration. A wavelength tuning range of 1184–1198 nm was obtained from the fiber output port of the laser. The spectral width was measured to be around 0.02 nm over the entire tunable range and a maximum output power of 81.6 mW at 1192 nm was obtained at a pump power of 1.97 W. The wavelength tunable range was found to be limited by the transmission of the fiber-optic wavelength division multiplexer and coupler. A broader wavelength tuning range of 1177–1201 nm was obtained with a simpler fiber laser construction from the zero-order diffraction output of the bulk grating.

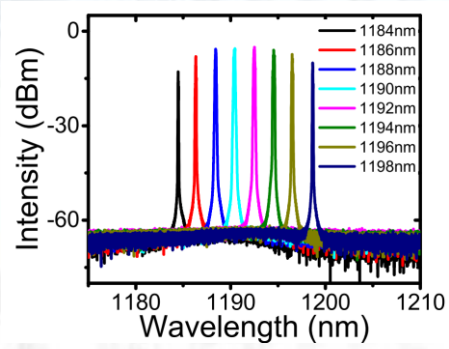

图 26. 1.97W 泵浦功率下波长可调谐掺钬 ZBLAN 光纤激光器 1184-1198nm 典型波长的光谱。

Fig. 26. Optical spectra of the wavelength tunable Ho^{3+}-doped ZBLAN fiber laser at typical wavelengths from 1184 nm to 1198 nm at the maximum available pump power of 1.97W.

光群速调控在光陀螺等探测设备中具有很重要的应用，以往光群速的调控主要是通过激发EIT、受激布里渊散射（SBS）等非线性效应实现的。在光纤中，自激发的SBS效应只能产生光群速减慢，而光群速加快则需要非常昂贵的射频发生器将探测光调控在SBS的反常色散区。近年来，回音廊模微腔因其极高的品质因数、极小的模式体积，在其中的SBS可以极大地降低泵浦功率，其结构也非常有利于小型化，探索其中的快光产生有着非常重要的意义。我们使用调制的泵浦光，在实验中观测到了自泵浦的光群速加快。随着调制频率的增加，光群速改变逐渐由群速加快（-91μs）逐渐变为群速减慢（2.6μs）。这个装置不但具有的配置简单、结构稳定、功耗小、容易调节等优势，而且自泵浦快光不需要昂贵的射频设备，为它以后的广泛应用奠定了基础。

The gyroscope plays a great role in the measurement of rotation, which has great applications in the fields of navigation, phone sensor, aircraft, satellite, and gravito-magnetic effects. The features of compact size and high sensitivity are expected for the future gyroscope. In 2007, M. S. Shahriar etc. demonstrated a resonator-based optical gyroscope whose sensitivity could be enhanced via the fast light from anomalous dispersion. There are various methods to control the dispersion to realize group velocity control in a fiber or photonic crystals. With the help of an expensive radio-frequency (RF) signal generator, the signal in the SBS amplifier configuration could be set in the abnormal dispersion window to generate fast light. In this letter, self-pumped SBS-induced fast light was demonstrated in a micro-sphere cavity, in which no RF signal generator was applied. The group delay from -91.0 to 2.6 μs could be modified by changing the modulation frequency of the pump light, and the optically induced thermal effect in the cavity was found to play an important role in the dispersion modification.

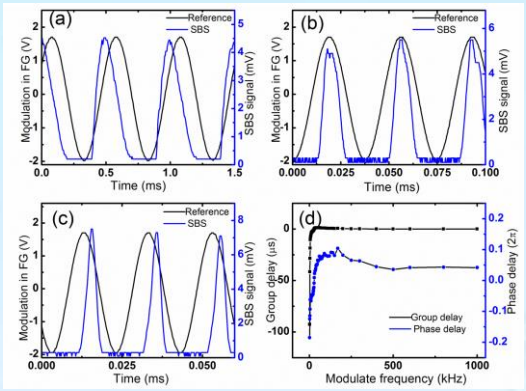

图 27. （a）、（b）、(c)分别是调制频率在 2 kHz、27 kHz、和 50 kHz 时调制相位和光强相位的对比图像，光群速逐渐由加快变为减慢；d 图显示了群速延时和相应的相位延时。

Fig. 27. （a）、（b）、(c) is the group delay examples at a modulation of 2 kHz, 27 kHz and 50 kHz, respectively; (d) showed the group delays and the phase delays accordingly.

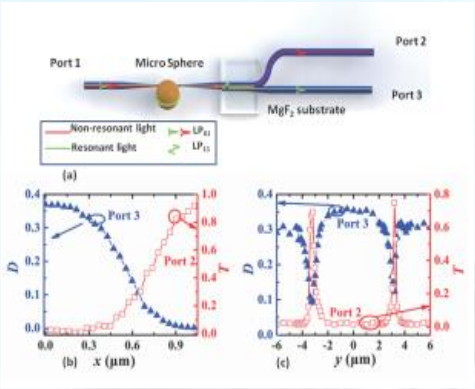

图28. （a）实验配置图，采用典型的少模光纤耦合微腔，并利用另一根锥形光纤导出高阶模；（b）和（c）分别显示的是x与y方向的位移和通道耦合效率的变化关系。

Fig. 28. (a) is the configuration of the experiment. A typical fewmode-TF coupled microsphere was adopted; (b) and (c) is relationship between the coupling efficiencies and the shift in *x* and *y* direction, respectively.

我们在理论和实验两方面证实了回音廊模微腔的准临界耦合效应。在此配置下，具有和输入模式相同衰减的另一模式作为微腔的损耗补偿，使得体系整体的耦合效率更加稳定；同时，随着微腔与锥形光纤（波导）的间距变化，耦合效率的变化为单调函数。Drop通道的效率在锥形光纤或波导贴近微腔时最高，并具有相同的稳定性，这方面的研究对于利用微腔实现滤波，以及滤波的相关应用（比如超窄线宽激光器等）有着非常重要的意义。利用此种配置结合光纤布拉格光栅，我们实现了C波段线宽3kHz的连续可调超窄线宽激光器。

A quasicritical coupling state was demonstrated both in theory and experiment with a few-mode tapered-fiber (TF) coupled whispering-gallery-mode (WGM) cavity. In such a configuration, the coupling mode to activate the WGM and the drop mode are in the same TF and of almost the same decay rate with the variation of the gap between the TF and WGM cavity. Consequently, when the gap decreases to zero, the transmission of the coupling mode decreases monotonously to zero at the resonance wavelength, while the transmission of the drop mode increases monotonously to unit, which means that neither the coupling efficiency in the coupling mode nor the transmission of the drop mode will decrease in the traditional overcoupling region. Thus a steadily high coupling efficiency can be achieved accordingly, which we defined as quasicritical coupling. Such a coupling state will be helpful to develop WGM-cavity-based filters and benefit the fabrication of ultranarrow-linewidth lasers. With such technique, a tunable laser with a line width less than 3 kHz covering the whole C-band was demonatrated with the help of FBGs.

手性液晶中缺陷模式的耦合。手性液晶可以看作是一维光子晶体，具有光子禁带。利用我们最近提出的液晶面外定向技术，可以构建一维的聚合物条带结构，在结构中充入手性液晶，可以实现手性液晶的均一取向。聚合物条带在手性液晶中起到了缺陷的作用，从而在光子禁带中出现了缺陷模式，具有很高的光子态密度。我们使用FDTD方法模拟了该类结构中缺陷模式的耦合效应。类比于固体物理中众所周知的紧束缚模型，当手性液晶中出现多个缺陷层时，缺陷模式会发生劈裂，甚至会在带隙中形成迷你能带。

该类结构在低阈值激光器和多波长滤色器方面具有潜在的重要应用。

Cholesteric liquid crystal structures with multiple isotropic defect layers exhibit localized optical modes (defect modes). Coupling effects between these modes were simulated using the finite difference time domain method. Analogous to the well-known result of the tight-binding approximation in solid state physics, splitting of the defect modes takes place, as soon as the structure contains more than one defect layer. The dispersion relation of the mini-bands forming within the photonic band gap of the structure is calculated numerically. The structures might have promising applications for multiwavelength filters and low-threshold lasers.

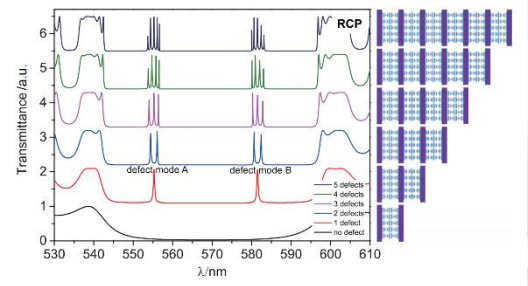

图 29. 右旋圆偏光通过具有不同数目缺陷的手性液晶的透射谱。手性液晶和聚合物条带的厚度分别为 4 μm and 2 μm。

Fig. 29. Transmission spectra (for RCP light) of composite structures with varying number of structural units. The thicknesses of the CLC and polymer layer are 4 μm and 2 μm, respectively.

3. 超分辨成像及其应用

采用一块动态调制关联位相屏，我们基于经典光实现了空间分辨率可达海森堡极限的相关成像。实验中，我们利用纯位相型空间光调制器动态调制出射光的位相空间分布，使之兼具透镜和空间关联位相分布的功能。进一步采用点扫描照明方式，我们在实验上利用经典光源如激光、准热光等实现了空间分辨率达到海森堡极限的相关成像。

We demonstrated experimentally a correlation imaging scheme with its spatial resolution reaching the fundamental Heisenberg limit by using a dynamically phase-correlated lens screen. The dynamically phase-correlated lens screen was realized experimentally through a commercial spatial light modulator by dynamically loading computer generated phase patterns, and the scanning-focused-beam illumination mode was employed to achieve the Heisenberg-resolution imaging with classical light such as laser and pseudo-thermal light.

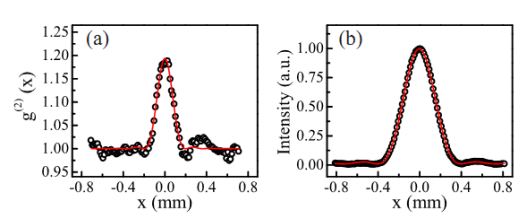

图 30. (a) 具有海森堡空间分辨率极限的二阶关联成像点扩散函数；(b) 传统的透镜辅助的强度成像点扩散函数。

Fig. 30. (a) The point spread function of the Heisenberg-resolution imaging scheme, and (b) the point spread function of the traditional lens-assisted intensity imaging scheme.

超分辨光学成像揭示生理状态红细胞骨架精细结构。人红细胞呈现特有的双凹圆饼状形态并具有极强的变形性和稳定性，保证其在120天寿命中往返动静脉上百万次，行程约480 km循环过程中不破损。红细胞虽已被人类认知300多年，但是诸多的机制仍尚不清楚，如细胞骨架组织特性等。我们基于随机光学重构超分辨成像技术研究了红细胞骨架生理结构特性，同时依靠最近距离法、二维自相干分析法和二维互相关分析法，并结合理论建模，证明在近无损生理状态下红细胞骨架连接复合体之间的距离即血影蛋白长度约为80 nm，而不是前人利用电镜观察得到的200 nm、46 nm或60 nm，并分析发现红细胞骨架体系处于动态的结合和解离状态。相关结果可为揭示红细胞极强变形性内在机制提供了新的实验支撑，也为理解血影蛋白相关的细胞骨架的构建提供新的启示。

The erythrocyte cytoskeleton is a textbook prototype for the submembrane cytoskeleton of metazoan cells. While early experiments suggest a triangular network of actin-based junctional complexes connected by ~200 nm-long spectrin tetramers, later studies indicate much smaller junction-to-junction distances in the vast range of 25-60 nm. Through super-resolution microscopy, we resolve the native ultrastructure of the cytoskeleton of membrane-preserved erythrocytes. This allows us to determine a ~80 nm junction-to-junction distance, a length consistent with relaxed spectrin tetramers and theories based on spectrin abundance. Through two-color data, we further show that that the cytoskeleton meshwork often contains nanoscale voids where the cell membrane remains intact, and that actin filaments and capping proteins localized to a subset of, but not all junctional complexes. Together, our super-resolution results thus call for both experimental and theoretical reassessments of the structure and function of the erythrocyte cytoskeleton, and more generally, the spectrin-actin-based cortical cytoskeleton of metazoan cells.

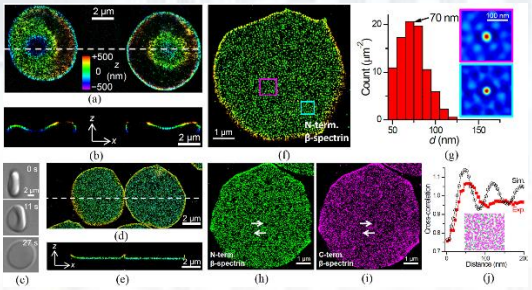

图 31. 超分辨光学成像揭示红细胞骨架精细结构特性.

Fig. 31. The native ultrastructure of the erythrocyte membrane skeleton revealed by super resolution fluorescence microscopy.

光刻图案化技术揭示细胞间通讯时空传递机制。小胶质细胞是中枢神经系统的第一道也是最主要的一道免疫系统防线，属于空间组织结构离散的功能系统，当脑部受到创伤或感染时，小胶质细胞可迅速动员并聚集，在正常细胞和受损细胞间形成一个保护屏障，但其如何实现快速有效通讯机制仍不明确。我们利用光刻技术实现细胞在基底的图案化分布，同时结合快速显微荧光成像技术，应用微局域机械力刺激手段，以胞间钙波传递为胞间通讯的观察载体，体外定量、可控地实现了小胶质细胞间通讯的时空传递机制研究。主要结果显示小胶质细胞间钙波通讯存在中继机制，即细胞在感受到信使分子之后自身又会分泌额外的信使分子，扩大信号传递的范围，提高传播速度和效率，首次实验上直观可信的验证了细胞间通讯存在中继站效应。相关结果可为阐明小胶质细胞快速有效的保护中枢神经系统机制提供新的实验支撑，也为体外研究细胞间通讯特性提供新的实验方案。

As the first line of immune defense in the central nervous system, microglia could rapidly congregate together and establish a potential barrier between healthy and damaged tissue after the brain injury. However, little is known about how microglial cells communicate with each other effectively following the injury. Micropatterned substrates offer a unique possibility to define and control spatial organization of biological cells at the microscale. Here, we developed a simple micropatterning strategy to resolve various spatiotemporal characteristics of intercellular calcium wave (ICWs) communication among isolated BV-2 microglial cells. we mainly observed that additional transmitter was released from the cells located at the intermediate rings. This revealed that neighboring cells acted as regenerative amplifiers for the ICWs generated by the central cell. We believe that our micropatterning strategy paves a way towards specifically designed experimental investigations on cellular assemblies and consequently towards improved understanding of ICWs-based cell-cell communications.

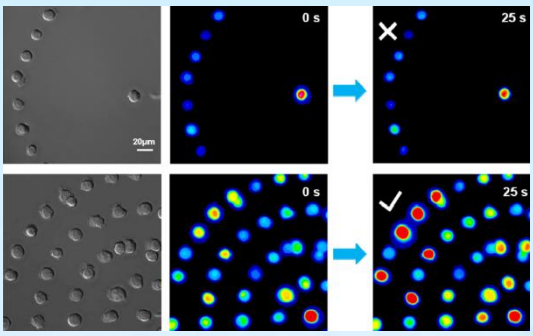

图 32. 图案化控制实验直接证明小胶质细胞间通讯存在中继传播特性。

Fig. 32. Our results directly provided the first experimental evidence of a regenerative amplification process, which were associated with the so-called relay station cells acting as regenerative amplifiers.

非线性物理与光子技术/ Nonlinear Physics and Photonics Techniques

负责人：田建国

本方向涉及石墨烯光学性质、等离子激元、超材料、光学传感、光在介质中的传播、光子带隙材料、亚波长微结构等方面。本年度发表论文 24 篇；申请或授权专利 7 项。在研课题经费 3855 万元。2018 年度“非线性物理与光子技术”方向主要在以下方面取得了进展：

In this field, we mainly focused on optical properties of graphene, plasmonics, metamaterials, optical sensor, one dimensional photon crystal, and sub-wavelength microstructure. 24 papers have been published in international academic journals, and 7 patents applicanted. The total researching founds are 38.55 millions. This year, we obtained some important results as following:

(1) 将 p 型的黑磷与其它二维材料叠加而成的范德华异质结构在光电子器件中有着潜在的应用，如逻辑整流、偏振灵敏光电探测器等。因此，我们选取少层黑磷作为研究对象来验证我们的预测。通过显微加工与工艺优化，我们实现了通过改变电荷沿不同方向传输来影响其光电性质的黑磷晶向诱导二极管。实验结果表明，不同的结构有着不同的整流比，分别为 6.8、22 和 115。同时结合扫描光电流成像实验，发现电荷传输的性质是由“晶向势垒”决定。理论分析表明，这种“晶向势垒”是由两个垂直的晶向中各向异性的载流子有效质量与费米能级形成。除此之外，对于晶向垂直的黑磷晶体管，在可见光范围内还展示出了明显的偏振依赖光电特性，这源于黑磷本身的二向色性与不同偏振光入射下的载流子动力学。尽管通过 p 型黑磷与其他二维材料结合制备的范德瓦尔斯 p-n 异质结可以用来实现逻辑整流器，光电探测器以及其他设备应用，通过化学掺杂的技术修饰黑磷也可以用来实现高整流比的 n 型晶体管和 p-n 结器件，相关的工作均已经被报道。然而，这种利用无掺杂和单一材料的操作方法同样展示了其优势所在。这种基于晶向诱导的光电器件不仅为二维各向异性材料提供了新的自由度，同时也为基础物理的发展提供了新的机会。

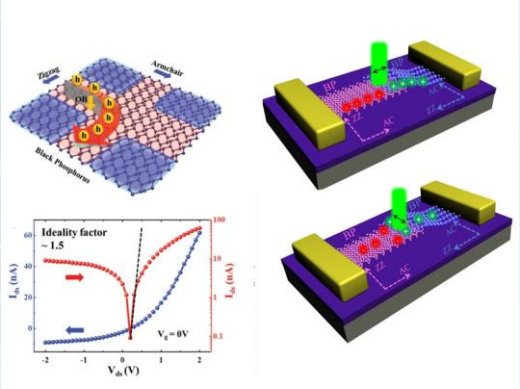

图 1. 晶向依赖的黑磷光电响应示意图。

Fig. 1. photoelectric response of black phosphorus junctions.

Van der Waals p-n heterostructures based on p-type black phosphorus (BP) integrated with other two-dimensional (2D) layered materials have shown potential applications in electronic and optoelectronic devices, including logic rectifiers and polarization-sensitive photodetectors. However, the engineering of carrier’s transport anisotropy, which is related to the linear dichroism, have not yet been investigated. Here, we demonstrate a novel van der Waals device of orientation-perpendicular BP homojunction based on the anisotropic band structures between the armchair and zigzag directions. The structure exhibits good gate-tunable diode-like rectification characteristics caused by the barrier between the two perpendicular crystal orientations. Moreover, we demonstrate that the unique mechanisms of the polarization-sensitivity properties of this junction are involved with the linear dichroism and the anisotropic carriers transport engineering. These results were verified by the scanning photocurrent images experiments.

This work paves the way for 2D anisotropic layered materials for next-generation electronic and optoelectronic devices.

(2) 黑磷这种二维材料因其独特的带隙结构，高速的载流子迁移率和显著的光学各向异性而引起了大家广泛的研究兴趣。尤其是黑磷具有高的消光系数和有效的光热转换效率并且对生物组织的无毒性的特点，这也使黑磷被广泛的应用于光热治疗等领域。在我们的研究中，我们发展了一种新型的泵浦探测技术，这项技术基于黑磷在全内反射条件下的偏振依赖吸收的光学性质。基于这项技术，黑磷的光热信号能够被实时的探测。黑磷的光热各向异性也能被定量的测试出来。黑磷面内光热各向异性的比值达到了2.9，这比文献当中报道的热导率和电导率的各向异性都要强很多。通过改变泵浦光的偏振方向，黑磷的光热型号发生了明显的变化，这也可以被用来进行黑磷晶向的判定。在我们的研究中，黑磷不仅作为吸收泵浦光并产生热量的载体，更是在探测光路中检测微小折射率变化的传感层。基于以上发现光热探测技术在生物检测和成像领域有着非常大的潜在应用。

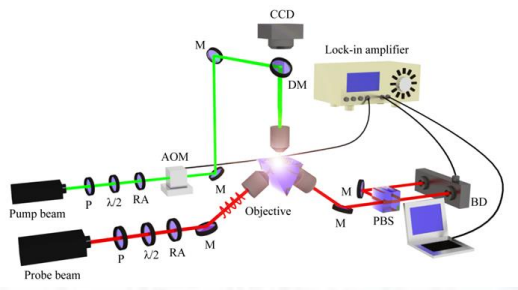

图 2. 黑磷光热效应测量装置示意图。

Fig. 2. Scheme diagram of the experimental setup used for the photothermal detection.

Black phosphorus (BP) attracts increasing attention due to its moderate bandgap, high carrier mobility, and striking in-plane anisotropy. In particular, its high-extinction coefficient combined with elevated photothermal conversion efficiency and nontoxicity in biological tissues would make BP promising in photothermal therapy. In this study, a new pump-probe technique for photothermal measurement is developed based on polarization-dependent absorption of BP under total internal reflection. The photothermal anisotropy of BP is experimentally observed for the first time. The values of photothermal anisotropy reach 2.9, which is stronger than thermal and electrical conductivity anisotropic ratios. The difference in crystal orientations of BP can accurately be distinguished by analyzing the relationship between the polarization of pump light and photothermal signal. Also, it is found that the BP not only exists as heat source yielding changes in refractive index of the photothermal media but also can detect minor photothermal signals as sensing layer. Overall, these findings that BP surface and the media significantly impact the photothermal signal provide not only an accurate way for measuring crystal orientation but also can expand the practical applications of biosensors.

(3) 我们用光热探测技术测量了黑磷和二硒化铼的光热各向异性，随后我们用光热信号的最大值和最小值的比值定义了光热对比度参数。通过探究入射泵浦光的偏振方向和光热信号强度的关系，我们可以获取不同厚度的黑磷和二硒化铼样品的光热对比度参数。研究结果证明，黑磷的光热对比度参数随着样品的厚度发生了明显的变化，但是二硒化铼样品的光热对比度参数随着样品的厚度改变并没有发生明显的变化。除此以外我们还探究了黑磷和二硒化铼异质结的光热各向异性。我们证明异质结的光热对比度参数随着堆叠角度的变化而明显的不同。我们的发现对于基于二维材料的新型微纳光学器件有着重要的意义，并有望应用于光电子器件的开发。

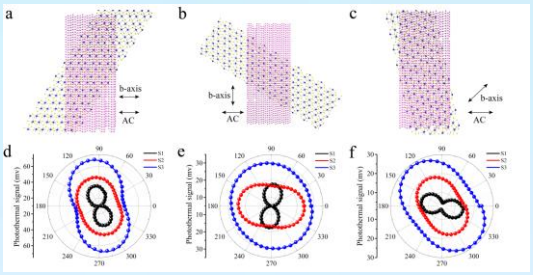

图 3. 黑磷和二硫化铼异质结构光热效应。

Fig. 3. Photothermal detection of BP/$ReSe_2$ heterostructures.

Manipulating the polarization of an incident beam using two dimensional materials have become an important research direction towards the development of nano-optical devices. Black phosphorus (BP) and rhenium diselenide ($ReSe_2$) possess excellent inplane optical anisotropy with optical birefringence in the visible region, which has led to novel applications in polarizing optics and optoelectronics. Herein, the polarization-dependent absorption of BP and ReSe2 and a modulated pump beam is utilized to obtain the photothermal signal from them. The photothermal anisotropy of BP and ReSe2 has been explored using photothermal detection. Then we have defined the photothermal contrast using the ratio of the maximum to the minimum of the photothermal signal. The photothermal contrast of BP and $ReSe_2$ can be obtained accurately by the relationship between the polarization angle of the pump light and the photothermal signal. We demonstrate that a layered BP with different thicknesses can remarkably change the photothermal contrast. In contrast, the photothermal contrast of ReSe2 does not change with the different thicknesses of the samples. Further, the photothermal anisotropies of BP/ReSe2 heterostructures were also explored. The photothermal contrasts of samples were observed to change with different stacking angles indicating that the photothermal anisotropy of heterostructures is dependent on the stacking angle. Our findings provide new prospects for designing novel optical devices based on two-dimensional anisotropic materials, with potential applications in electronics, photonics, and optoelectronics.

(4) 撰写综述文章总结了超表面调制电磁波相位及其在纳米光子学中的应用：相对于传统的相位调制光学元件，超表面显示出了新的光学现象，并有望实现可应用于更紧凑平台上的和具有更简单的制造工艺的功能性器件。光波前可以通过调控空间相位变化而被调制成任意形状，这使得探索新现象和集成超薄光学设备成为可能。该综述从超表面实现 2π的物理机制出发，将不同的机制分成了三种基本形式—谐振相位、贝里相位及传输相位，每种相位机制又可分为等离激元超表面、电介质超表面以及非线性超表面。在应用部分首先总结了利用基于相位调控的超表面实现的基础应用，随后又对能容纳更大信息容量、能实现多功能以满足现代光子学发展需求的超表面进行了总结，包括超全息、编码超表面以及多功能超表面等。我们还对于基于相位调控超表面的几个有发展应用潜力的方面进行了展望，包括基于波导的超表面、动态可重构超表面、高转化效率非线性超表面以及量子超表面等。

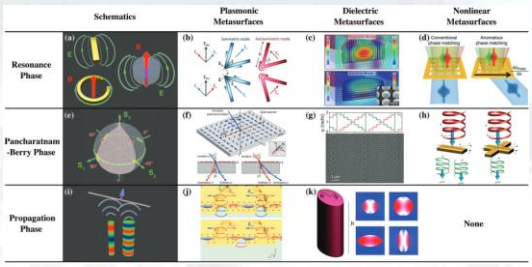

图 4. 利用不同的谐振单元如等离子谐振子、电介质谐振子、非线性谐振子进行相位调控的不同方式。

Fig. 4. Different ways for phase manipulation of optical waves with artificial nano structures.

Invited review of phase Manipulation of Electromagnetic Waves with Metasurfaces and Its Applications in Nanophotonics: Relative to conventional phase- modulation optical elements, metasurfaces (i.e., 2D versions of

metamaterials) have shown novel optical phenomena and promising functionalities with more compact platforms and more straightforward fabrication processes. With the ability to generate a spatial phase variation, optical wavefront can be manipulated into arbitrary shapes at will, enabling new phenomena and integrated ultrathin optical devices to be explored. This review is focused on recent developments regarding phase manipulation of electromagnetic waves with metasurfaces. Starting from their underlying physics for realizing full 2π phase manipulation, an overview of the applications of such metasurfaces in nanophotonics is discussed, concluding with a discussion of future prospects in this field.

(5) 撰写综述文章总结了应用于超薄光学器件上的几何超表面：超表面是由单层或少层人工微结构组成的平面超材料，它不仅是基础物理研究领域的一大基石，而且具有重大的技术意义。超表面可在亚波长范围内局域改变光学性质，因此便于器件小型化和系统集成。超表面在局域调制光的振幅、相位、偏振方面展示了非凡的能力，并产生了大量的新型应用，比如展示了广义斯涅尔定律和光子自旋霍尔效应。该综述聚焦于几何超表面基础研究领域和其在超薄光学器件方面的最新进展，介绍了包括平面超透镜、螺旋多路复用全息、可切换功能性器件、偏振光束分束器、矢量光束产生、任意偏振控制等应用。这些几何超表面器件的紧凑性、易于制造性及其特异的功能使得它们在新应用（例如加密、成像、防伪、光通信、量子科学和基础物理）方面很有吸引力。

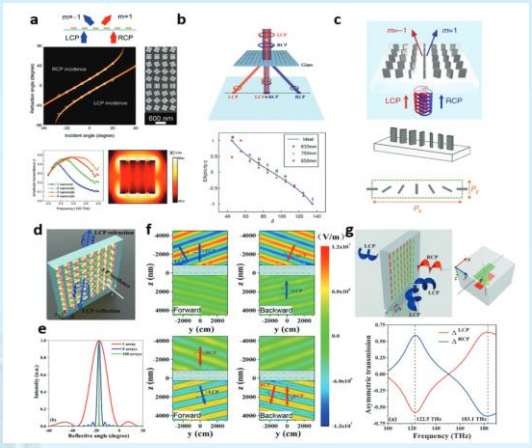

图 5. 几何超表面用于实现电磁波前的精确控制等应用。

Fig. 5. Metasurfaces for precisely manipulating the phase of electromagnetic waves and its applications

Invited review of Geometric Metasurfaces for Ultrathin Optical Devices: metasurfaces, planar metamaterials consisting of a single layer or several layers of artificial structures, not only form the basis for fundamental physics research but also have considerable technological significance. Metasurfaces can locally modify the optical property within a subwavelength range, which can facilitate device miniaturization and system integration. Metasurfaces have shown extraordinary capabilities in the local manipulation of the light's amplitude, phase, and polarization, leading to a plethora of novel applications such as generalized Snell's law of refraction and photonic spin Hall effect. This progress report is focused on the recent advancements in the fundamental research of geometric metasurfaces and their applications in ultrathin optical devices, including planar metalenses, helicity multiplexed holograms, functionality switchable devices, polarization beam splitters, vector beam generation, arbitrary polarization control, and so on. The compactness, ease of fabrication, and unusual functionalities of these devices render geometric optical metasurface devices very attractive for new applications such as encryption, imaging, anti-counterfeiting,

optical communications, quantum science, and fundamental physics. This paper aims to bring readers some new insights, and to broaden the applications of geometric metasurfaces in more research fields of science and technology.

(6) 实现了人工微结构非傍轴傅里叶透镜：傅里叶透镜作为光场空间变换的基础性元件，在光学校正、空间滤波等领域具有广泛的应用。传统的傅里叶透镜利用薄透镜或复杂透镜组来实现，前者只能工作在傍轴条件下，后者虽然可以实现宽场入射却因复杂设计与庞大体积限制了光学系统的微型化与集成化。我们利用大高宽比的非晶硅波导结构设计实现了突破傍轴条件的宽带微结构傅里叶透镜。这种超表面利用了非晶硅的高折射率特性，当入射电磁波耦合到高度约为一个波长的微结构中会激发出波导模式，通过波导的宽度参数的改变可以实现出射电磁波相位的调控。对于不同入射角度与入射波长这种非晶硅波导都具有显著的模式保护特性，从而可以实现突破傍轴条件的宽带微结构设计。另一方面，借助于优化的相位设计，我们进一步实现了具有大数值孔径的微结构傅里叶透镜。通过与商业傅里叶透镜测试对比，该微结构透镜明显拓宽了视场范围，对于高级次傅里叶分量实现了高度再现。这种基于微结构的高性能透镜研究，对于光学系统的集成化设计以及光学计算芯片的开发具有重要意义，并可以应用于超分辨成像、图像处理、微纳加工等领域，相关成果发表在 Adv. Mater. 30, 1706368 (2018)。

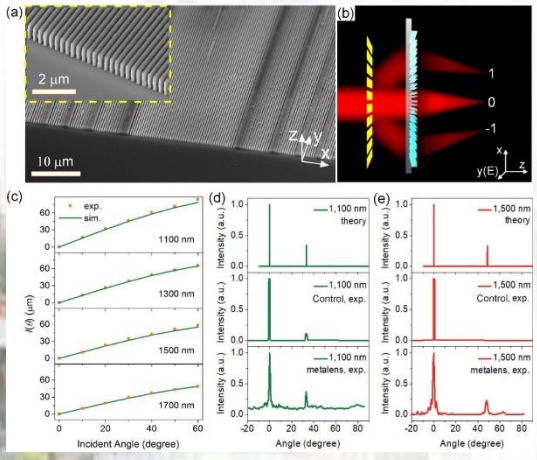

图 6. 人工微结构傅里叶透镜及其光学特性。

Fig. 6. Fourier lens based on artificial nanostructures and its optical function.

Realizing of metasurface Enabled Wide-Angle Fourier Lens: Fourier optics, the principle of using Fourier transformation to understand the functionalities of optical elements, lies at the heart of modern optics, and it has been widely applied to optical information processing, imaging, holography, etc. While a simple thin lens is capable of resolving Fourier components of an arbitrary optical wavefront, its operation is limited to near normal light incidence, i.e., the paraxial approximation, which puts a severe constraint on the resolvable Fourier domain. As a result, high-order Fourier components are lost, resulting in extinction of high-resolution information of an image. Other high numerical aperture Fourier lenses usually suffer from the bulky size and costly designs. In our research, a dielectric metasurface consisting of high-aspect-ratio silicon waveguide array is demonstrated experimentally, which is capable of performing 1D Fourier transform for a large incident angle range and a broad operating bandwidth. Thus, the device significantly expands the operational Fourier space, benefitting from the large numerical aperture and negligible angular dispersion at large incident angles. The Fourier metasurface will not only facilitate efficient manipulation of spatial spectrum of free-space optical wavefront, but also be readily integrated into micro-optical platforms due to its compact size.

(7) 实现了多通道非线性聚焦涡旋光传输：不同拓扑荷数的涡旋光在光场信息传输领域有着重要的应用。我们利用超表面同时产生的基频及二倍频信号携带的相位信息不同，提出了一种能够存储三个拓扑荷数不同的涡旋光高容量器件。由于微纳结构在产生高次谐波过程中需要遵循对于圆偏入射

光的选择规则：当微结构存在某种旋转对称性时，只有某些级次的高次谐波能够产生，并且高次谐波信号的自旋态也受到限制；满足选择规则的高次谐波信号的相位则与高次谐波的级次以及信号的自旋态有关。因此非线性谐波的相位分布就与微纳结构的对称性及光的旋性产生的关联，同时我们在相位因子中加入聚焦项，大大提升了非线性涡旋光的强度，实现了三个不同拓扑荷数的涡旋光能够在不同的焦距实现聚焦。为非线性光信息传输提供了新的提高光通信信道容量及信息安全的思路，相关成果发表在 Laser Photonics Rev. 12, 1800164 (2018)。

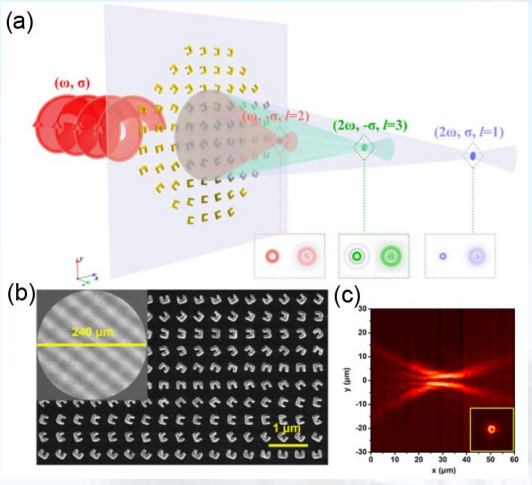

图 7. 非线性超表面功能示意图。

Fig. 7. A schematic of nonlinear metasurface.

Tripling the Capacity of Optical Vortices by Nonlinear Metasurface: Optical vortices have emerged as a potential approach to enhance data capacity for its extra degree of freedom of orbital angular momentum. Although linear metasurfaces have been used to generate optical vortices, their capacity can be further increased by involving nonlinear frequency conversions, providing new channels for data storage. In our research, by introducing second harmonic Pancharatnam–Berry phase, one linear and two second harmonic optical vortices with different topological charges focused into different focal lengths can be generated simultaneously from the proposed metasurface, which can store threefold optical vortices compared with the conventional linear geometric metasurfaces have been demonstrated. Besides, the 2D multifocal metalens with same strength for each focus emerged from the parabolic phase factor has been experimentally observed. This nonlinear optical vortex generation process represents a new strategy for enhancing the capacity of optical communications and multi-channels integrated optical communications.

(8) 实现了色调饱和度同时可调的偏振相关结构色：不同于传统化学颜料和染料，超表面可以对电磁波的波前及谐振强度进行深度的调控，具有低污染，不褪色，耐高温和高分辨率的优点。利用电介质材料实现的结构色，避免了等离子超表面高损耗和易腐蚀的弊端，可以产生高纯度高效率的结构颜色。我们利用 TiO2 在可见光波段高折射率低损耗的特性产生高效率（反射效率理论上接近 100%）、高分辨率和高纯度的颜色。特别的，为了同时实现颜色中色调与饱和度的调控，我们还对超表面的结构各向异性进行了进一步的设计，即对 x 轴和 y 轴的周期与椭圆直径进行单独的调节。这个关键性的设计策略不仅使结构色随着入射光偏振角度变化而明显的变化，甚至可以得到了 RGB 三原色转换；还可以实现在垂直偏振状态下对色调和饱和度的分别调控，通过改变 x(y) 轴方向的周期参数而保持 y(x)轴周期不变，可以得到在 x(y)偏振入射光下的饱和度变化和在 y(x)偏振下的色调变化，实现了对颜色三性质中色调与饱和度的分别调控，可以被广泛的应用于众多光信息及光成像领域，如信息编码，高密度信息存储，防伪标识，偏光显微镜以及高光谱显微镜等，相关工作发表在 Adv. Opt. Mater. 6, 1701009 (2018)。

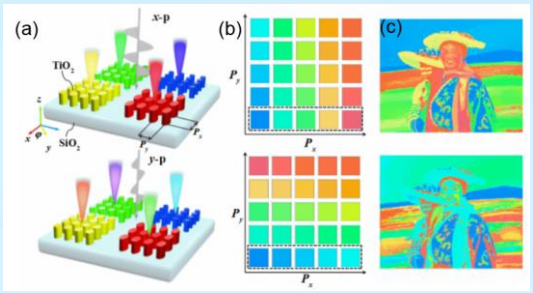

图 8. 电介质超表面实现各向异性结构色示意图。

Fig. 8. A schematic of anisotropic structural color in dielectric metasurfaces.

Realizing of Polarization-Sensitive Structural Colors with Hue-and-Saturation Tuning Based on All-Dielectric Nanopixels: Structural colors generated by the plasmonic resonance of metallic nano-structures, particularly aluminum, have been intensively studied in recent years. However, the inherent Ohmic loss and interband transitions in metals hinder the high efficiency and narrow bandwidth required for pure colors. In our research, arrays of asymmetric titanium oxide elliptical nanopixels on a silica substrate are utilized to realize polarization-sensitive structural colors with high saturation, high efficiency (more than 90%), and high resolution. Owing to Fano resonance resulting from the interference between the radiating waves of dipole resonances and directly reflected waves, perfect narrow reflected spectra can be formed with nearly ideal efficiency in the visible spectrum based on this all-dielectric nanostructure. In particular, hue- and saturation-tuned colors can be simultaneously obtained under two orthogonally polarized incident lights with apparent color contrast. Based on the superior properties of the titanium oxide metasurface, the proposed design strategy is anticipated to form a new paradigm for practical applications, such as high-density optical data storage, nanoscale optical elements, sensing, security, and so on.

(9) 实现了基于偏振与相位联合调控的远场超分辨聚焦：在人工微结构的应用领域，微纳光学透镜由于高性能、微体积被视为传统物镜的重要替代器件，是光场波前调控的重要基础，然而如何通过人工微结构联合调控的设计来实现突破衍射极限的超分辨成像，是目前该领域的重要难点。我们利用了电介质人工微结构对光场偏振与相位的联合调控，提出利用微结构增强的矢量光场干涉理论来降低聚焦光斑的大小，并突破了标量光场理论的 Abbe 衍射极限，将远场聚焦半径缩小到 0.4λ 附近（数值孔径为 0.95）。我们进一步提出了两种优化的超分辨设计方案，即利用优化的附加相位分布及附加光瞳的方式来进一步减小光斑大小，使得在入射波长为 1μm 时，光斑的半峰宽减小为约 0.38λ。这种基于微结构光场联合调控来突破标量光场衍射极限的新设计，将推动微结构功能材料与器件的开发，并推动光学显微技术的发展，促进光学成像在亚衍射极限表征、测试等方面的应用，相关成果发表在 Adv. Opt. Mater. 6, 1800795 (2018)。

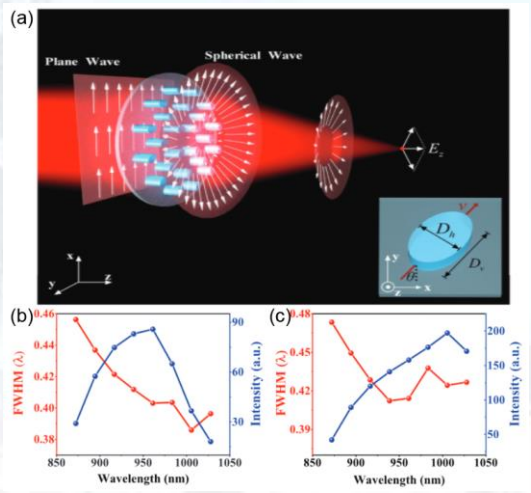

图 9. 电介质超表面实现超分辨成像示意图。

Fig. 9. A schematic of dielectric metasurfaces for breaking the diffraction limit.

Breaking the Diffraction Limit with Radially Polarized Light Based on Dielectric Metalenses: dielectric metalenses with high efficiency and compact size have been widely investigated recently, but still suffer from Abbe diffraction limit. In our research, with linear polarization incidence, a dielectric

metalens is demonstrated to efficiently generate and focus radially polarized light simultaneously. Two novel methods are proposed to achieve super-resolution. First, a circular high-pass aperture is utilized to enhance the longitudinal field component in the vicinity of focus with the focal spot size of $0.138\lambda^2$, much smaller than the theoretical limit of $0.212\lambda^2$. The key parameters that impact the focusing size are explored in detail, such as radius of the circular aperture and numerical aperture of the metalens. Second, an extra phase distribution is added on the metalens to filter the transversely polarized component, which leads to a focal spot size of $0.144\lambda^2$. The approach provides a wide platform for sub-resolution focusing and imaging, which offers the capability of subdiffraction techniques for microscopy systems and information processing with extensive channels.

(10) 基于外差探测-光学克尔门法测量单层 MoS_2 的三阶极化率张量元的值：我们使用外差探测-光学克尔门技术研究了化学气相层积法生长的单层 MoS_2 薄膜在 800nm 下的非线性。单层 MoS_2 的三阶极化率张量(即 $\chi^{(3)}_{xxyy} + \chi^{(3)}_{xyyx}$) 的值被决定为 1.4×10^{-9} esu。超快时间响应说明非线性极化率来源于非共振电子极化。基于 Kleinman 对称性，极化率张量元的值可进一步地决定。这些结果有利于 MoS_2 在非线性光子器件上的应用。相关成果发表在 Appl. Phys. Lett. 113(5), 051901 (2018).

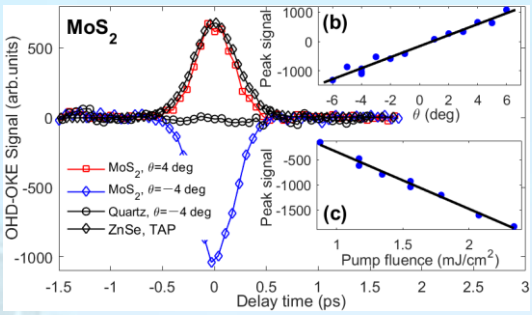

图 10. 单层 MoS_2 的外差探测-光学克尔门测量。

Fig. 10. Time-resolved OHD-OKE results of MoS_2 film and the quartz substrate.

Measuring third-order susceptibility tensor elements of monolayer MoS_2 using the optical Kerr effect method: We present a femtosecond optical heterodyne detection of optical Kerr effect study on Chemical Vapor Deposition-grown monolayer MoS_2 film at 800 nm. The third-order nonlinear optical susceptibility (i.e. $\chi^{(3)}_{xxyy} + \chi^{(3)}_{xyyx}$) of monolayer MoS_2 is determined to be 1.4×10^{-9} esu, and the ultrafast temporal response process indicates that the susceptibility origins from the nonresonant electronic polarization. Based on the Kleinman symmetry, the susceptibility tensor elements are determined, further, the nonlinear refractive indexes of any elliptically polarized light could be calculated for MoS_2. These results will benefit for the application of MoS_2 in nonlinear photonic devices.

光子学材料及先进制备技术/ Photonics Materials and Advanced Fabrication Techniques

负责人：孔勇发

本方向涉及多功能光学晶体、低维功能材料、软物质、微晶玻璃陶瓷、光子学微结构等方面。本年度发表论文 20 篇，申请发明专利 2 项，授权专利 2 项（其中国际专利 1 项），在研课题经费 945.8 万元。取得的代表性成果如下:

In this field, we mainly focused on the multi-functional optical crystals, low-dimensional functional materials, soft matter, nano-crystalline glass ceramics, and photonic microstructure. 20 papers were published in international academic journals, and 2 patents were applied and 2 authorized patents were granted (including one International patent). The total researching founds are 9.458 million. This year, we obtained some important results, they are mainly shown as following:

本课题组通过第一性原理计算分析，得出了同成分铌酸锂晶体中本征缺陷的最稳定结构形态，无论在纯 LN 还是掺杂 LN 中，四个锂空位都分居在 2 个最近邻和 2 个次近邻位置。同时，此状态下的缺陷偶极矩对晶体极化没有直接贡献。图 1 给出了掺 Mg, Sc, Zr 晶体中稳定的缺陷结构形态。该结论为缺陷团簇与晶体极化之间的关系提供了新的认识。

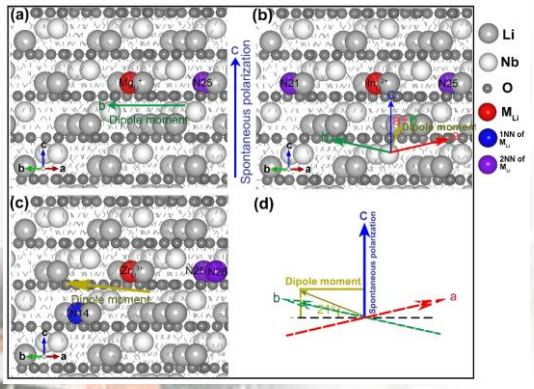

图 1. LN:Mg(a)、LN:Sc(b)和 LN:Zr(c)的最稳定缺陷结构模型。掺杂离子 Mg^{2+}、Sc^{3+}、Zr^{4+}分别用图中的红球表示。蓝球和紫球是掺杂离子 1NN 和 2NN 位置上的锂空位。蓝色箭头表示晶体的自发极化方向，绿色箭头和黄色箭头表示(a)、(b)和(c)中的偶极矩方向。(d)是偶极矩的放大结构，红色绿色和蓝色箭头表示晶体中 a、b 和 c 轴的方向，黄色箭头表示偶极矩的方向。

Fig. 1. The most stable model of LN:Mg (**a**), LN:Sc (**b**) and LN:Zr (**c**). The dopants ions Mg^{2+}, Sc^{3+}, and Zr^{4+} are represented by red balls in the figure respectively. Blue and purple balls are lithium vacancies in 1NN and 2NN site of dopant ions. And the blue arrow shows the direction of spontaneous polarization of crystal, while green arrows and yellow arrows indicate the direction of the dipole moment in (**a**), (**b**) and (**c**). (**d**) is the amplification structure of dipole moment; the red green and blue arrows represent the direction of a, b and c axis in crystal, and yellow arrow show the direction of dipole moment.

Through first-principles calculation and analysis, the most stable structure of intrinsic defects in the congruent lithium niobate (LN) crystals is obtained. In both pure and doped LN, four lithium vacancies are located in two nearest neighbors and two second nearest neighbors. Besides, the defect dipole moment in this state has no direct contribution to the crystal polarization. Fig. 1 shows the stable defect morphology in Mg, Sc, Zr doped crystals. This conclusion provides a new understanding of the relationship between defect clusters and crystal polarization.

研究了掺钼系列双掺铌酸锂晶体 LN:Mo,Me (Me=Mg^{2+}, Zn^{2+}, In^{3+}, Zr^{4+})的光折变性能，研究结果发现抗光折变离子的价态并不是影响掺钼系列铌酸锂晶体性能的决定性因素.掺杂离子的个性如价态、电负性以及离子半径等对光折变过程至关重要。

The photorefractive properties of LN:Mo,Me (Me=Mg^{2+}, Zn^{2+}, In^{3+}, Zr^{4+}) crystals were studied. The results show that the valence of anti-photorefractive ions is not the decisive factor affecting the properties of

LN doped with molybdenum. The individuality of doped ions, such as valence, electronegativity and ion radius, is very important to the photorefractive process.

在以 Nb(0.7%wt):STO 为缓冲的 Pt(111)/Ti/SiO_2/Si 衬底上，采用脉冲激光沉积(PLD)技术成功地制备了 La 和 Co 共掺杂 $BiFeO_3$ 薄膜。X-射线衍射分析表明，0.2Pa 生长的薄膜主要取向为（111），表面均方根粗糙度（RMS）为 0.96 nm。薄膜（111）的饱和磁化强度达到 25.3 emu/cm^3，是薄膜（110）的 6 倍(如图 2 所示)。提高饱和磁化强度主要归因于 La-Co 共掺杂 BFO 的主导取向和晶粒尺寸。同时，该薄膜还具有良好的铁电性能(图 3)。我们的工作将促进薄膜作为高密度信息存储材料的应用。

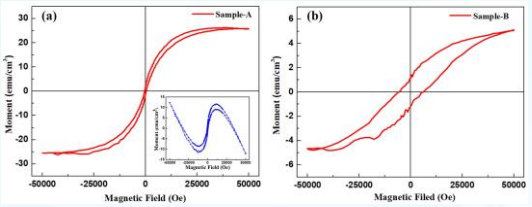

图 2. (a)主要取向为(111)的样品 A 的磁滞回线。内图为原始数据。在 300K 下用 H=1T 磁化样品，然后冷却到 2K 后进行 M-T 测量。(b)样品 B 的磁滞回线，其主要取向为(110)。所有测量均在面内进行。

Fig. 2. (a) Magnetic hysteresis loops of sample A with a main orientation of (111). Inset is the raw data. The M-T measurement performed after magnetizing the sample at 300 K with H = 1 T and then cooling to 2K. (b) Magnetic hysteresis loops of sample B with a main orientation of (110). All the measurements were performed in-plain.

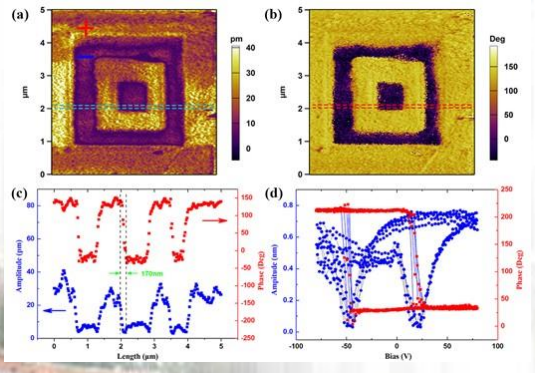

图 3. BLFCO 薄膜的面外压电力显微镜振幅（a）和压电力相位（b）图像。(c) 在 a、b 局部区域内的数值变化。(d) 振幅信号和相位信号的局域压电力回线。

Fig. 3. PFM out-of-plane amplitude (a) and phase (b) images were recorded after writing with ±40V using a conductive tip. c, The phase and amplitude steps over the strip area shown in a, b. d, Local PFM hysteresis loops of phase signal and amplitude signal.

The La and Co co-doped $BiFeO_3$ thin films were successfully fabricated on the Pt(111)/Ti/ SiO2/Si substrate buffered by Nb (0.7%wt):STO via pulsed laser deposition (PLD). The X-Ray Diffraction revealed that the film grew at 0.2Pa was predominant orientations of (111), and its surface root-mean-square roughness (RMS) was 0.96 nm. The saturation magnetization of film (111) reached 25.3 emu/cm3, which was 6 times larger than that of the film (110) (as shown in Figure 2). The enhanced saturation magnetization can mainly ascribe to the predominant orientation and the grain size of La-Co co-doped BFO. Besides, this film has good ferroelectric properties (Fig. 3). Our work will promote the application of the films as high-density information storage materials.

研制了一种基于铌酸锂(LN)电光调Q的高重复频率窄脉宽短腔激光器。首先通过测量激光穿过置于正交偏振镜间的电光晶体后，透射强度随晶体上施加的脉冲高压的变化情况，探究了不同尺寸LN晶体中的压电振铃效应，并与磷酸钛氧铷(RTP)晶体中的压电振铃效应进行了比较；发现块状LN晶体中的压电振铃效应严重，而小尺寸LN晶体中的压电振铃效应和RTP晶体中的相似，基本可以忽略。结合压电效应理论得出，压电振铃效应的强弱与外加电压大小及晶体固有的压电共振频率有关，电压越低，压电共振频率越大，压电振铃效应越弱。在此基础上，制备了可高重频应用的尺寸为1.2 mm×9 mm×9.4 mm (X×Y×Z) 的LN调Q开关，并实现了LN晶体的高重频调Q运转。激光增益介质采用具有较大受激发射截面和较短荧光寿命的Nd：YVO_4晶体，其一端镀有1.064 μm的全反膜，另一端沿布儒斯特角切割，从而省去了全反镜和偏振镜，缩短了腔

长。泵浦源采用中心波长为808 nm的光纤耦合激光二极管。通过上述设计，谐振腔长度仅为20 mm。在退压式电光调Q运转下，获得了最大重复频率为15 kHz，脉宽为5.4 ns，峰值功率为2.94 kW的稳定的激光输出。

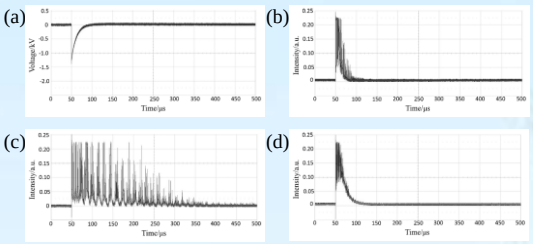

图 4. 小尺寸 LN 晶体、块状 LN 晶体及 RTP 晶体中压电振铃效应的定量比较（a）外加电压脉冲，（b）透过 RTP 普克尔盒的光强随时间的变化情况；（c）透过块状 LN 普克尔盒的光强随时间的变化情况；（d）透过小尺寸 LN 普克尔盒的光强随时间的变化情况。

Fig. 4. Qualitative comparison of piezoelectric ringing in miniature LN, block LN and RTP, (a) Applied voltage pulse, (b) Temporal behavior of the intensity transmitted through the RTP PC, (c) Temporal behavior of the intensity transmitted through the block LN PC, (d) Temporal behavior of the intensity transmitted through the miniature LN PC.

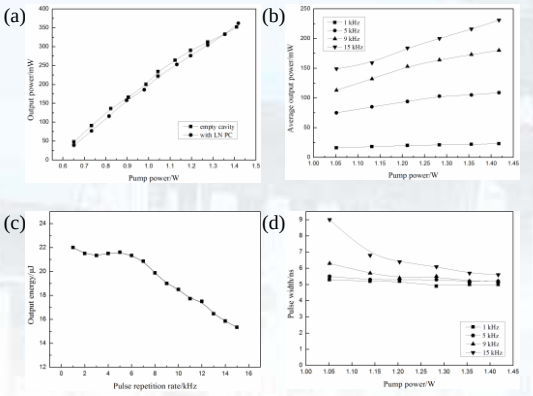

图 5. 连续激光和 Q 开关脉冲激光的输出情况；（a）连续激光输出功率随泵浦功率的变化；（b）Q 开关脉冲激光输出功率随泵浦功率的变化；（c）不同重复频率下的输出能量；（d）不同重复频率下，脉冲宽度随温度的变化。

Fig. 5. The performances of CW and Q-switched pulsed lasers, (a) Output power versus pump power of CW laser, (b) Output power versus pump power of Q-switched pulsed laser, (c) Output energy versus pulse repetition rate, (d) Pulse vs. pump power at different repetition rates.

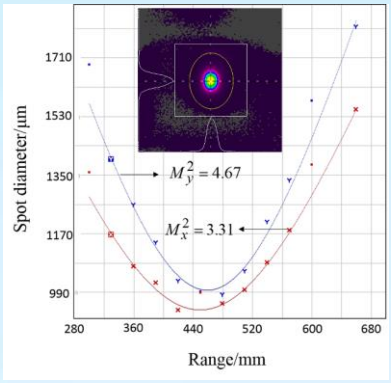

图 6. 泵浦功率为 1.41W 时，重复频率为 15kHz 的调 Q 脉冲激光的光束质量。

Fig. 6. Beam quality for 15 kHz Q-switched laser at a pump power of 1.41W.

With a $LiNbO_3$ crystal as the electro-optic Q-switch, a compact Q-switched laser with a high repetition rate and a narrow pulse width was developed. Firstly, the piezoelectric ringing effects in $LiNbO_3$ crystals with different dimensions were investigated. The crystal was sandwiched between two crossed polarizers, then the variation of the laser transmitted intensity with the pulsed high voltage applied to the crystal was measured. Additionally, the piezoelectric ringing effects in $LiNbO_3$ crystals were compared with that of a $RbTiOPO_4$ crystal. The results show that the block $LiNbO_3$ crystal suffers enormously from piezoelectric ringing, while the piezoelectric ringing in the miniaturized $LiNbO_3$ crystal is similar to that of the $RbTiOPO_4$ crystal and is negligible. Combining with the piezoelectric effect theory, it is derived that the acoustic ringing is influenced by the applied voltage and the piezoelectric resonance frequency, the acoustic ringing decreases with the decreasing of applied voltage and the increasing of piezoelectric resonance frequency. Based on these results, a miniaturized LN EO Q-switch that can operate at a high repetition rate was prepared, its dimensions is 1.2 mm×9 mm×9.4 mm (X×Y×Z). The miniature LN crystal was

successfully used for high repetition rate EO Q-switching. A Nd:YVO_4 crystal possessing a large emission cross-section and a short fluorescence lifetime was used as the gain medium. One side of the Nd:YVO_4 crystal was high-reflection coated at 1064 nm, and another side was cut along the Brewster angle, then a reflecting mirror and a polarizer was saved and the cavity length was shortened. The pump source was a fiber-coupled laser diode with a central wavelength of 808 nm. Based on the above design, a compact cavity with a length of only 20 mm was achieved. In the pulse-off Q-switching operation, a stable pulsed laser operating at a maximum repetition rate of 15 kHz with a pulse width of 5.4 ns and a peak power of 2.94 kW was obtained.

本年度延续上一年度的研究内容，重点为掺杂离子在晶格中占位及晶场环境对离子发光的影响，以及探索具有高热稳定性的新型发光材料。

The research is focus on the occupancy of the doping ions in host, the influence of different crystal field environment on luminescent properties, and developing novel phosphors with high thermal stability.

过渡族金属离子Mn^{2+}，由于其裸露在外的d电子受晶场环境影响较大，在不同基质中可发射多种波长的光，从而受到广泛的关注。在四配位的弱晶场环境下，Mn^{2+}离子多发射绿光，而在八面体配位的强晶场环境下，Mn^{2+}离子多发射橙一红色光。但近年来一些研究发现，在四配位的晶场环境下，Mn^{2+}离子也可出现红色的反常发光。以往的研究多集中在Mn^{2+}离子占据四及六配位的晶场环境，本年度，我们通过高温固相反应制备了$LiMgBO_3$:Mn^{2+}荧光粉，结合X射线衍射，荧光光谱和第一性原理计算，研究了Mn^{2+}占据扭曲的五配位晶场环境下的发光特点及其成因。在该基质中，Mn^{2+}在晶格中占据两个非满占位的Li位。高度扭曲的五配位晶体学环境，使其在427nm光激发下，发射705nm的长波红光。同时，研究了阳离子取代对材料发光的影响。

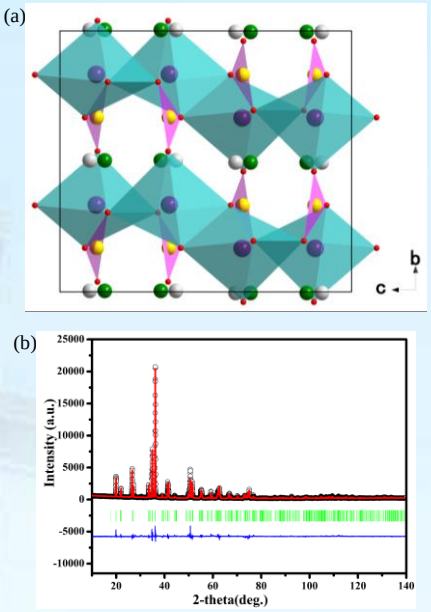

图7. (a) $LiMgBO_3$的晶体结构图和(b) $LiMgBO_3$:Mn^{2+}的结构精修XRD图。

Fig. 7. (a) Crystal structure of $LiMgBO_3$, and (b) the final Rietveld refinement plot of the XRD pattern of $LiMgBO_3$:Mn^{2+}.

Mn^{2+} is attracting much attention due to its potential application as an activated ion in the phosphors. A rare-earth free phosphor $LiMgBO_3$: Mn^{2+} was synthesized by high temperature solid-state reaction method. Combined with X-ray diffraction and PL/PLE as well as the first-principle theory calculation, the coordination environment of Mn^{2+} was disclosed that Mn^{2+} ions were inclined to occupy two partially filled Li sites. Under the 427nm excitation, an abnormal deep red emission band centered at 705nm was observed, which was due to the strong crystal field environment of Mn^{2+} induced by the extremely distorted five-coordinated sites and proved by the electronic band structure through density functional theory calculations. In addition, the luminescence intensity and thermal stability of $LiMgBO_3$:Mn^{2+} was significantly enhanced with Li^+ replaced by Na^+ and K^+. This work disclosed the origin of

the abnormal luminescent properties of Mn^{2+} in $LiMgBO_3$ and further enriched the understanding of abnormal luminescence of Mn^{2+} in special crystal structure (five-coordinated configuration).

提高发光材料热稳定性的方法之一是利用“自还原”。例如在Eu^{2+}的获得上，人们已经取得了很大进展。可以在非还原性气氛下将Eu^{3+}还原为Eu^{2+}，但至今并没有对于$Mn^{4+}\rightarrow Mn^{2+}$在非还原性气氛下制备的系统研究。除采用电荷补偿的方法以及几种正锗酸盐外，空气中制备样品所含的痕量Mn^{2+}仅在EPR谱中显示，而无法在光谱中探测到。大多数Mn^{2+}激活的发光材料，依然采用了常规的还原性气氛制备。能够在非还原气氛下制备出性能优异的发光材料具有显著优势，一方面，该材料在长时间高温使用状态下不会由于被氧化而出现色度坐标的偏移；另一方面，简化的制备手段有利于工业生产的普及。我们近期在几种磷酸盐基质中，实现了Mn^{2+}的非还原性气氛制备，并发现其在高温下依然保持与室温相似的发光强度，具有极强的实际应用潜力。

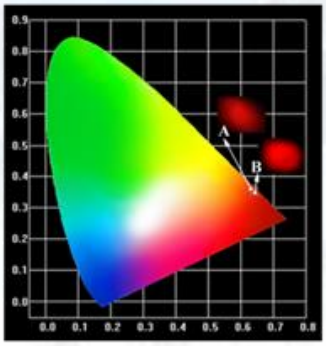

A: $NaZn(PO_3)_3$:0.12Mn^{2+}

B: $NaZn_{0.28}Mg_{0.6}(PO_3)_3$:0.12$Mn^{2+}$

图 8 空气中制备的荧光粉色度坐标图及粉体照片。

Fig. 8. CIE chromaticity coordinates and the pictures of the phosphors.

One of the methods to improve thermal stability is 'self-reduction'. As we know, most of the low valence ion activated phosphors should be synthesized in reducing atmosphere. They will meet a problem of being oxidized after long time working at high temperature, which will lead to chromaticity coordination deviation, such as Eu^{2+} to Eu^{3+}, and Mn^{2+} to Mn^{3+}. An ideal way to solve the problem is to synthesize the low valence ion activated phosphors in ambient atmosphere. Then we can expect outstanding thermal stability at high temperature. People have found that Eu^{2+} can be stabilized in ambient atmosphere in some special host structure. But as to the Mn^{2+}, most of them are prepared in reducing atmosphere except several Germanates. Recently, we realized the self-reduction from Mn^{4+} to Mn^{2+} in phosphates. These phosphors are synthesized in moderate temperature and ambient atmosphere, which has outstanding thermal stability and can avoid being oxidized are high temperature.

为探索新型深紫外非线性光学材料，我们考察了锂与钙复合的磷酸盐体系，发现了一种新的磷酸盐化合物——$Li_2Ca(PO_3)_4$，采用蒸发溶剂法制备出 $Li_2Ca(PO_3)_4$ 和 $LiCa(PO_3)_3$ 单晶，测定了它们的晶体结构并进行了表征。

以 Li_2CO_3、$CaCO_3$ 和浓磷酸原料，通过蒸发溶剂法可得到 $LiCa(PO_3)_3$ 晶体；或者采用高温固相法制备多晶粉末。但 $Li_2Ca(PO_3)_4$ 晶体只能通过蒸发溶剂法制备，且不是唯一产物。$LiCa(PO_3)_3$ 晶体为三斜晶系 $P\bar{1}$ 空间群，晶胞参数为 a = 6.6779(7) Å、b = 6.9305(8) Å、c = 7.3417(10) Å、α = 83.697(10)°、β = 80.765(10)°、γ = 81.897(9)°、Z = 2。$Li_2Ca(PO_3)_4$ 晶体属于单斜晶系 $C2/c$ 空间群，晶胞参数为 a = 16.2147(15)Å、b = 7.1231(4) Å、c = 9.2644(11) Å、β = 124.674(15)°、Z = 4。$Li_2Ca(PO_3)_4$ 的结构不同于以往任何化学式为 $M^{i}_{2}M^{ii}(PO_3)_4$ 的多聚偏磷酸。两种晶体中，基本结构基元 PO_4 四面体都是通过共用氧原子形成一维无限长链 $[PO_3]_\infty$，但 $LiCa(PO_3)_3$ 的 $[PO_3]_\infty$ 为之字形折叠链，重复周期为 $[PO_3]_3^{3-}$，而 $Li_2Ca(PO_3)_4$ 的为螺旋链，重复周期为 $[PO_3]_4^{4-}$。Li^+ 与 Ca^{2+} 居于链之间，连接起周围的 $[PO_3]_\infty$ 长链形成三维结构，并

起到平衡电荷的作用。此外，通过粉末 X 射线衍射、傅里叶变换红外光谱、拉曼光谱、紫外-可见粉末漫反射谱、差示扫描量热和热重等分析方法对两种晶体进行了表征。由于 $LiCa(PO_3)_3$ 和 $Li_2Ca(PO_3)_4$ 在结构上都具有对称中心，所以不具有倍频效应。

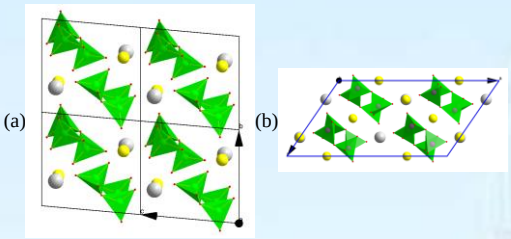

图 9. $LiCa(PO_3)_3$（a）和 $Li_2Ca(PO_3)_4$（b）的晶体结构图（绿色的四面体为 PO_4，黄色和白色的球分别为 Li^+和 Ca^{2+}）。

Fig. 9. The projection of the crystal structures of $LiCa(PO_3)_3$ (a) and $Li_2Ca(PO_3)_4$ (b) (Green tetrahedra represent PO4, and yellow and white balls represent Li^+ and Ca^{2+}, respectively).

To explore new deep-ultraviolet nonlinear optical materials, the phosphate system of lithium and calcium was investigated, and a new metaphosphate compound, $Li_2Ca(PO_3)_4$, was found. $Li_2Ca(PO_3)_4$ and $LiCa(PO_3)_3$ crystals were prepared by the evaporation method of solvent, their crystal structures were determined by single crystal X-ray diffraction.

$LiCa(PO_3)_3$ was not only prepared by the evaporation method of solvent (Li_2CO_3, Ca_2CO_3 and phosphoric acid as raw materials), but also by the high-temperature solid state reaction. However, $Li_2Ca(PO_3)_4$ can only be prepared by the evaporation method of solvent, and moreover, it's not the only product. $LiCa(PO_3)_3$ crystallizes in triclinic crystal system, $P\bar{1}$ space group, and its cell parameters are a = 6.6779(7) Å, b = 6.9305(8) Å, c = 7.3417(10) Å, α = 83.697(10)°, β = 80.765(10)°, γ = 81.897(9)°, Z = 2, and $Li_2Ca(PO_3)_4$ crystallizes in monoclinic crystal system, $C2/c$ space group, and its cell parameters are a = 16.2147(15) Å, b = 7.1231(4) Å, c = 9.2644(11) Å, β = 124.674(15)°, Z = 4. The crystal structure of $Li_2Ca(PO_3)_4$ is differ with those of any known $M^i_2M^{ii}(PO_3)_4$ compounds. The common structural feature of both compounds is infinite chain of $[PO_3]_\infty$ formed by sharing oxygen atoms of basic unit PO_4. The chain is zigzag and the repetition period is $[PO_3]_3^{3-}$ for $LiCa(PO_3)_3$, and helical chain and repetition period of $[PO_3]_4^{4-}$ for $Li_2Ca(PO_3)_4$. Li^+ and Ca^{2+} are among the chains of $[PO_3]_\infty$ to connect them by ion bonds and to balance electronic charge. $LiCa(PO_3)_3$ and $Li_2Ca(PO_3)_4$ were characterized by powder X-ray diffraction, FTIR spectroscopy, Raman spectroscopy, UV-visible powder diffuse reflectance spectroscopy, and differential scanning calorimetry and thermogravimetry, respectively. Both of $LiCa(PO_3)_3$ and $Li_2Ca(PO_3)_4$ cannot exhibit the effect of powder second-harmonic generation due to their centrosymmetric crystal structures.

超快（亚纳秒）并且具有高探测效率的闪烁体是核探测领域的核心技术与研究热点。本研究的目标在于寻找一种或几种可实现超快闪烁的闪烁材料，因此研究主要围绕芯带-价带发光材料以及闪烁量子点展开。对于最主要的芯带-价带发光材料 BaF_2 晶体发光中存在慢分量的问题，在与中科院上海硅酸盐研究所和北京玻璃研究院共同合作的研究中发现，通过稀土离子的掺杂可以有效抑制 BaF_2 中的慢发光成分，同时还可以保留快发光成分。还对对晶体生长中存在的问题、对掺杂剂的含量与慢分量抑制之间的关系进行了深入研究。

The scintillator with ultrafast (sub nanosecond) scintillation and high detection efficiency is the frontier of radiation detection research, which is also the main goals of our group's research. At present, our investigations are focusing on the cole-valence scintillation material and quantum dots. We have cooperated with SICCAS and BGRI to

suppress the slow scintillation component in the BaF_2.It is demonstrated the rare-earth doping is an efficiency approach to suppress the slow scintillation component in the BaF_2 without losing the fast scintillation component. At the same time, the issues in crystals growth and relations between dopant concentration and slow component suppression have also been investigated.

图 10(a)展示了 10 块 La 掺杂晶体照片，图 10(b)展示了这些标为 P1 到 P10 的晶体在红光 LED 照射下的照片，可以看出晶体内部存在大量包裹体，这些包裹体主要集中在晶体靠近籽晶端 P6。通过对这些样品进行 SEM/EDS 测试后发现，这些包裹体的成分与基质的成分一致，同时包裹体形貌研究也可以发现，这些包裹体具有与晶体结构一致的几何外形如图 11，所以可以总结出这些包裹体是晶体生长中出现的负晶。这是由于晶体生长时，靠近籽晶端一开始散热较好，因此晶体结晶速度大于晶体生长速度，导致晶体生长的固液界面出现失稳，从而将一些气泡或者过冷熔体包裹进生长的晶体内。当过冷熔体在晶体内析晶后，体积收缩，因此留下与晶体晶型一致的空洞，也就是负晶。

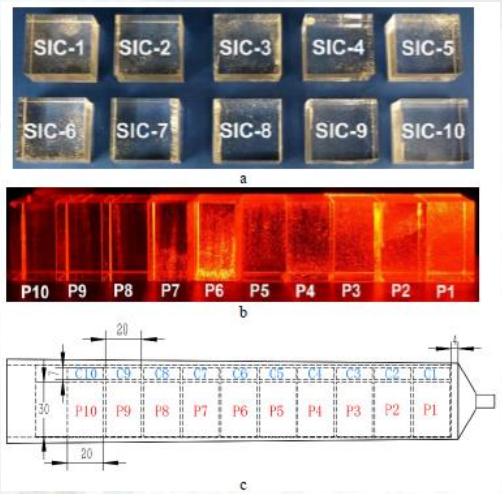

图 10. SIC 制备 La 掺杂 BaF2 晶体照片：(a) 沿晶体长轴方向切割十个样品；(b) 红光照射下晶体照片；(c) 样品在晶体内部位置示意图。

Fig. 10. (a). A photo showing ten La-doped samples; (b). These samples under illumination by a red LED; and (c). The position of twenty samples in the La doped ingot.

(a)

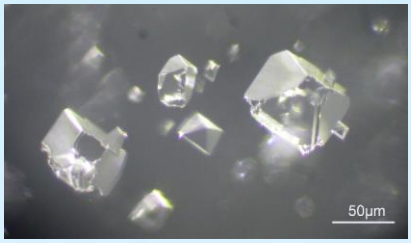

(b)

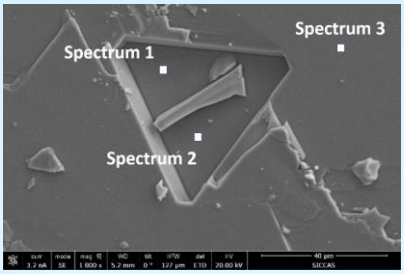

图11. 散射包裹体的显微照片：(a)显微镜照片；(b) SEM照片.

Fig. 11. Images of scattering centers observed by (a) an optical microscopy and (b) a SEM/EDS spectroscopy.。

Fig. 10(a) shows ten BaF_2 samples cut from a La doped ingot. Fig. 10(b) shows these samples marked as P1 to P10 under a red LED illumination, revealing scattering centers in all samples with the most severe in the sample P6. In Fig. 11, it shows consistent shape and stoichiometric ratios measured by the SEM/EDS analysis for scattering centers (Spectrum 1 and 2) and background (Spectrum 3). This consistency indicates that the scattering centers are voids or bubbles, known as negative crystals formed according to the Roedder's liquid-inclusion formation mechanism. While the shape and formation mechanism of negative crystal were investigated for pure BaF_2 crystals, its existence in La doped BaF_2 crystals indicates a morphological instability of the solid-liquid interface during crystal growth. Such instability is caused by an out of controlled crystallization velocity, which occurs often at a high thermal gradient zone such as the seed end. To grow scattering center free crystals, the crystal growth parameters need to be further optimized.

图 12 展示了 La 掺杂晶体 La 的浓度与晶体质量之间的关系，通过计算可以获得在

此生长速度下 La 的有效分凝系数为 1.53。同时对晶体刚开始生长时的几个 La 浓度点的分析也可知在晶体生长靠近籽晶的时候，晶体结晶的速度是大于晶体生长速度，所以晶体中的 La 浓度低于理想状态下的浓度。这一结果同样也从侧面证明了晶体中的包裹体是负晶这一结论。

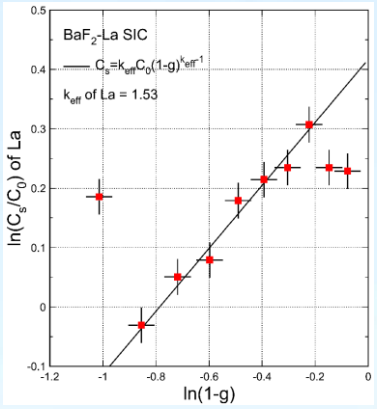

图 12. La 掺杂晶体中 La 的浓度与晶体质量之间的关系。

Fig. 12. Relative concentration of La as a function of solidification fraction.

Fig. 12 shows relation between La concentration and crystal solidification fraction, where the effective segregation coefficient for La in BaF_2 is determined to be 1.53±0.09 for a crystal growth velocity of 2 mm/h. According to a few abnormal concentration points at the beginning of crystal growth, it is also demonstrated crystallization velocity was out of control. Therefore, the La concentration in these points are lower than the theoretical concentration, which also demonstrates the scattering centers are negative crystals.

图 13 展示了 La/Ce 共掺杂晶体中 La 和 Ce 的浓度与晶体质量之间的关系，并列出 La 和 Ce 在该生长速度下的有效分凝系数。从图中可以看出 La 和 Ce 拥有近乎一致的有效分凝系数，这是由于这两种元素的离子半径相近。

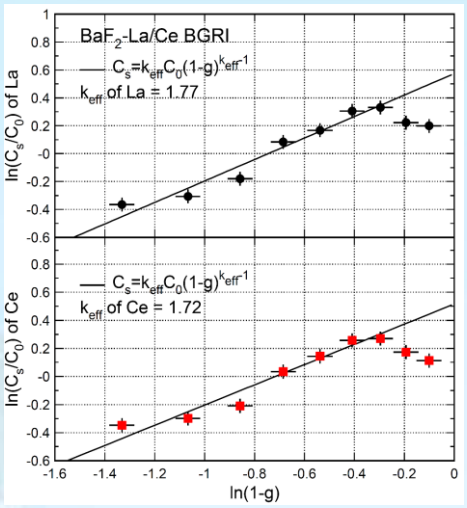

图 13. La/Ce 共掺杂晶体中 La 和 Ce 的浓度与晶体质量之间的关系。

Fig. 13. Relative concentration of La (top) and Ce (bottom) as a function of solidification fraction in La/Ce co-doped BaF_2 samples.

Fig. 13 shows fit results of 1.77±0.09 and 1.72±0.09 respectively for La and Ce with the crystal growth velocity of 1.5 mm/h. The consistent effective segregation coefficients of La and Ce in BaF_2 are due to their similar ion radius and valance.

图 14 展示了 220 nm 发光的 EWLT 以及 300 nm 发光的 EWLT 与 La 和 Ce 浓度之间的关系。从图中可以看出 220 nm 发光的 EWLT 与 La 的浓度之间有着非常好的负线性关系，而 300 nm 发光的 EWLT 与 Ce 的浓度之间有着非常好的负线性关系。这一方面说明 La 的掺杂对于 220 nm 快衰减发光有吸收，而 Ce 的掺杂对于 300 nm 慢衰减发光有吸收，还说明可以通过测试透过光谱的方法获得晶体中 La 与 Ce 的掺杂浓度。

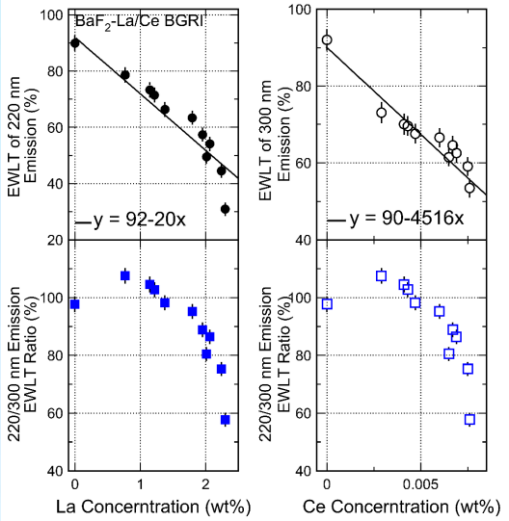

图 14. 220 nm 发光的 EWLT 以及 300 nm 发光的 EWLT 与 La 和 Ce 浓度之间的关系。

Fig. 14. The values of EWLT for the fast (220 nm, top left) and slow (300 nm, top right) scintillation component as well as their ratio (bottom) are shown as a function of the La (left) and Ce (right) concentrations.

Fig. 14 shows correlations between the values of EWLT for the fast (220 nm, top left) and slow (300 nm, top right) scintillation component as well as their ratio (bottom) as a function of the La (left) and Ce (right) concentrations. The excellent linearity observed in two top plots indicates that the La/Ce concentration may be extracted from the EWLT data. The ratio distributions indicate that the optimized doping level for La and Ce is 0.77 and 0.0029 wt% respectively for slow component suppression in the La/Ce co-doped BaF_2. While the self-absorption effect induced by La doping reduces the fast component, the self-absorption effect induced by Ce doping reduces the slow component only, so improves the F/S ratio. The La and Ce concentration can be extracted through transmittance spectrum.

图 15 展示了快发光损失与 220nm 的 EWLT 损失关系和慢发光损失与 300nm 的 EWLT 损失关系。从图中可以看出快发光损失与 220 nm 的 EWLT 损失成明显的正线性关系，这意味着快发光损失主要由 La 掺杂引起的透过率损失造成。而慢发光损失与 300 nm 的 EWLT 损失没有的线性关系，这意味着慢发光损失不是全部由的透过率损失造成。这也证明了我们一个推论，即三价稀土离子掺杂会在晶体中引入阳离子空位或间隙阴离子，而这些缺陷的存在会显著破坏晶体中的自陷激子发光，也就是慢发光，从而使晶体中的慢发光获得抑制。

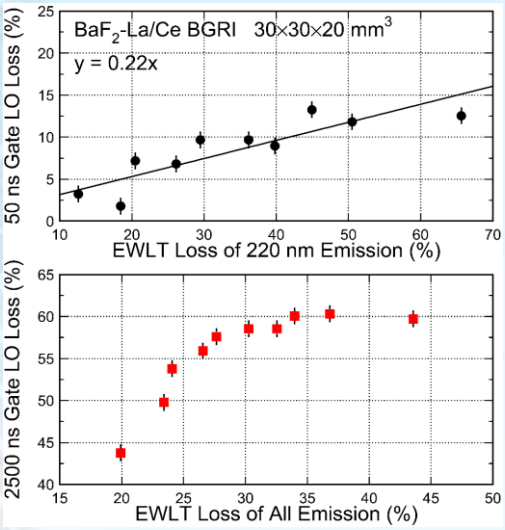

图15. 快发光损失与220nm的EWLT损失关系和慢发光损失与300nm的EWLT损失关系。

Fig. 15. Light output in 50 (top) and 2,500 ns gate (bottom) is shown as a function the EWLT loss for La/Ce co-doped BaF_2.

Fig. 15 shows the light output losses in ten La/Ce co-doped BaF_2 samples compared to the pure sample in 50 (top) and 2,500 (bottom) ns gate as a function of the EWLT loss. A good correlation is observed between the losses of the light output in 50 ns gate and the EWLT of the 220 nm emission, indicating the loss of the fast scintillation component is due to the absorption induced by La doping. No correlation is observed between the losses of the light output in 2,500 ns gate and the EWLT for the entire emission, indicating an additional quenching effect beyond absorption. The reduction of the fast component is attributed to a slightly reduced efficiency of the cross-luminescence in La doped BaF_2. The reduction of the slow component is attributed to the quenching centers introduced by the La

doping, which leads to non-radiative decays of self-trapped excitons (STE) of the slow component. The trivalent rare earth ions (La^{3+}) replace Ba^{2+} ions in the lattice, leading to a charge imbalance. The overall charge is balanced by defects, such as interstitial F− complexes or O− centers due to oxygen contamination. These defects may act as quenching centers. The phenomenon has been observed in serval trivalent rare earth (La, Ce and Y) doped BaF_2 crystals.

无序结构晶体是一类庞大的无机晶体材料，因其优异的光学、磁学和电学性能在激光、照明、量子电子学、光通信以及生物成像等领域都具有广泛的应用。其中稀土掺杂的 β-$NaREF_4$（RE=rare earth metal）家族化合物就是一种具有优良光学性能的无序结构晶体材料。采用“高温固相法”制备了不同稀土掺杂浓度的六方相 $NaGdF_4$ 和 $NaEuF_4$。通过扩展 X 射线精细结构（Extend X-ray Absorption Fine Structure, EXAFS）以及荧光光谱等手段清晰、系统地研究了无序结构晶体 β-$NaREF_4$ 的局部结构，以及无序晶体结构内部存在的本征畸变对稀土离子光学性质的影响。结果表明，无序的 1f 阳离子格位上 RE^{3+}离子和 Na^+离子沿晶格的 c 方向有序交替排列，而在晶格的 a 和 b 方向上 RE^{3+}和 Na^+离子却随机分布于 1f 格位。由于 1f 格位上阳离子替位无序的存在以及 RE^{3+}离子和 Na^+离子半径的不匹配，使得 β-$NaREF_4$ 晶格内部出现了即使在完美的 β-$NaREF_4$ 晶格内也存在的本征畸变。由于本征畸变的存在，将极大的影响着处于晶格中的稀土离子的发光性质。我们的工作不仅明确了 β-$NaREF_4$ 家族化合物的结构以及其结构对稀土离子发光性质的影响；还为其它无序晶体结构的研究以及探究无序结构晶体的微观结构对其宏观物理性质的影响提供了一种新的思路。对无序结构晶体材料的设计、改性以及应用等

近红外激光激发下的上转换发光一直是生物荧光探针候选材料之一，与传统的紫外光激发相比，近红外光激发时可以实现生物分子的活性检测。如果激发光和上转换荧光均位于生物通讯窗口，则有望在生物化学领域有重要应用。稀土掺杂的氟氧化物玻璃陶瓷兼具氟化物发光特性和氧化物稳定性，是最佳稀土发光材料之一。我们研究了 Yb^{3+}/Tm^{3+}共掺氟氧化物玻璃陶瓷在 976 nm 激光激发下的上转换发光特性，首次观察到 800 nm 附近近单色近红外上转换发光现象，发光源于 $^3H_4 \rightarrow {}^3H_6$ 的辐射跃迁，与蓝光辐射跃迁强度之比为 9633。通过对玻璃陶瓷中稀土掺杂氟化铅的结构和 Yb^{3+}/Tm^{3+}之间能量传输过程的分析，认为稀土周围的低声子能量环境和 Yb^{3+}/Tm^{3+}之间的能级失配是 $^3H_4$ 能级激发态粒子布居数相对于其他能级迅速增加的主要原因，导致 $^3H_4 \rightarrow {}^3H_6$ 的单带辐射跃迁强度增加。通过对上转换发光过程和荧光寿命的研究，发现 Tm^{3+}离子之间的交叉弛豫过程也会调制激发态粒子在各能级的重新布居，Tm^{3+}浓度增加会进一步增加 $^3H_4$ 能级激发态粒子布居数。976 nm 激光激发下获得的单带近红外发光可能在生物活性成像检测方面获得广泛应用。

Disordered crystals are a type of inorganic crystal, which have applications in laser, illumination, quantum electronics, optical communication and biological imaging, due to their excellent optical, magnetic and electrical properties. The rare earth doped $NaREF_4$ family compound is a disordered structure crystal material with excellent optical properties. Hexagonal $NaGdF_4$ and $NaEuF_4$ crystal materials with different rare earth doping concentrations were prepared by high temperature solid method. Extended X-ray Absorption Fine Structure (EXAFS) and fluorescence spectroscopy were used to clearly and systematically study the local structure of the disordered structure crystal β-$NaGdF_4$ and the intrinsic distortion existing within the disordered crystal structure. A local structure model of the disordered structure crystal β-$NaGdF_4$ is proposed. In this

structural model, Gd^{3+} ions and Na^{+} ions are arranged alternately along the c-direction of the lattice in disordered 1f cation positions, while Gd^{3+} and Na^{+} ions tend to be disordered in the a and b directions of the lattice. Due to the mismatch of ion radii between the disordered cations, lattice distortions occur within the β-$NaGdF_4$ crystal lattice. This kind of lattice distortion exists even in the perfect β-$NaGdF_4$ crystal lattice. Due to the presence of intrinsic distortion, the luminescent properties of the rare earth ions in the crystal lattice are greatly affected. Our work not only defines the structure of the β-$NaREF_4$ family of compounds and the effect of their structure on the luminescent properties of rare earth ions; it also provides insights into the structure of other disordered crystals and explores the effects of the disordered structure's microstructure on its macroscopic physical properties. It is of great significance to the design, modification and application of disordered crystal materials.

Up-conversion fluorescence materials that excitation by infrared laser is one of candidates of biological fluorescence probe. The infrared laser is safe for activated bio-molecular. Both wavelength of excitation laser and up-conversion fluorescence are in the infrared. It implied this kind of materials will be signification for biological and chemical research. An ultrapure near infrared (NIR) emission entered at 800 nm upon 976 nm laser excitation (NIR-to-NIR) was observed in β-PbF_2:Yb^{3+}/Tm^{3+} glass ceramics (GCs). The ultrapure NIR-to-NIR single band emission originated from the $^3H_4 \rightarrow {}^3H_6$ transition of Tm^{3+} with the ratio of NIR emission, and a blue band up to 9,633 was obtained. Through detailed analysis of the crystal structure and the energy transfer between Tm^{3+} and Yb^{3+}, it is elucidated that the host lattice with low phonon energy cooperative with the energy mismatch results in a dramatic population of the $^3H_4$ state as well as ultrapure NIR-to-NIR single band emission. Moreover, up-conversion (UC) emission properties and the decay lifetimes of β-PbF_2:Yb^{3+}/Tm^{3+} in GCs were explored thoroughly. The results illustrate that efficient cross relaxation (CR) processes between Tm^{3+} generate the energy redistribution in UC emission spectra, further concentrating energy to NIR emission. These two issues can be treated as crucial factors on ultrapure NIR-to-NIR single band emission in β-PbF_2:Yb^{3+}/Tm^{3+} in GCs. The ultrapure NIR-to-NIR single band emission through 976 nm laser excitation is advantageous for enhancing resolution and has potential application in bio-imaging fields.

本方向主要涉及典型软物质体系的计算模拟研究。本年度发表论文 3 篇文章，该研究成果发表在 ***Macromolecules***, 51, 3050-3058 (2018), **Soft Matter** 14,1887--1896(2018) 和 ***Polymer***, 140, 278-289 (2018)。在研课题经费 333 万元。取得的代表性成果如下：

In this field, we mainly focused on computational and simulation studies of typical soft matter. 3 papers were published in international academic journal of ***Macromolecules***, 51, 3050-3058 (2018), Soft Matter 14,1887--1896(2018) and ***Polymer***, 140, 278-289 (2018). The total researching founds are more than 3.33 million. The typical result we obtained this year is shown as following:

聚合物链和纳米粒子通过化学键连接可形成一类新型分子，称为巨分子。这类巨分子的自组装行为已成为软物质领域的研究热点之一。近期，我们利用布朗动力学模拟系统地研究了巨分子在选择性溶剂中的自组装行为、以及聚集体（特别是囊泡）的形成过程。我们的模型中，每个巨分子由一

个纳米粒子接枝 1-5 条聚合物链组成。我们系统研究了溶剂的选择性、巨分子浓度、每个分子中聚合物链的数目、聚合物的链长、体系的温度、以及纳米粒子尺寸等对聚集体形态和形成过程的影响。我们构建了随不同参数变化的形态相图。我们发现当溶剂选择纳米粒子时，体系可形成球状胶束、柱状胶束、囊泡以及大复合胶束。当溶剂选择聚合物链时，体系还可形成片状结构、管状囊泡、球状或柱状多室囊泡等。我们利用堆积参数解释了不同形态之间的转变。我们观测到两种囊泡形成路径，称为机制 I 和机制 II。我们发现随着单个巨分子中聚合物链数目的增加、或链长增长、或巨分子浓度的减小，都可发生囊泡形成路径从机制 I 到机制 II 的转变。我们从体系的吸引能和排斥能的变化解释了上述转变。

We study the self-assembly and formation process of vesicles of giant molecular shape amphiphiles in a selective solvent using the Brownian dynamics approach. Each amphiphile is composed of one hydrophilic nanoparticle tethered with one to five hydrophobic polymer tail(s), and the number of coarse-grained beads in each polymer tail is comparable to the number of repeating units in shape amphiphile used in the experiments. The effects of various parameters, such as the number of polymer tails, the length of each tail, the concentration of amphiphile beads, the size of the nanoparticle, and the temperature of the system on the self-assembled aggregate morphologies are investigated. Morphological phase diagrams are constructed in different parameter spaces, and multiple morphological transitions are predicted and explained based on packing parameter. The formation pathways of vesicles are examined systematically and mechanism II is identified for the first time in such shape amphiphilic systems. Transition between mechanism I and mechanism II can occur by varying several parameters, and principles controlling the different pathways are elucidated. The simulation results are compared with available experimental and simulation results of related systems.

我们借助格点自洽场理论对平板接枝环形均聚物刷子在无热溶剂（χ=0）中自组装行为进行了理论研究。我们的计算体系有三种，分别是体系 I，接枝环形刷子是不受任何挤压作用的；体系 II，接枝环形刷子受到一个表面性质均匀但不可穿透型中性平面硬壁所施加给的垂直挤压作用；体系 III，接枝环形刷子受到一个等同刷子所施加给的垂直挤压作用。为了方便对比分析，对满足链长（N_L）为环形链长（N_R）的一半（$N \equiv N_L = N_R/2$）但接枝密度是环形情况的两倍的“等价”线形均聚物刷子的自组装行为也进行了相同的计算。对三种计算体系，我们均计算了接枝层高度（h）和链节密度分布。链节密度分布包括属于所有链节的密度分布（$\phi(x)$）和仅属于第 N 个链节的密度分布（$\phi_N(x)$）。对于体系 II 和 III 来说，我们均定量计算了接枝刷子在垂直挤压作用下所呈现出的垂直反作用压强（P^*）；对于体系 III，我们还定量计算了属于两个刷子的渗透厚度。计算结果很清晰地显示环形刷子并不完全等同于“等价”线形刷子。由于环形刷子的链拉伸程度相对“等价”线形刷子来说较小，因此环形刷子的高度和压强均略微偏小，这些差别尤其在高链接枝密度下会变的相对更加明显些。对于环形刷子和线形刷子来说，尽管在$\phi(x)$，h 及 P^*上的差别在数值大小上均是非常小的，但是在$\phi_N(x)$和渗透厚度上的差别是相对更加显著。另外，对于体系 III 来说，我们的数据显示接枝环形刷子与等价线形刷子的压强大小比值是可以等于 1/2 且可以随接枝链在体系中的平均体积分数变化而变化的。这与 Erbas 和 Paturej 所给出的在熔体密度下，压强比值大小为固定值 1/2 的结论不同。

We reported the first systematic study using lattice self-consistent field (LSCF)

calculations of ring homopolymer brushes grafted onto a flat and homogeneous surface and immersed in an explicit and athermal solvent, which are either uncompressed, compressed by a flat and impenetrable surface, or compressed by an identical brush. Our results clearly show that ring brushes are slightly less stretched than, thus nearly but not completely identical to, the “equivalent” linear brushes having half the chain length and double the grafting density. Our LSCF results are consistent with the molecular simulation results reported in the literature (Reith et al., Europhys. Lett. 2011, 95, 28003; Erbas and Paturej, Soft Matter 2015, 11, 3139), except that Erbas and Paturej reported that the normal pressure of two opposing ring brushes is only half of the “equivalent” linear brushes at melt density.

我们借助格子自洽场理论对平板接枝 ABA 线形三嵌段共聚物在选择中间 B 嵌段的选择性溶剂中的自组装行为进行了理论研究。我们对链接枝密度、共聚物成分及不同物种之间的相互作用对接枝 ABA 共聚物自组装行为的影响进行了系统性的计算研究。我们定量地计算了接枝聚合物层在沿垂直于接枝平面方向上的高度、接枝层表面层成分、链节密度分布、链构象相对分数、均方末端距及相应的单链额外自由能、单链焓能及单链熵能等表征量。计算结果显示两大类相结构可稳定存在，即包含单个 A 富集层状相畴的相结构和包含两个 A 富集层状相畴的相结构。这些相结构之间的转化是由熵能和焓能之间的竞争来决定的。在这两大类相结构中有三种链构象，即桥式构象、中间构象及 loop 构象。这两大类相结构有着不同的链构象、不同的主导性的表面层成分和不同的形成条件。

The effects of chain-grafting density, chain composition, and interactions between different species on the self-assembled structures and chain conformations of planar grafted ABA triblock copolymers in a solvent selective for the middle B-block are investigated systematically using 3-dimensional lattice self-consistent field calculations. Structures with one A-rich layer (S1Aa and S1Ab) and with two A-rich layers (S2A) are predicted and the corresponding formation conditions are identified. It is the competition between the entropy and enthalpy that results in the formation of different structures. The copolymer chain composition affects the balance between entropy and enthalpy, and therefore has a significant influence on the resulting structure and chain conformations. In structures S1Aa and S1Ab, the free A-blocks fold into the B-rich domain and the grafted A-rich domain, respectively, whereas in structures S2A the free A-blocks do not fold. Our results are compared with available experimental and simulation results of related systems

MoS_2修饰 C_3N_4（g-C_3N_4/MoS_2X）催化剂的能带结构和光催化降解HCHO的机理研究。

The band structure and photocatalytic mechanism of MoS_2-modified C_3N_4 photocatalysts with improved visible photocatalytic activity on the photodegradation of HCHO.

一组不同浓度 MoS_2 修饰 g-C_3N_4（g-C_3N_4/MoS_2X）光催化剂被制备。采用 XRD、 HR-TEM、吸收光谱和XPS等研究了光催化剂的晶体结构、形态、异质结构、载流子的行为和氧化还原能力。结果表明，MoS2在g-C_3N_4纳米片表面形成微区异质结，能够促进可见光的吸收和载流子的有效分离。另外，研究了光催化剂产生氧活性物种（例如 $O^{2-}$and OH）的能力。因此，与g-C_3N_4和MoS_2相比，g-C_3N_4/MoS_2X催化剂显示出较高的降解HCHO的可见光催化性质。

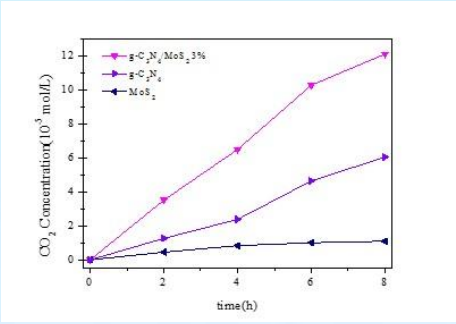

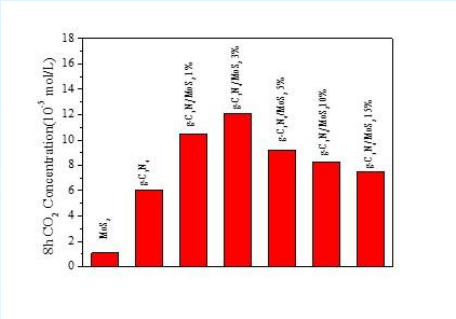

图 16. 在 λ>420 nm 可见光照射下， MoS_2, g-C_3N_4, g-C_3N_4/MoS_2X 催化剂降解 HCHO 生成 CO_2 浓度和反应时间的关系曲线。

Fig. 16. CO_2 concentration vs reaction time under λ>420 nm visible light irradiation for MoS_2, g-C_3N_4, g-C_3N_4/MoS_2X.

(a) (b)

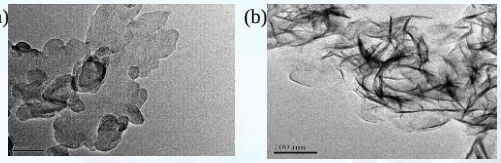

(c) (d)

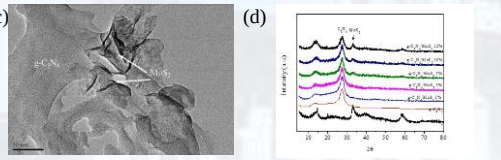

图17. (a) g-C_3N_4, (b) MoS_2 and (c) g-C_3N_4/MoS_2 X催化剂的 TEM 照片和XRD谱。

Fig. 17. TEM images of (a) g-C_3N_4, (b) MoS_2 and (c) g-C_3N_4/MoS_2 3%; XRD patterns of MoS_2, g-C_3N_4 and g-C_3N_4/MoS_2X.

(a)

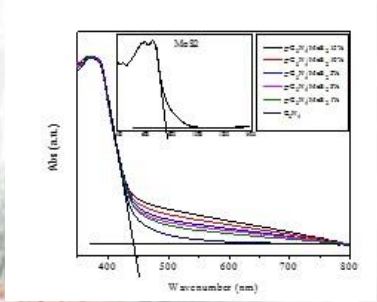

(b)

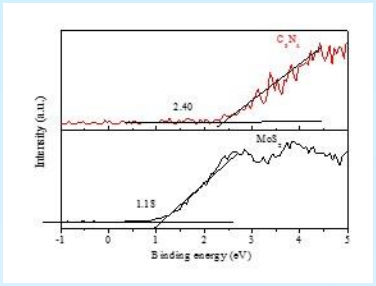

图18. MoS_2、g-C_3N_4和 g-C_3N_4/MoS_2X催化剂的(a)吸收光谱和(b)XPS价带谱。

Fig. 18. (a) Diffuse reflectance absorption spectra and (b) XPS valence band spectra for MoS_2, g-C_3N_4 and g-C_3N_4/MoS_2X.

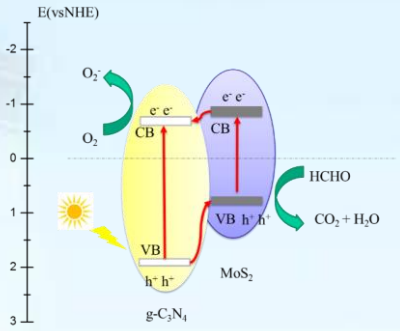

图19. g-C_3N_4/MoS_2X催化剂的光催化机理示意图。

Fig. 19. Schematic diagram of the photocatalytic mechanism for the g-C_3N_4/MoS_2X.

A series of g-C_3N_4/MoS_2X photocatalysts were prepared by modifying g-$C_3N_4$with different concentration of MoS_2 via a water exfoliation method. The crystal structure, morphology, band structure of heterojunction, behaviors of charge carries and the redox ability were characterized by XRD, HR-TEM, absorption spectra, XPS, PL, cyclic voltammetry curves and transient photocurrent spectra. It is revealed that the introduction of MoS_2 on the surface of g-C_3N_4 nanosheets to form micro-heterojunction could enhance the visible response and separate photogenerated charge carriers effectively. Moreover, the ability of the photocatalyst for generating reactive oxygen species (ROS, such as O^{2-} and OH) was also investigated. Therefore, g-C_3N_4/MoS_2X samples exhibit better photocatalytic performance for the photodegradation of HCHO than g-C_3N_4 and MoS_2 under visible irradiation.

对于提高催化剂可见光催化活性，TiO_2 中 N^{3-}、In^{3+} 和 Sn^{4+} 掺杂离子的协同作用。

Synergetic effect of N^{3-}, In^{3+} and Sn^{4+} ions in TiO_2 towards efficient Visible Photocatalysis

采用溶胶-凝胶法，制备出 N、Sn 和 In 离子掺杂的 TiO_2 光催化剂(TiO_2-N-Sn-In)。研究结果表明，Sn 离子是以取代式掺杂的方式占据 TiO_2 的 Ti 离子晶格，而 N 和 In 分别以 NO_x 和 O-In-Cl_x 表面物种的形式存在于 TiO_2 的表面。N、Sn 和 In 离子的引入，能够调控 TiO_2 的能带结构，促进紫外和可见光的吸收，阻止光生载流子的复合，导致了光催化活性的有效提高。实验证明，这种掺杂结合表面修饰调控催化剂能带结构是提高催化剂光催化活性的有效方法。

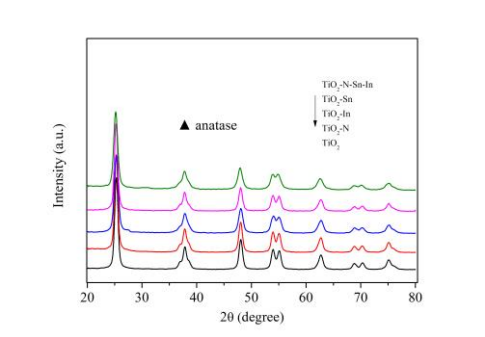

图 20. TiO_2、TiO_2-N、TiO_2-In、TiO_2-Sn 和 TiO_2-N-Sn-In 的 XRD 谱。

Fig. 20. XRD patterns of TiO_2, TiO_2-N, TiO_2-In, TiO_2-Sn and TiO_2-N-In-Sn.

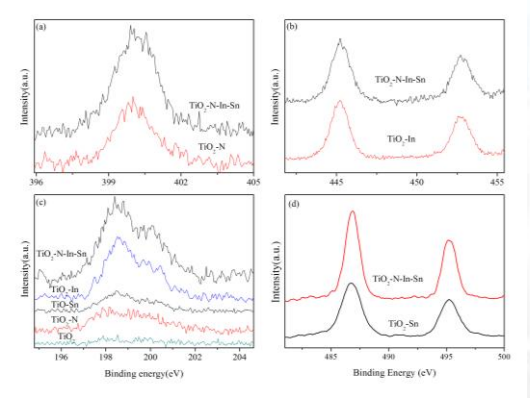

图 21. TiO_2-N-In-Sn 样品的 XPS 谱：(a) N 1*s*、(b) In 3*d*、(c) Cl 2*p* 和 (d) Sn 3*d*。

Fig. 21. XPS spectra of N 1*s* (a), In 3*d* (b), Cl 2*p* (c) and Sn 3*d* (d) for TiO_2-N-In-Sn sample.

(a)

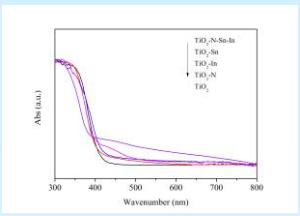

(b)

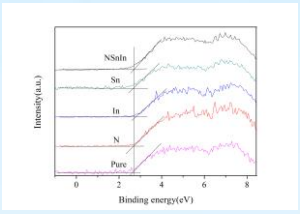

图 22. TiO_2、TiO_2-N、TiO_2-In、TiO_2-Sn 和 TiO_2-N-Sn-In 的吸收光谱(a)和 XPS 价带谱(b)。

Fig. 22. Diffuse reflectance absorption spectra (a) and XPS valence band spectra (b) of TiO_2 ,TiO_2-N, TiO_2-In, TiO_2-Sn, TiO_2-N-Sn-In.

(a) (b)

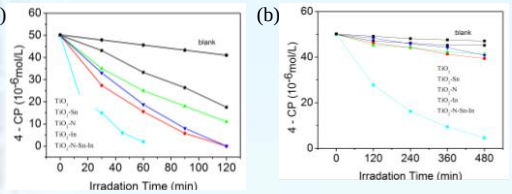

图 23. TiO_2、TiO_2-N、TiO_2-In、TiO_2-Sn 和 TiO_2-N-Sn-In 的紫外（λ>340nm）、可见（λ>400nm）光催化降解对氯苯酚的浓度曲线。

Fig. 23. Curves of the photodegradation of 4-CP for pure TiO_2, N-TiO_2, Sn-TiO_2, In-TiO_2 and TiO_2-N-Sn-In under UV irradiation and visible light) irradiation.

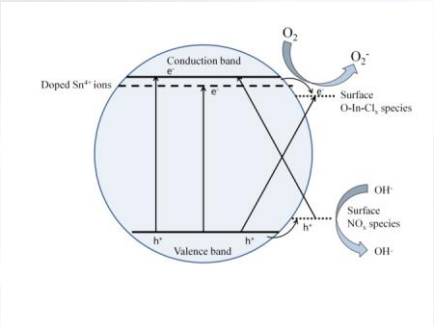

图 24. TiO_2-N-Sn-In 催化剂光催化机理图。

Fig. 24. Schematic diagram of photocatalytic mechanism for TiO_2-N-Sn-In photocatalyst.

Nitrogen, tin and indium doped TiO_2 photocatalyst (TiO_2-N-Sn-In) was prepared by a simple sol-gel method. It was revealed that tin was incorporated into TiO_2 crystal lattice in substitutional mode, while nitrogen and indium were present as surface species (NO_x

and O-In-Cl_x). The introduction of nitrogen, indium and tin into TiO_2 system could adjust the band structure, enhancing the absorption in visible light region and inhibiting the recombination of photogenerated charge carriers, resulting in an improved photocatalytic activity, compared with pure TiO_2, TiO_2-N, TiO_2-In and TiO_2-Sn for degradation of 4-chlorophenol under both visible and UV-light irradiation. The adjustment of the band structure for TiO_2 by doping and modification is a feasible way to improve the photocatalytic activity of TiO_2.

对于催化剂光催化还原 CO_2 生成 CH_4，TiO_2 中 Zn 和 Pd 离子的协同作用。

Synergetic effects of Zn and Pd ions in TiO_2 towards efficient Photo-Reduction of CO_2 into CH_4.

Zn 和 Pd 修饰 TiO_2 光催化剂（TiO_2-PdX-ZnY）表现出优异还原 CO_2 生成 CH_4 光催化性质。研究表明，引入的 Zn 和 Pd 离子分别以 O-Zn-Cl 和 O-Pd-O 物种的形式存在于 TiO_2 的表面，产生了可见光吸收的增强和载流子的有效分离。理论计算和实验结果证明，O-Zn-Cl 和 O-Pd-O 物种能级与还原 CO_2 生成 CH_4 的氧化还原电位很好的匹配，导致了 TiO_2-PdX-ZnY 催化剂光催化活性的有效提高。

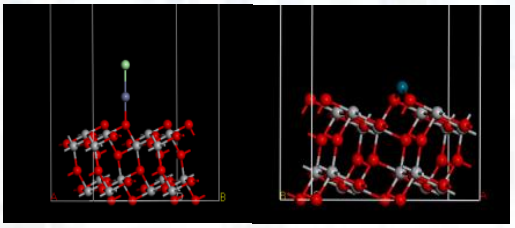

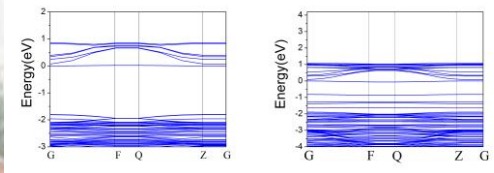

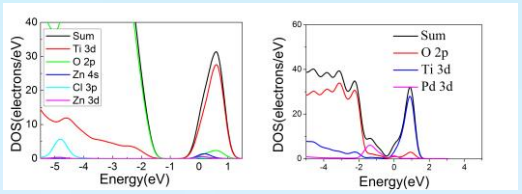

图 25. TiO_2-Zn 和 TiO_2-Pd 样品的能带结构和态密度。

Fig. 25. Theoretical calculated band structure and Projected density of states (PDOS) for the TiO_2-Zn and TiO_2-Pd.

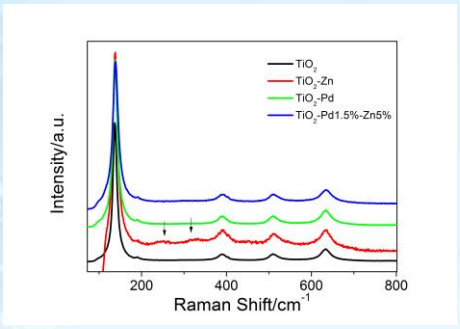

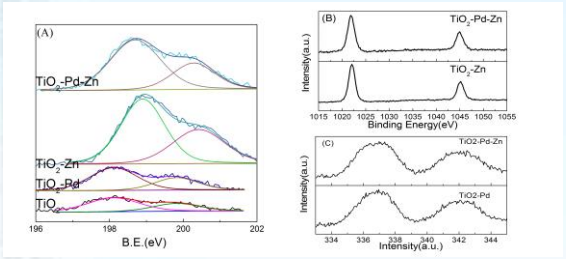

图 26. TiO_2, TiO_2-Pd, TiO_2-Zn and TiO_2-Pd-Zn 样品的 Raman 谱和 Cl 2p (a), Zn 2p (b), Pd 3d (c) XPS 谱。

Fig. 26. Raman spectra and XPS Cl 2p (a), Zn 2p (b), Pd 3d (c) spectra of TiO_2, TiO_2-Pd, TiO_2-Zn and TiO_2-Pd-Zn.

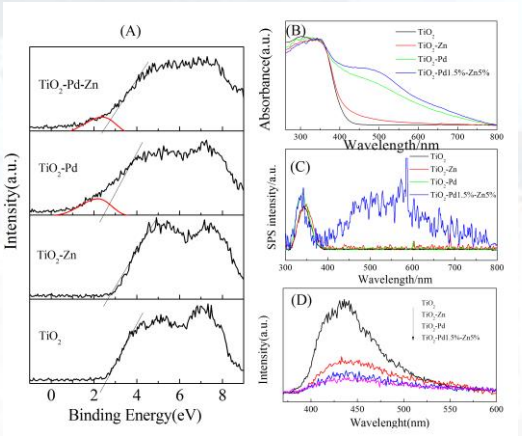

图 27. TiO_2, TiO_2-Pd, TiO_2-Zn and TiO_2-Pd-Zn 样品的 XPS 价带谱（A）、吸收谱（B）、光电压谱（C）和荧光谱（D）。

Fig. 27. XPS valence band spectra（A）, absorption spectra（B）, surface photovoltaic spectra （C）and photoluminescence spectra （D）of TiO_2, TiO_2-Zn, TiO_2-Pd and TiO_2-Pd-Zn.

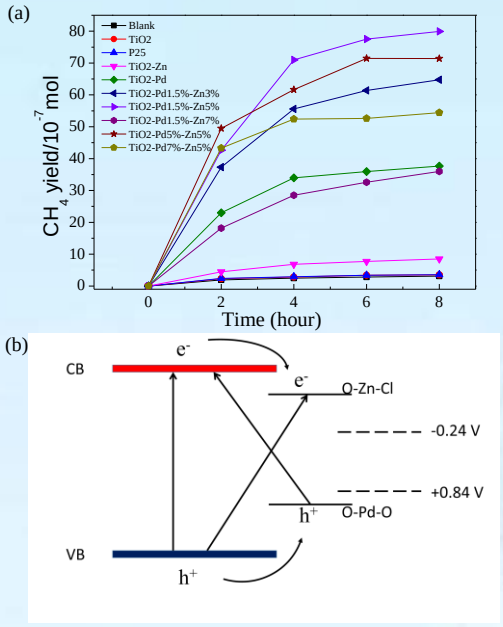

图 28. TiO_2, TiO_2-Pd, TiO_2-Zn and TiO_2-PdX-ZnY 催化剂光催化还原 CO_2 生成 CH_4 的浓度曲线(a)；TiO_2-PdX-ZnY 催化剂的能带结构和光催化机理(b)。

Fig. 28. (a). CH_4 generation of TiO_2, TiO_2-Pd, TiO_2-Zn and TiO_2-PdX-ZnY; (b). Schematic band structure and the photocatalytic mechanism of TiO_2-PdX-ZnY.

The Zn and Pd co-modified TiO_2 photocatalyst (TiO_2-PdX-ZnY) exhibit remarkably enhanced photocatalytic activity on photo-reduction of CO_2 with H_2O into CH_4. It is revealed that the introduced Zn and Pd exist as unique O-Zn-Cl and O-Pd-O species on the surface of TiO_2, resulting in the enhanced absorption in visible region and efficient separated charge carriers. It can be deduced from the theory calculation and experiment results that the energy level of O-Zn-Cl and O-Pd-O match the redox potential, leading to the improvement of photocatalytic performance.

光场调控及其应用/Manipulation of Optical Fields and Its Application

负责人：王慧田

本方向主要开展新型矢量光场的调控生成、焦场工程、新颖光学轨道角动量的设计、非线性光学效应、微加工和微操纵及新材料的理论预测等方向的研究。取得的代表性成果如下：

In our direction, we mainly focused on the generation of the new kind of vector optical fields, the focusing engineering, the design of the orbital angular momentum of photons, the nonlinear effect, the micro-manipulation and fabrication by the new optical fields. This year, we obtained some respective results as following.

（一）基于位相嵌套光束的光丝延长/Extending optical filaments with phase-nested laser beams

为满足实际应用需要，人们一直期望延长飞秒激光成丝的长度。在本工作中，我们通过构一种位相嵌套型光束，在 BK7 玻璃中实现了显著的单丝延长。这种位相嵌套光束使得基于单一的光束即可实现成丝及对其后续传播的能量补充。该光束的中心部分即圆孔截取的高斯光束，被聚焦到一点以产生一根短光丝；余下的环状部分逐渐向中心轴汇聚，持续地为光丝的再生提供能量补充。光束的共路生成系统保证了产生光丝的稳定性，同时由于其灵活性，使得我们可以简单的通过优化光束参数来获得最长的高质量光丝。此外，我们还探讨了连续的能量补充对光丝延长的重要性以及基于我们的方法实现更长光丝的可能性。

Extending the length of femtosecond laser filamentation has always been desired for practical applications. Here, we demonstrate that significant extending of a single filament in BK7 glass can be achieved by constructing phase-nested beams. The filamentation and the following energy replenishment are assembled in a single phase-nested beam. The central part of the phase-nested beam is an apertured Gaussian beam, which is focused into one focal spot to produce a short filament. In contrast, the rest of the annular part converges gradually towards the central axis to continuously replenish the energy for supporting the regeneration of filaments. The common-path generating system ensures the stability of generated filaments and easily optimizes the beam parameters to obtain the longest high-quality filament due to its flexibility. In addition, we discuss the significance of continuous replenishment for extending filaments and the potential for generating more extended filaments based on this method.

从如图1所示的实验结果中我们不难发现，相比于传统的高斯光束，这种嵌套结构光束在不增加脉冲能量的情况下，其在 BK7 玻璃中的成丝长度实现了约 7.6 倍的延长。此外这种特殊的嵌套结构可有效地抑制多丝的产生。该工作发表于《Photon. Res. 6, 1130 (2018)》上

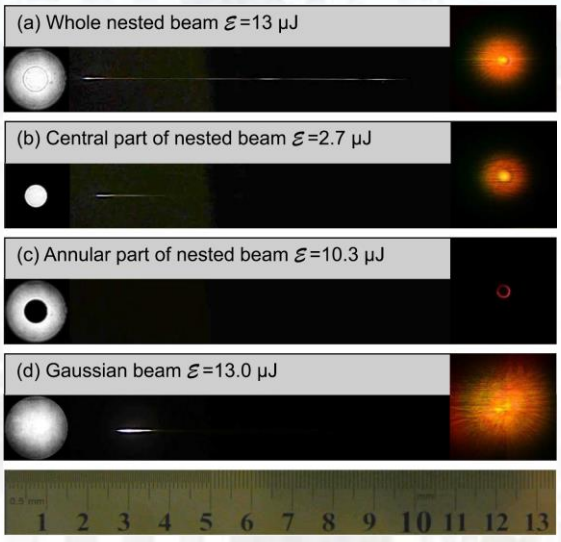

图 1. 利用嵌套结构光场延长飞秒激光成丝实验结果。(a)整个

嵌套结构光场，(b)嵌套结构光场的中心部分，(c)嵌套结构光场的环状部分和(d)高斯光场的成丝效果。左侧为相应的入射场强度分布，右侧为相应的远场辐射。

Fig. 1. Experimental results of the filament extended by the phasenested beam. (a) Filament produced by the phase-nested beam. (b) Filament produced by the central part of only the phase-nested beam. (c) No filament is formed by the annular part of the phasenested beam. (d) Filament generated by the Gaussian beam with same pulse energy and beam width as the whole phase-nested beam. The corresponding input beams are shown in the left side, while the corresponding far-field patterns are shown in the right side.

From Fig. 1, it is obvious that the filamentation was extended by 7.6 times for the phase-nested optical beam, compared with the traditional Gaussian beams in BK7 glass. Additionally, this kind of phase-nested beam can suppress the multi-filamentation. This work was published in [Photon. Res. 6, 1130 (2018)].

此外，基于光场调控，首次提出并利用偏振结构和介质的光学各向异性的协同作用实现了可控的飞秒成丝，课题组在各项异性材料中的实现了稳定的成丝控制。相关工作发表于《Opt. Express 26, 27726 (2018)》上。

Additionally, we put forward the idea to combine the polarization manipulation and optical birefringence to achieve stable filamentation, and realized stable femtosecond filamentation in birefringence media. This work was published in [Opt. Express 26, 27726 (2018)].

（二）钠硼化合物最新研究进展/ Ground-state structure of sodium boride

碱金属硼化物，作为潜在的新型电池负极材料、储氢或超导材料等颇受关注。该类化合物的典型代表，钠硼化合物 Na_2B_{30} 或 Na_2B_{29} 早在 1969 年就被合成，迄今近 50 年，然而有关它的基态晶体结构和电子性质还存在争议。我们基于进化算法结构预测软件 USPEX 的变组分模块，意外发现实验合成的 Imma-Na_2B_{30} 并不是基态结构，而是另一个正交相 $I2_12_12_1$-Na_2B_{30}，两者皆由 Na 原子，B_{12} 团簇和填隙 B 原子构成。与 Imma-Na_2B_{30} 的三角形填隙硼单元不同，$I2_12_12_1$-Na_2B_{30} 的填隙原子形成螺旋状硼链。如此细小的结构差别导致 XRD 或 HRTEM 很难区分，因为 $I2_12_12_1$-Na_2B_{30} 和 Imma-Na_2B_{30} 具有非常接近的晶格常数。有趣的是，细小的结构差别竟然产生完全不同的电子性质。一直以来 Imma-Na_2B_{30} 被视为金属性材料，第一性原理计算发现 Imma-Na_2B_{30} 是拓扑节线半金属。基于紧束缚模型的 WannierTools 软件显示第一布里渊区有两个正交的 nodal rings 分别位于 *kxkz* 和 *kykz* 平面内，受时间-空间反演保护，具有潜在的优越输运性质。与之对比，$I2_12_12_1$-Na_2B_{30} 是具有 1.6 eV 带隙的间接半导体，根据微观硬度模型，理论 Vickers 硬度约为 37.4GPa，接近超硬材料(> 40GPa)。此外，$I2_12_12_1$-Na_2B_{30} 的三维硼网格具有开放式骨架结构，Na 原子位于沿[010]晶向的特殊通道中，若 $I2_12_12_1$-Na_2B_{30} 被实验合成，通过退火蒸发 Na 原子的办法，有望获得新型亚稳单质硼(B_{30})。该工作以快讯(Rapid Communication)的方式发表于 2018 年的《Phys. Rev. B, **97**, 100102(R) (2018)》。

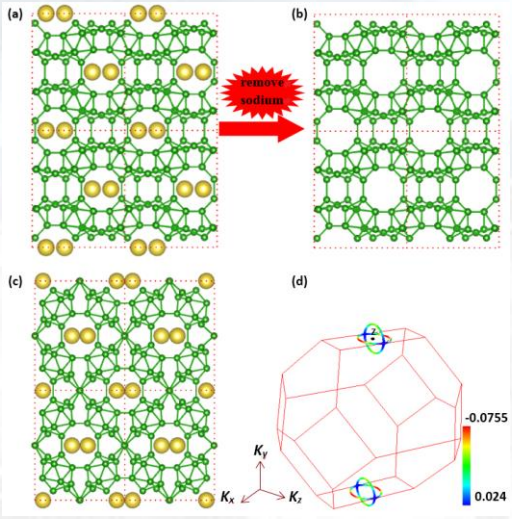

图 2. (a)，(b) $I2_12_12_1$-Na_2B_{30} 和 $I2_12_12_1$-B_{30} 结构；(c)，(d) Imma-Na_2B_{30} 结构及相应节-线图。

Fig. 2. (a) Crystal structure of $I2_12_12_1$-Na_2B_{30}. (b) Crystal structure of $I2_12_12_1$-B_{30}. (c) Crystal structure of Imma-Na_2B_{30}. (d)

Nodal rings of *I*mma-Na_2B_{30} in the Brillouin zone.

Boron-rich solids are an important class of materials, combining high-temperature superconductivity, superhardness, ferromagnetism and quantum topological properties, which attracted broad interest all along owing to many interesting fundamental issues and huge potential applications. Binary borides had been a subject of extensive research. However, it is inconceivable that the exact compositions and crystal structures of sodium borides remained controversial even that sodium boride (Na_2B_{30}) was first synthesized about 50 years ago. Here our work presented an instructive case of controversy in this "simple" system, which showed that very different structures can have very similar XRD and TEM patterns, making structure determination ambiguous, and in such cases input from theory is invaluable. In brief, we found unusual structure and novel properties in sodium borides (Na_2B_{30} or Na_2B_{29}), that is,

1. Discovery of new ground state phase $I2_12_12_1$-Na_2B_{30} with unusual open-framework boron structure, which may have potential advanced applications.

2. Rediscovery of old experimental phase Imma-Na2B30 with novel topological property, which possesses superior transport properties.

This work was published in [Phys. Rev. B, **97**, 100102(R) (2018)] as Rapid Communication.

光谱表征及传感技术/Spectral Charaterization and Sensing Techniques

负责人：宋峰

本方向涉及稀土材料发光制备和性质的研究、石墨烯光电性质研究、表面增强拉曼光谱研究、超分辨成像研究、空气和水的光学监测等方面。本年度发表论文 13 篇。2018 年度本方向主要在以下方面取得了进展：

Our groups mainly focused on the preparation and the spectral properties of the luminescent materials, optical properties and electrical properties of graphene, surface enhanced Raman scattering, super resolution imaging, optical monitoring of air and water, etc. 13 papers have been published in international academic journals, 17 patents were applied for and 2 patents were authorized. This year, we obtained some important results as following:

(1) 碳点和 $NaLuF_4$ 结合的微米材料通过水热法制备，可以发现在 365nm 激发下材料在固态和液态时可以观察到蓝光发射。材料的碳点固态不猝灭特点进行了深入的探究，通过改变柠檬酸和乙二胺的浓度关系。结果表明碳点可以有效的分散到 $NaLuF_4$ 表面，从而抵制团簇引起的猝灭。而且在 980nm 激发下，上转换发光也可以实现。碳点和 $NaLuF_4$ 结合，不仅仅可以分别实现碳点和 $NaLuF_4$ 的上转换发光，而且可以优化碳点的特性。我们提出了一种新的防止固态碳点猝灭的方法，而且也探究了其潜在的应用，例如变温探测，固态显示以及安全印刷。

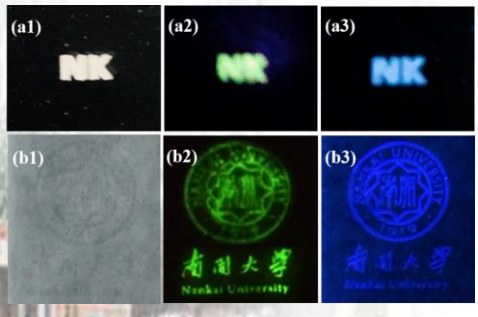

图 1.（a1）、（a2）和（a3）为刻蚀在 PMMA 上面的“NK”字样，里面填充碳点/$NaLuF_4$ 微米晶体在自然光照射下，980nm 激光器照射下以及 365nm 激发下的照片；（b1）、（b2）和（b3）分别为在无荧光纸上的印刷结果，且在自然光下，980nm 激发下以及 365nm 激发下的照片。

Fig. 1. (a1), (a2) and (a3) The “NK” loaded on the PMMA using solid state carbon dots/$NaLuF_4$ microcrystals under natural light, a 980nm laser and 365nm UV light; (b1), (b2) and (b3) The logo of Nankai loaded on a fluorescer-free paper using carbon dots/$NaLuF_4$ microcrystals under natural light, a 980nm laser and 365nm UV light, respectively

The carbon-dots/$NaLuF_4$ microcrystals have been synthesized by the hydrothermal method and bright blue emission from carbon dots is observed in aqueous and solid state under 365nm excitation. Self-quenching property of the carbon-dots/$NaLuF_4$ microcrystals under solid state was deeply investigated, by changing the ratio of citric acid (CA) and ethylenediamine (DHE). The results indicate that the carbon dots can be effectively adsorbed and dispersed on the surface of $NaLuF_4$ microcrystals, suppressing the aggregation of carbon dots. Furthermore, the upconversion luminescence can also be realized under 980nm laser excitation. From the above observations, the carbon-dots/$NaLuF_4$ microcrystals not only reveal emission property of carbon dots and $NaLuF_4$, respectively, but also optimize the property of carbon dots. It provides a promising new strategy to prevent the carbon dots quenching in solid state and the carbon-dots/$NaLuF_4$ microcrystals may have potential multi-applications in different fields including temperature sensing, solid-state display lighting as well as security inks.

(2) 通过水热法制备了以 $NaYF_4$:Yb/Er 为核，以 NaYF4:Ce/Tb/Eu 为壳制备核壳微米棒，实现了双模发射且在时域上多色发光可调。该双模核壳结构棒通过调节泵浦光波长

（紫外，近红外），壳层中稀土掺杂浓度以及探测延迟时间可实现多色发光调控。此外，材料的微米尺寸使其不仅具有高发光效率并且制备程序简单低耗，不需包敷隔离层和最外惰性层以切断核壳间能量传递和抑制表面猝灭效应。因此，双模核壳发光材料可作为多色发光标签应用在安全防伪领域。

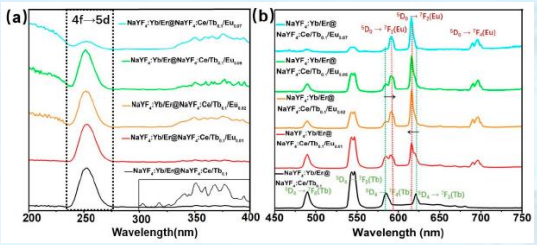

图 2. （a）检测 Tb^{3+} 发射 544nm 时核壳结构微米棒的激发光谱；（b）在 252nm 激发下样品的发射光谱。

Fig. 2. (a) Photoluminescence excitation (PLE) spectra of core–shell-structured microrods monitored at 544 nm from Tb^{3+}. (b) Emission spectra of corresponding samples at 252 nm excitation under the same condition.

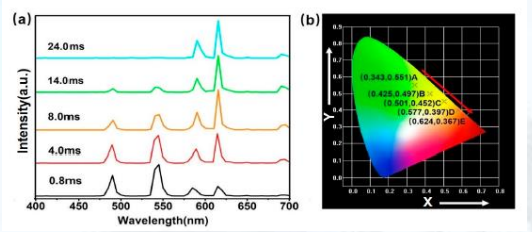

图 3. 在 252nm 激发下，$NaYF_4$:Yb/Er@$NaYF_4$:Ce/$Tb_{0.1}$/$Eu_{0.05}$ 微米棒的时间分辨发射谱以及其对应的 CIE 图。

Fig. 3. Time-resolved emission spectra for $NaYF_4$:Yb/Er@ $NaYF_4$:Ce/$Tb_{0.1}$/$Eu_{0.05}$ microrods at 252 nm excitation, and the CIE coordinates of the sample at various delay times.

The dual-mode emission and multicolor outputs in the time domain from core–shell microcrystals are presented. The core–shell microcrystals, with $NaYF_4$:Yb/Er as the core and $NaYF_4$:Ce/Tb/Eu as the shell, were successfully fabricated by employing the hydrothermal method, which confines the activator ions into a separate region and minimizes the effect of surface quenching. The material is capable of both upconversion and downshifting emission, and their multicolor outputs in response to 980 nm near-infrared (NIR) excitation laser and 252 nm, and 395 nm ultraviolet (UV) excitation light have been investigated. Furthermore, the tunable color emissions by controlling the Tb^{3+}–Eu^{3+}ratio in shells and the energy transfer of Ce^{3+}→Tb^{3+}→Eu^{3+} were discussed in details. In addition, color tuning of core–shell-structured microrods from green to red region in the time domain could be obtained by setting suitable delay time. Due to downshifting multicolor outputs (time-resolved and pump-wavelength-induced downshifting) coupled with the upconversion mode, the core–shell microrods can be potentially applied to displays and high-level security.

(3) 利用三明治结构石墨烯可饱和吸收体（GSA）实现了被动同步掺铒镱光纤激光器的 Q 开关，产生以 1530nm 和 1060nm 为中心的光脉冲。在该激光器中，1530nm 激光脉冲影响 1060nm 光通过 GSA 的传输，并诱导两个脉冲激光的同步。在这种被动同步调 Q 激光器中，通过调节泵浦功率，不仅可以连续地调节脉冲持续时间和脉冲能量，而且可以连续地调节重复频率。在实验数据的基础上，我们建立了饱和吸收特性的简化理论模型，并得到了在 GSA 的双波长交叉吸收调制期间（XAM）调制光对信号光输出性能影响的仿真结果。互调特性的双波长之间的理论模型与实验结果吻合得很好。这在激光非线性频率转换，多色泵浦-探测光谱和拉曼散射光谱上有很多潜在的应用。

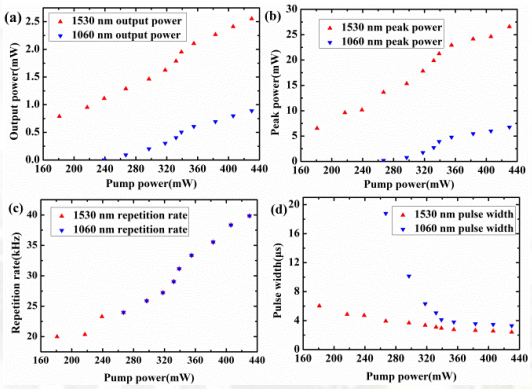

图 4. Er 激光和 Yb 激光作为泵浦源的(a)输出能量、(b)峰值能量、(c)重复速率和(d)脉宽。

Fig. 4. (a) Output power, (b) peak power, (c) repetition rate and (d) pluse width of Er-laser and Yb-laser as a function of pump power.

We demonstrate a passively synchronized erbium and ytterbium doped fiber laser Q-switched by a common graphene saturable absorber (GSA), which generates optical pulses centered at 1530nm and 1060nm. In this laser, 1530 nm laser pulses affect the transmission of 1060 nm light through GSA, and induce synchronization of the two pulsed laser lights. In this passively synchronized Q-switched laser, not only pulses duration and pulses energy but also repetition rate can be continuously tuned by adjust the pump power. Based on the experimental data, we build a simplified theoretical model of saturated absorption characteristics in GSA during the dual wavelength cross absorption modulation (XAM) process and present the simulation results of the impact on the output performance of the signal light. The theoretical model of intermodulation characteristic between the dual wavelength agrees well with the experimental results. This laser has many potential applications such as nonlinear frequency conversion, multi-color pump probe spectroscopy and Raman scattering spectroscopy.

(4) **银胶的制备** 近年的实验研究表明，表面增强拉曼散射能够使拉曼信号增强10^{14}-10^{15}倍，极大地提高了拉曼散射的强度，使拉曼散射得到了更加深入和广泛的应用。由于表面增强拉曼是实现单分子的拉曼光谱检测的必要手段，因此如何制备出高效的表面增强拉曼散射衬底就更加重要。银胶以其制备方法简单多样、增强效果显著而得到了广泛的应用。其性能与纳米银粒子的聚集状态、大小和形状密切。我们使用硼氢化钠还原硝酸银制备得到银溶液，其特点是纳米银颗粒粒径大小均一。同时我们使用柠檬酸钠还原硝酸银制备得到银溶液，其特点是纳米银颗粒浓度较高。

单位mM	10.30	11.01	11.05.1	11.05.2	11.07.1	11.07.2	11.08.3	标准
柠檬酸钠	30	**30**	30	30	30	30	30	30
PVP	0.7	**0.7**	0.7	0.7	0.7	0.7	0.7	0.7
$AgNO_3$	0.0965	**0.0965**	0.0965	0.0989	0.1000	0.1089	0.1119	0.1
$NaBH_4$	0.5551	**0.5815**	0.7402	0.7402	0.7534	0.5815	0.6344	0.3~1

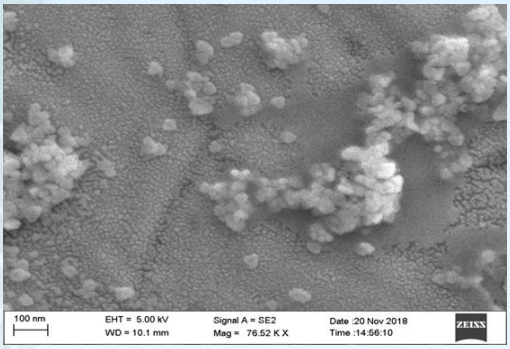

图 5. 硼氢化钠还原硝酸银。

Fig. 5. Sodium borohydride reduction of silver nitrate.

单位g	11.09.1	11.09.2	11.10.1	11.16	19.01.04
柠檬酸钠（%）	1.0013	1.0013	1.0013	1.0013	0.1005
$AgNO_3$（g）	0.0098	0.0103	0.0096	0.0092	0.8989

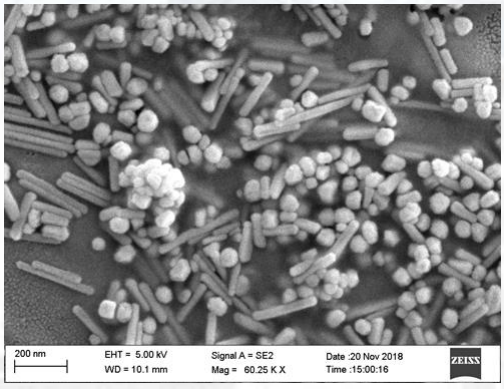

图 6. 柠檬酸钠还原硝酸银。

Fig. 6. Sodium citrate reduction of silver nitrate.

Preparation of Ag nanopaiticles Recent experimental studies have shown that

surface-enhanced Raman scattering, and the Enhancement factor almost be 10^{14} -10^{15}, greatly improving the intensity of Raman scattering, and making Raman scattering more in-depth and widely used. Since surface-enhanced Raman is a necessary means to achieve single-molecule Raman spectroscopy, it is more important to prepare a highly efficient surface-enhanced Raman scattering substrate. Silver gum has been widely used due to its simple and diverse preparation method and remarkable enhancement effect. Its performance is closely related to the aggregation state, size and shape of the nano silver particles.

(5) **MXene 材料** MXene 材料是一类具有二维层状结构的金属碳化物和金属氮化物材料，具有良好的导电性、亲水性以及机械性能。MXene 材料的化学式为 $M_{n+1}AX_n$，其中（n = 1–3），M 代表早期过渡金属，比如 Sc、Ti、Zr、V、Nb、Cr 或者 Mo；A 通常代表第三主族和第四主族化学元素；X 代表 C 或 N 元素。二维 MXene 相纳米片层结构主要通过液相剥离的方法合成得到，主要的原理是利用其前驱体 MAX 材料中不同原子层间作用力的差异，通过条件可控的刻蚀过程来实现 A 层原子的抽出，进而实现 MX 层（即 MXene）的剥离。MXene 因其本身丰富的理化性能被用于能源储存和转换、水体净化、化学传感、光或电催化和静电屏蔽等领域，并被期待在纳米生物医学领域有所突破。

MXexe MXene material is a kind of metal carbide and metal nitride material with two-dimensional layer structure, which has good electrical conductivity, hydrophilicity and mechanical properties. The chemical formula of MXene material is $M_{n+1}AX_n$, where (n = 1–3), M represents an early transition metal such as Sc, Ti, Zr, V, Nb, Cr or Mo; A usually represents the third main group and the fourth main Family chemical element; X represents a C or N element. The two-dimensional MXene phase nanosheet structure is mainly synthesized by liquid phase stripping method. The main principle is to realize the layer A by the conditional controllable etching process by using the difference of the force between different atomic layers in the precursor MAX material. The extraction of the atoms further realizes the stripping of the MX layer (ie MXene). MXene is used in energy storage and conversion, water purification, chemical sensing, photo or electrocatalysis and electrostatic shielding due to its rich physical and chemical properties, and is expected to make breakthroughs in nano biomedical fields.

对于表面增强拉曼光谱，以 $Ti_3C_2T_x$ 混合银纳米颗粒作为增强基底，可获得 10^5 增强效果；以 $Ti_3N_2T_x$ 直接作为增强基底，可获得 10^{12} 增强效果。但由于 Ti_3AlN_2 合成困难且稳定性差，目前的研究集中于过渡金属碳化物。$Ti_3C_2T_x$ 制备过程中的刻蚀剂主要有两种：① HF 刻蚀；② LiF+HCl 刻蚀。使用的刻蚀剂不同，得到的 MXene 纳米片也不同。

For surface-enhanced Raman spectroscopy, $Ti_3C_2T_x$ with silver nanoparticles were used as the reinforcing substrate to obtain 10^5 enhancement effect; $Ti_3N_2T_x$was directly used as the reinforcement substrate to obtain 10^{12} enhancement effect. However, due to the difficulty in synthesis and poor stability of Ti_3AlN_2, current research has focused on transition metal carbides. There are two main types of etchants in the preparation of $Ti_3C_2T_x$: ① HF etching; ② LiF+HCl etching. The etchants used are different, and the resulting MXene nanosheets are also different.

(6) **石墨烯材料拉伸阻抗测试** 我们设计了简单的弹性材料拉伸阻抗测试装置。利用该装置我们对碳纳米管复合弹性材料

结构进行了拉伸阻抗测试。同一频率下，样品的阻抗随拉伸幅度的增加而增加。我们测量了样品拉伸 0%、25%、50%、75%、100%、125%的多种情况，我们发现：相同拉伸程度，幅度不随频率的变化而变化，基本保持不变；相同频率，幅度随拉伸程度的变大而变小，阻抗随拉伸程度的变大而变大。

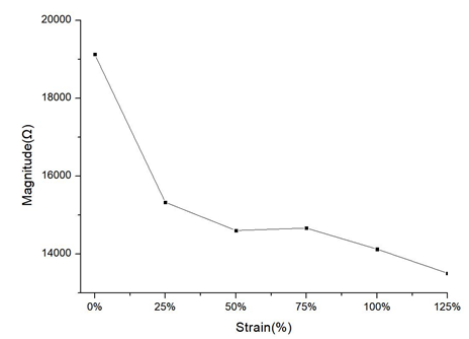

图 7. 拉伸阻抗测试中幅度随拉伸长度变化曲线。

Fig. 7. Amplitude versus stretch length curve in tensile impedance test.

Tension impedance testing of graphite materials A simple device for measuring the tensile impedance of elastic materials is designed. With this device, the tensile impedance of carbon nanotube composite elastic material was measured. At the same frequency, the impedance of the sample increases with the increase of the tensile range. We measured a variety of stretching conditions of 0%, 25%, 50%, 75%, 100% and 125% of the samples. We found that at the same stretching degree, the amplitude does not change with the change of frequency; at the same frequency, the amplitude decreases with the increase of the stretching degree, and the impedance increases with the increase of the stretching degree.

(7) 制备表面有金字塔型周期结构的琼脂糖凝胶用于 SERS 检测 凝胶呈多孔结构，有利于纳米颗粒的聚集以及分析物的聚集与吸附，有效增加“热点”，提高灵敏度。我们采用有规则倒金字塔周期结构的硅基（2μm 为一个周期，金字塔底长宽为 1.5μm）作为模板，把流动的琼脂糖压印在该硅基上，待其冷却后翻出，在琼脂糖表面可获得形貌较好且面积较大的周期金字塔结构，单个金字塔长宽为 1.5μm，与硅基上倒金字塔的长宽一致。我们在该结构表面通过连续激光曝光得到银纳米颗粒，在该基底上可检测 10^{-9}M 浓度罗丹明的拉曼信号。

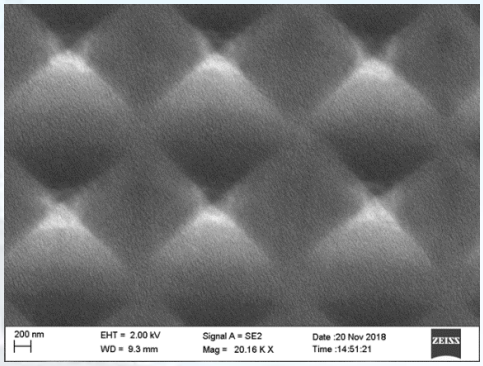

图 8. 琼脂糖凝胶微结构 SERS 检测基底。

Fig. 8. Agar gel microstructural substrates for SERS detection.

Preparation of agarose gel with Pyramid type periodic structure for SERS detection The gel has a porous structure, which is beneficial to the aggregation of nanoparticles and the aggregation and adsorption of analytes, the structure effectively increasing "hot spots" and improving sensitivity of sensing. We use a silicon wafer with a regular inverted pyramid periodic structure (period is 2μm, the base length of the pyramid is 1.5μm) as a template, and the flowing agarose is imprinted on the silicon base, after it is cooled, turned over on the agar. A periodic pyramid structure with good morphology and large area can be

obtained on the agarose surface. The length and width of a single pyramid are 1.5μm, which is consistent with the length and width of the inverted pyramid on the silicon wafer. We obtained silver nanoparticles by continuous 532nm laser exposure on the surface of the structure, on which the Raman signal of R6G at a concentration of 10^{-9} M was detected.

发表论文/Publications in Journal

1. Wei Xin, Xiao-Kuan Li, Xin-Ling He, Bao-Wang Su, Xiao-Qiang Jiang, Kai-Xuan Huang, Xiang-Feng Zhou, Zhi-Bo Liu*, and Jian-Guo Tian, "Black-Phosphorus-Based Orientation-Induced Diodes," Adv. Mater., 30(2), 1704653 (2018). †
2. Wenwei Liu, Zhancheng Li, Hua Cheng, Chengchun Tang, Junjie Li, Shuang Zhang, Shuqi Chen*, and Jianguo Tian, "Metasurface enabled wide-angle Fourier lens," Adv. Mater., 30, 1706368 (2018). †
3. Xiao-Guang Gao, Guo-Xing Chen, De-Kang Li, Xiao-Kuan Li, Zhi-Bo Liu*, and Jian-Guo Tian, "Modulation of photothermal anisotropy using black phosphorus/rhenium diselenide heterostructures," Nanoscale, 10(23), 10844-10849 (2018). †
4. Bao-Wang Su, Xiao-Kuan Li, Xiao-Qiang Jiang, Wei Xin, Kai-Xuan Huang, De-Kang Li, Hao-Wei Guo, Zhibo Liu*, and Jian-Guo Tian, "Carrier Engineering in Polarization-Sensitive Black Phosphorus van der Waals Junctions," ACS Applied Materials & Interfaces, 10(41), 35615–35622 (2018). †
5. Zhi Li, Wenwei Liu, Zhancheng Li, Chengchun Tang, Hua Cheng, Junjie Li, Xianzhong Chen, Shuqi Chen*, and Jianguo Tian, "Tripling the capacity of optical vortices by nonlinear metasurface," Laser Photonics Rev. 12, 1800164 (2018). †
6. Shuqi Chen*, Zhi Li, Yuebian Zhang, Hua Cheng, and Jianguo Tian, "Phase manipulation of electromagnetic waves with metasurfaces and its applications in nanophotonics," Adv. Opt. Mater. 6, 1800104 (2018). †
7. J. Q. Lv, P. P. Li, D. Wang, C. H. Tu, Y. N. Li, and H. T. Wang, "Extending optical filaments with phase-nested laser beams," Photon. Res. 6(12), 1130-1136 (2018). †
8. G. G. Liu, K. Wang. Y. H. Lee, D. Wang, P. P. Li, F. W. Gou, Y. N. Li, C. H. Tu, S. T. Wu, and H. T. Wang, "Measurement of the topological charge and index of vortex vector optical fields with a space-variant half-wave plate," Opt. Lett. 43(4), 823-826 (2018). †
9. D. Wang, G. G. Liu, J. Q. LÜ, P. P. Li, M. Q. Cai, G. L. Zhang, Y. N. Li, C. H. Tu, and H. T. Wang, "Femtosecond polarization-structured optical field meets an anisotropic nonlinear medium," Opt. Express 26(21), 27726-27747 (2018). †
10. Shiqi Xia, Ajith Ramachandran, Shiqiang Xia, Denghui Li, Xiuying Liu, Liqin Tang, Yi Hu, Daohong Song, Jingjun Xu, Daniel Leykam, Sergej Flach, Zhigang Chen, "Unconv entional Flatband Line States in Photonic Lieb Lattices", Phys. Rev. Lett. 121, 263902 (2018). †
11. Lei-Ting Pan, Rui Yan, Wan Li, Ke Xu*, "Super-resolution microscopy reveals the native ultrastructure of the erythrocyte cytoskeleton", Cell Reports 22, 1151-1158 (2018). †
12. Fu-Lin Xing, Ping Zhang, Peng-Chong Jiang, Zi-Yuan Chen, Jian-Yu Yang, Fen Hu, Irena Drevenšek-Olenik, Xin-Zheng Zhang, Lei-Ting Pan*, Jing-Jun Xu*, "Spatiotemporal characteristics of intercellular calcium waves communication in micropatterned assemblies of single cells", ACS Applied Materials & Interfaces 10, 2937-2945 (2018). †

† 选录论文/Selected papers

13. Li Li, Wei Cai, Chenglin Du, Zhongyuan Guan, Yinxiao Xiang, Zenghong Ma, Wei Wu, Mengxin Ren, Xinzheng Zhang, Aiwei Tang, and Jingjun Xu, “Cathodoluminescence nanoscopy of open single-crystal aluminum plasmonic nanocavities”, Nanoscale 10, 22357-22361 (2018). †

14. Chenglin Du, Wei Cai, Wei Wu, Li Li, Yinxiao Xiang, Mengxin Ren, Xinzheng Zhang and Jingjun Xu, “Evolution and coupling of plasmonic modes in single-crystal aluminum nanoridge antennas”, ACS Photon. 5, 2983-2989 (2018). †

15. Wei Cai, Ori Reinhardt, Ido Kaminer, and F. Javier Garcia de Abajo, “Efficient orbital angular momentum transfer between plasmons and free electrons”, Phys. Rev. B 98, 045424 (2018). †

16. Di Zhang, Mengxin Ren, Wei Wu, Ninghui Gao, Xuanyi Yu, Wei Cai, Xinzheng Zhang, Jingjun Xu, "Nanoscale beam splitters based on gradient metasurfaces", Opt. Lett. 43, 267 (2018). †

17. Liming Li, Peilong Hong, and Guoquan Zhang, “Experimental realization of Heisenberg-limit resolution imaging through a phase-controlled screen with classical light”, Optics Express 26(15), 18950-18956 (2018). †

18. Qingxiao Li, Zheng Wang, Yuhua Yin, Run Jiang, Baohui Li, “Self-assembly of Giant Amphiphiles Based on Polymer-Tethered Nanoparticle in Selective Solvents”, Macromolecules 51, 3050-3058 (2018). †

19. Yu Yanlong, Huang Shaolei, Gu Yao, Yaan Cao*, “Study of $PbBiO_2X$ (X = Cl, Br and I) square nanoplates with efficient visible photocatalytic performance”, Appl Surf Sci, 428, 844-850 (2018). †

20. Li-Wei Wu, Yu-Xing Bai, Li Wu*, Huan Yi, Xin-Zheng Zhang, Li-Xin Zhang, Yong-Fa Kong, Yi Zhang*, Jing-Jun Xu, "Analysis of the structure and abnormal photoluminescence of a red-emitting $LiMgBO_3:Mn^{2+}$ phosphor", Dalton Transactions, 47, 13094-13105 (2018). †

21. Aihua Zhou, Feng Song*, Yingdong Han et al, “Simultaneous size adjustment and upconversion luminescence enhancement of β-$NaLuF_4:Yb^{3+}/Er^{3+}$, Er^{3+}/Tm^{3+} microcrystals by introducing Ca^{2+} for temperature sensing”, CrystEngComm, 20, 2029-2035 (2018). †

22. Kang Zhang, Ming Feng, Yangyang Ren et al, “Q-switched and mode-locked Er-doped fiber laser using $PtSe_2$ as a saturable absorber”, Photonics Research, 6, 893-899 (2018). †

23. Jiuyang Lu, Chunyin Qiu*, Weiyin Deng, Xueqin Huang, Feng Li, Fan Zhang, Shuqi Chen*, and Zhengyou Liu*, “Valley topological phases in bilayer sonic crystals,” Phys. Rev. Lett. 120, 116802 (2018).

24. Qiushuai Shi, Wen-Yuan Zhou, Wangwei Hui, Kaicheng Huang, Hongyang Zhao, and Jianguo Tian, “Phase imaging using single-pixel detection in the spatial spectrum plane”, Optical Engineering 57(11), 114104 (2018).

25. Zhichao Deng, Jin Wang, Zhixiong Hu, Jianchun Mei, Shike Liu, Ningning Huang, Qing Ye*, and Jian-Guo Tian. “Complex Refractive Index Dispersion of Strong Absorbing

Material Determined Using Internal Reflectance Spectra Measurement", Applied Spectroscopy, 72(9), 1349-1353, (2018).

26. Xiufeng Xin, Fang Liu, Xiao-Qing Yan*, Wwangwei Hui, Xin Zhao*, Xiaoguang Gao, Zhi-Bo Liu, and Jian-Guo Tian*, "Two-photon absorption and non-resonant electronic nonlinearities of layered semiconductor $TlGaS_2$," Opt. Express 26(26), 33895-33905 (2018).

27. Kang Zhang, Ming Feng*, Yangyang Ren, Fang Liu, Xingshuo Chen, Jie Yang, Xiao-Qing Yan*, Feng Song, and Jianguo Tian, "Q-switched and mode-locked Er-doped fiber laser using PtSe2 as a saturable absorber," Photon. Res. 6, 893-899 (2018).

28. Fang Liu, Xin Zhao, Xiao-Qing Yan*, Xiufeng Xin, Zhi-Bo Liu, and Jian-Guo Tian*, "Measuring third-order susceptibility tensor elements of monolayer MoS2 using the optical Kerr effect method," Appl. Phys. Lett. 113, 051901 (2018).

29. Wen-Shuai Jiang, Chao Yang, Guo-Xing Chen, Xiao-Qing Yan, Shao-Nan Chen, Bao-Wang Su, Zhi-Bo Liu*, and Jian-Guo Tian, "Preparation of high-quality graphene using triggered microwave reduction under an air atmosphere," Journal of Materials Chemistry C, 6(7), 1829-1835 (2018).

30. Xiao-Guang Gao, Wen-Shuai Jiang, Guo-Xing Chen, Xiao-Kuan Li, De-Kang Li, Kai-Xuan Huang, Wei Xin, Zhi-Bo Liu*, and Jian-Guo Tian, "Visualizing Photothermal Anisotropy in Black Phosphorus by Total Internal Reflection Pump-Probe Technique," Advanced Materials Interfaces, 5(8), 1701605 (2018).

31. Xiaoguang Gao, Guoxing Chen, Dekang Li, Xiaokuan Li, Zhibo Liu*, and Jianguo Tian, "High-accuracy measurement of the crystalline orientation of anisotropic two-dimensional materials using photothermal detection," Journal of Materials Chemistry C, 6(22), 5849-5856 (2018).

32. Wei Xin, Hao-Bo Jiang, Xiao-Kuan Li, Xiang-Feng Zhou, Jin-Long Lu, Jian-Jun Yang, Chunlei Guo*, Zhi-Bo Liu*, and Jian-Guo Tian, "Photoinduced Orientation-Dependent Interlayer Carrier Transportation in Cross-Stacked Black Phosphorus van der Waals Junctions," Advanced Materials Interfaces, 5(20), 1800964 (2018).

33. Xiao-Kuan Li, Xiao-Guang Gao, Bao-Wang Su, Wei Xin, Kai-Xuan Huang, Xiao-Qiang Jiang, Zhi-Bo Liu*, and Jian-Guo Tian, "Polarization-Dependent Photocurrent of Black Phosphorus/Rhenium Disulfide Heterojunctions," Advanced Materials Interfaces, 5(22), 1800960 (2018).

34. Xiang Yin, Hua Zhu, Huijie Guo, Ming Deng, Tao Xu, Zhijie Gong, Xun Li, Zhi Hong Hang, Chao Wu, Hongqiang Li, Shuqi Chen, Lei Zhou, and Lin Chen, "Hyperbolic metamaterial devices for wavefront manipulation," Laser Photonics Rev. 12, 1800081 (2018).

35. Dandan Wen, Fuyong Yue, Wenwei Liu, Shuqi Chen*, and Xianzhong Chen*, "Geometric metasurfaces for ultrathin optical devices," Adv. Opt. Mater. 6, 1800348 (2018).

36. Ruizhi Zuo, Wenwei Liu, Hua Cheng, Shuqi Chen*, and Jianguo Tian, "Breaking the diffraction limit with radially polarized light based on dielectric metalenses," Adv. Opt. Mater. 6, 1800795 (2018).

37. Chao Wang, Wenwei Liu, Zhancheng Li, Hua Cheng, Zhi Li, Shuqi Chen*, and Jianguo Tian, "Dynamically tunable deep sub-wavelength high-order anomalous reflection using graphene metasurfaces," Adv. Opt. Mater. 6, 1701047 (2018).

38. Yuebian Zhang, Wenwei Liu, Zhancheng Li, Zhi Li, Hua Cheng, Shuqi Chen*, and Jianguo Tian, "High-Quality-Factor multiple Fano resonances for refractive index sensing," Opt. Lett. 43, 1842 (2018).

39. Zhangren Zhang, Dandan Wen, Chunmei Zhang, Ming Chen, Wei Wang, Shuqi Chen, and Xianzhong Chen, "Multifunctional light sword metasurface lens," ACS Photonics 5, 1794 (2018).

40. Hua Zhu, Tao Xu, Zhuo Wang, Junhao Li, Zhihong Hang, Lei Zhou, Shuqi Chen, Xun Li, and Lin Chen, "Flat metasurfaces to collimate electromagnetic waves with high efficiency," Opt. Express 26, 28531 (2018).

41. G. L. Zhang, X. Z. Gao, Y. Pan, M. D. Zhao, D. Wang, H. H. Zhang, Y. N. Li, C. H. Tu, and H. T. Wang, "Inverse method to engineer uniform-intensity focal fields with arbitrary shape," Opt. Express 26(13), 16782-16796 (2018).

42. X. Z. Gao, Y. Pan, M. D. Zhao, G. L. Zhang, Y. Zhang, C. H. Tu, Y. N. Li, and H. T. Wang, "Focusing behavior of the fractal vector optical fields designed by fractal lattice growth model," Opt. Express 26(2), 1597-1614 (2018).

43. J. Q. Lv, P. P. Li, D. Wang, C. H. Tu, Y. N. Li, and H. T. Wang, "Control on helical filaments by twisted beams in a nonlinear CS_2 medium," Opt. Express. 26(22), 29527-29538(2018).

44. P. P. Li, M. Q. Cai, J. Q. Lu, D. Wang, G. G. Liu, C. H. Tu, Y. N. Li, and H. T. Wang, "Unveiling of control on the polarization of super continuum spectra based on ultrafast birefringence induced by filamentation," J. Opt. Soc. Am. B 35(11), 2916-2922(2018).

45. D. Wang, Y. Pan, J. Q. Lu, P. P. Li, G. G. Liu, M. Q. Cai, Y. N. Li, C. H. Tu, and H. T. Wang, "Controlling optical field collapse by elliptical symmetry hybrid polarization structure," J. Opt. Soc. Am. B 35(10), 2373-2381(2018).

46. R. Liu, L. J. Kong, Z. X. Wang, Y. Si, W. R. Qi, S. Y. Huang. C. H. Tu, Y. N. Li, and H. T. Wang, "Two-Photon interference constructed by two Hong-Ou-Mandel effects in one Mach-Zehnder interferometer," Chin. Phys. Lett. 35(9), 090303 (2018).

47. M. D. Zhao, X. Z. Gao, Y. Pan, G. L. Zhang, C. H. Tu, Y. N. Li, and H. T. Wang, "Image encryption based on fractal-structured phase mask in fractional Fourier transform domain," J. Opt. 20, 045703 (2018).

48. YR Zhang, ZZ Zhang, JQ Yuan, W Wang, LQ Wang, ZX Li, RD Xue, and J Chen, "Anomalous amplified and bound-state-like optical transmissions via unidirectional interaction in parity-time symmetric metamaterials", J. Appl. Phys., 123, 103102 (2018).

49. YR Zhang, ZZ Zhang, JQ Yuan, W Wang, LQ Wang, ZX Li, RD Xue, and J Chen, "Parity-time symmetry in periodically curved optical waveguides", Opt. Express, 26, 27141 (2018).

50. Qiang Li, Qiang Wu*, Yanan Li, Chunling Zhang, Zixi Jia, Jianghong Yao, Jun Sun, Jingjun Xu,“Femtosecond laser-induced periodic surface structures on lithium niobate crystal benefiting from sample heating” Photonics Research, 6(8), 789-793 (2018).

51. Lei Wang, Wei Cai, Mengli Bie, Xinzheng Zhang, and Jingjun Xu, “Zak phase and topological plasmonic Tamm states in one-dimensional plasmonic crystals”, Opt. Express 26, 28963 (2018)

52. Xiaojie Jiang, Wei Cai, Weiwei Luo, Yinxiao Xiang, Ni Zhang, Mengxin Ren, Xinzheng Zhang, and Jingjun Xu, “Near-field imaging of graphene triangles patterned by helium ion lithography”, Nanotechnology 29, 385205 (2018).

53. Linyu Niu, Yinxiao Xiang, Wei Cai, Xiaomin Zhao, Ni Zhang, Jiwei Qi, Xinzheng Zhang, and Jingjun Xu, “Plasmonic Tamm states in insulator–metal–insulator waveguides”, J. Opt. Soc. Am. B. 35, 1368 (2018).

54. Ninghui Gao, Di Zhang, Mengxin Ren, Wei Wu, Wei Cai, Xinzheng Zhang, and Jingjun Xu, "Ultra-dispersive anomalous diffraction from Pancharatnam-Berry metasurfaces", Appl. Phys. Lett. 113, 113103 (2018).

55. Shaohua Gao, Yanzi Zhai, Xinzheng Zhang*, Xiao Song, Jiayi Wang, Irena Drevensek-Olenik*, Romano A. Rupp and Jingjun Xu, "Coupling of defect modes in cholesteric liquid crystals separated by isotropic polymeric layers", Polymers 10(7), 00805-9 (2018).

56. Xiaodan Xu, Bin Shi*, Xinzheng Zhang*, Yang Liu, Wei Cai, Mengxin Ren, Xiaojie Jiang, Romano A. Rupp, Qiang Wu, Jingjun Xu*, "Laser direct writing of graphene nanostructures beyond the diffraction limit by graphene oxidation", Opt. Exp. 26(16) 20726-20734 (2018).

57. Yao Lu, Qiang Wu*, Qi Zhang, Ride Wang, Wenjuan Zhao, Deng Zhang, Chongpei Pan, Jiwei Qi, and Jingjun Xu, “Propagation of THz pulses in rectangular subwavelength dielectric waveguides,” Journal of Applied Physics 123, 223103 (2018).

58. Ride Wang, Qiang Wu*, Qi Zhang, Yao Lu, Wenjuan Zhao, Wei Cai, Jiwei Qi, Jianghong Yao, and Jingjun Xu, “Conversion from terahertz-guided waves to surface waves with metasurface,” Opt. Express 26, 31233-31243 (2018).

59. Wenjuan Zhao, Qiang Wu*, Ride Wang, Jianshun Gao, Yao Lu, Qi Zhang, Jiwei Qi, Chunling Zhang, Chongpei Pan, Romano Rupp, and Jinjun Xu, “Transient establishment of the wavefronts for negative, zero, and positive refraction,” Opt. Express 26, 1954-1961 (2018).

60. M. Zhang, J. Qi, M. Jiang, Y. Li, J. Qian, J. Chen, Z. Chen, Q. Sun and J. Xu, "Screened bonding, antibonding and charge transfer plasmon modes in conductively connected nanorod heterodimer", Journal of Optics, 20, (2018).

61. Yane Wang, Jiwei Qi*, Chongpei Pan, Qiang Wu, Jianghong Yao, Zongqiang Chen, Jing Chen, Yudong Li, Xuanyi Yu, Qian Sun*, and Jingjun Xu, “Giant circular dichroism of large-area extrinsic chiral metal nanocrecents”， Scientific Reports, 8, 3351(2018).

62. Pengwei Xu, Mingsi Zhang, Zongqiang Chen, Jiwei Qi, Jing Chen, Jun Qian, Yudong Li,

Qian Sun, Jingjun Xu, “Unidirectional Optical Transmission in a Single-Layer Metallic Grating Consisting of Cambered Resonators”, IEEE Photonics Journal, 10, 4501308(2018).

63. Pengwei Xu, Xuefeng Lv, Jing Chen, Yudong Li, Jun Qian, Zongqiang Chen, Jiwei Qi, Qian Sun and Jingjun Xu, “Dichroic Optical Diode Transmission in Two Dislocated Parallel Metallic Gratings”, Nanoscale Research Letters 13, 392 (2018).

64. Yumiao Pei, Yi Hu, Cibo Lou, Daohong Song, Liqin Tang, Jingjun Xu, and Zhigang Chen, "Observation of spatial optical diametric drive acceleration in photonic lattices," Opt. Lett. 43, 118-121 (2018).

65. Xu Liu, Yi Hu, Pengbo Jia, Ping Zhang, Hao Wu, Zhenzhong Hao, Fang Bo, Zhigang Chen, and Jingjun Xu, "Free-space coupling enhancement of micro-resonators via self-accelerating beams," Opt. Express 26, 32055-32062 (2018).

66. Chang Pengfa, Li Xiaoting, Huang Ligang, Gao Feng* Zhang Wending, Bo Fang, Zhang Guoquan, Xu Jingjun, “Fast light in the generation configuration of stimulated Brillouin scattering based on high-Q micro-cavities,” Optics Express 26(12) 15377-15383(2018).

67. Wenbo Mao, Wei Deng, Fang Bo*, Feng Gao, Guoquan Zhang*, and Jingjun Xu*, "Upper temperature limit and multi-channel effects in ellipsoidal lithium-niobate optical parametric oscillators," Opt. Express 26, 15268-15275 (2018).

68. Xiaoting Li, Pengfa Chang, Ligang Huang, Feng Gao, Wending Zhang, Fang Bo, Guoquan Zhang, and Jingjun Xu, “Quasicritical coupling in a few-mode tapered-fiber coupled whispering-gallery-mode system”, Phys. Rev. A 98, 053814(2018).

69. ZhenZhong Hao, Li Zhang, Ang Gao, WenBo Mao, XiaoDan Lyu, XiaoMei Gao, Fang Bo*, Feng Gao, GuoQuan Zhang*, and JingJun Xu*, "Periodically poled lithium niobate whispering gallery mode microcavities on a chip," Sci. China-Phys. Mech. & Astron. 61, 114211 (2018).

70. L. Xu, M. Rahmani, D. Smirnova, K. Zangeneh Kamali, G. Zhang, D. Neshev, and A. Miroshnichenko, "Highly-Efficient Longitudinal Second-Harmonic Generation from Doubly-Resonant AlGaAs Nanoantennas," Photonics 5, 29 (2018).

71. Kaiwen Ji, Zengrun Wen, ZhenjuanLiu, Yanan Dai, Kun Han, Pingan Gao, Aihua Gao, Jintao Bai, Guoquan Zhang, and Xinyuan Qi, “Asymmetric localization induced by non-Hermitian perturbations with PT symmetry in photonic lattice”, Optics Letters 43(18), 4457-4460 (2018).

72. Li Wang, Cheng Wang, Jie Wang, Fang Bo*, Mian Zhang, Qihuang Gong, Marko Lončar*, and Yun-Feng Xiao*, "High-Q chaotic lithium niobate microdisk cavity," Opt. Lett. 43, 2917-2920 (2018).

73. K. Ji, X. Qi, S. Li, K. Han, Z. Wen, G. Zhang, and J. Bai, “Nonlinearity-dependent asymmetric transmission in a sawtooth photonic lattice with defects,” Laser Physics 28, 045404 (2018).

74. Jianji Liu, Zhixiang Li, Hongming Fan, and Guoquan Zhang, “Coherent Optical Field

Manipulation and Optical Information Processing Based on Electromagnetically-Induced Transparency Effect in Pr^{3+}:Y_2SiO_5 Crystal", Applied Sciences 8, 1179 (2018).

75. Jonathan Ward, Khosro Zangeneh Kamali, Lei Xu, Guoquan Zhang, Andrey E. Miroshnichenko and Mohsen Rahmani, "High-contrast and reversible scattering switching via hybrid metal-dielectric metasurfaces", Beilstein J. Nanotechnol. 9, 460-467 (2018).

76. Tengfei Kong, Hongde Liu, Xinyu Ge, Da Qu, Shiguo Liu, Shaolin Chen, Ling Zhang, Yongfa Kong, Romano Rupp & Jingjun Xu, "Room temperature 90° phase-matching in zirconium and magnesium co-doped lithium niobate crystals", Sci. Rept. 8, 3865 (2018).

77. Jianning Jin, Hua Yu, Liying Guo, Jinjin Liu, Bing Wu, Yuao Guo, Yuting Fu, Lijuan Zhao, "Crystallographic and spectroscopic evidence for intrinsic distortion in the disordered crystal β-$NaGdF_4$", Phys. Chem. Chem. Phys. 20, 15835 (2018).

78. Wenjuan Qiu, Baohui Li, Qiang Wang, "Lattice Self-Consistent Field Calculations of Ring Polymer Brushes", Soft Matter 14, 1887-1896 (2018).

79. Wenjuan Qiu, Zheng Wang, Yuhua Yin, Run Jiang, Baohui Li*, Qiang Wang *, "A Lattice Self-Consistent Field Study of Self-Assembly of Grafted ABA Triblock Copolymers in a Selective Solvent", Polymer, 140, 278-289 (2018).

80. Zijian Lan, Yanlong Yu, Enjun Wang, Yaan Cao*, "Synergetic effect of N^{3-}, In^{3+} and Sn^{4+} ions in TiO_2 towards efficient visible photocatalysis", Journal of Photochemistry & Photobiology, A Chemistry, 356, 123-127 (2018).

81. Zijian Lan, Yanlong Yu, Yaan Cao*, "The band structure and photocatalytic mechanism of MoS_2-modified C_3N_4 photocatalysts with improved visible photocatalytic activity", Materials Research Bulletin, 102, 433-439 (2018).

82. Yanlong Yu, Zijian Lan, Limei Guo, Yaan Cao*, "Synergistic effects of Zn and Pd species in TiO_2 towards efficient photo-reduction of CO_2 into CH_4", New Journal of Chemistry, 42, 483-488, (2018).

83. Ling Zhu, Dahuai Zheng, Hongde Liu, Shahzad Saeed, Shuolin Wang, Shiguo Liu, Shaolin Chen, Yongfa Kong, and Jingjun Xu, "Enhanced photorefractive properties of indium co-doped $LiNbO_3$:Mo crystals", AIP Adv. 8, 095316 (2018).

84. Ling Zhu, Dahuai Zheng, Shahzad Saeed, Shuolin Wang, Hongde Liu, Yongfa Kong, Shiguo Liu, Shaolin Chen, Ling Zhang and Jingjun Xu, "Photorefractive Properties of Molybdenum and Hafnium Co-Doped $LiNbO_3$ Crystals", Crystals 8, 322 (2018).

85. Fan Yang, Liyuan Zhang, Chen Hu and Renyuan Zhu,"Slow scintillation component and radiation induced readout noise in undoped CsI crystals", IEEE Transactions on Nuclear Science, 65, 2716-2723 (2018).

86. Chen Hu, Fan Yang, Liyuan Zhang, Renyuan Zhu, Jon Kapustinsky, Ron Nelson and Zhehui Wang, "Proton-induced radiation damage in BaF_2, LYSO and PWO crystal scintillators", IEEE Transactions on Nuclear Science, 65, 1018-1024 (2018).

87. Junfeng Chen, Fan Yang, Liyuan Zhang, Renyuan Zhu, Yong Du, Shaohua Wang, Shiyun Sun, and Xiang Li, "Proton-Induced radiation damage in BaF_2, LYSO and PWO crystal scintillators", IEEE T NUCL SCI., 65, 2147-2151 (2018).

88. Yang, Jinfeng, Mao Qianhui, Shang Jifang, Hao Haoshan, Li Qinglian, Huang Cunxin, Zhang Lin, Sun Jun. "Preparation and characterization of thick stoichiometric lithium tantalite

crystals by vapor transport equilibration method". Materials Letters, 232, 50-152 (2018).

89. Aihua Zhou, Feng Song*, Yingdong Han et al, "Color-tunable emission by adjusting sensitizer (Yb^{3+}) and excitation power of 980 nm in $NaGdTiO_4:Yb^{3+}/Tm^{3+}/Er^{3+}$ phosphors for light emitting diodes", Journal of Luminescence, 194, 225-230 (2018).

90. Aihua Zhou, Feng Song*, Feifei Song et al, "Optical thermometry using fluorescence intensities multi-ratios in $NaGdTiO_4:Yb^{3+}/Tm^{3+}$ phosphors color", Optical materials, 78, 438-444 (2018).

91. Aihua Zhou, Feng Song*, Weijing Yao et al, "Efficient solid-state and dual-mode photoluminescence of carbon-dots/$NaLuF_4$ microcrystals for multifunctional applications", Journal of Alloys and Compounds, 775, 457-465 (2019).

92. Yingdong Han, Chao Gao, Yangbo Wang, Dandan Ju, Aihua Zhou et al, "Spatially confined luminescence process in tip-modified heterogeneous-structured microrods for high-level anti-counterfeiting", Physical Chemistry Chemical Physics, 20, 9516-9522 (2018).

93. Dandan Ju, Feng Song*, Yingdong Han, Wenjing Cui, Feifei Song, Lisa Lui, Aihua Zhou et al, "Morphology control and upconversion luminescence enhancement of $Na_{1-x}Li_xY_{0.78-y}Lu_yF_4$: $Er_{0.02}$ $Yb_{0.2}$ microcrystals by doping ions with different valences". Journal of Luminescence, 198, 46-53 (2018).

94. Dandan Ju, Feng Song*, Jun Zhang, Chengguo Ming, Feifei Song, Adnan Khan, Aihua Zhou et al, "Enhancing the emission color sensitivity of bulk microcrystals in response to excitation power density and NIR wavelength by introducing Li^+/Lu^{3+} for anti-counterfeiting", Journal of Alloys and Compounds, 770, 1181-1188 (2019).

95. Dandan Ju, Feng Song, Adnan Khan et al, "Simultaneous dual-mode emission and tunablemulticolor in the time domain from lanthanide-doped core-shell microcrystals", Nanomaterials, 8, 1023 (2018)

96. Chengguo Ming, Manting Pei, Xiaobin Ren, Ning Xie et al, "Improving luminescent penetrability by Tm^{3+}/Ce^{3+} doped Y_2O_3 nanocrystals for optical imaging", Materials Letters 218, 154-156 (2018).

97. Chengguo Ming, Manting Pei, Feng Song et al, "Wide excitation spectra by $Nd^{3+}/Pr^{3+}/Yb^{3+}$ doped phosphateglassfor mono-crystalline silicon cells", Optik, 156, 754-757 (2018).

98. Sheng Li, Jun Zhang, Dandan Ju et al, "Flexible inorganic composite nanofibers with carboxyl modification for controllable drug delivery and enhanced optical monitoring functionality". Chemical Engineering Journal, 350, 645-652 (2018).

99. Jun Zhang, Sheng Li, Dandan Ju et al, "Flexible inorganic core-shell nanofibers endowed with tunable multicolor upconversion fluorescence for simultaneous monitoring dual drug delivery". Chemical Engineering Journal, 349, 554-561 (2018).

100. Ning Yuan, Dayu Liu, Xiaochen Yu, Hongxue Sun, Chengguo Ming, Winghan Wong, Feng Song et al, "A biological nano-thermometer based on ratiometric luminescent Er^{3+}/Yb^{3+}-codoped $NaGd(WO_4)_2$ nanocrystals", Materials Letters, 218, 337-340(2018).

101. 杨渤, 程化, 陈树琪*, 田建国, “基于傅里叶分析的超表面多维光场调控,” 《光学学报》(2018).

102. 蒋鹏翀，魏巍，胡芬，张心正，潘雷霆*，“基于激光消融技术的斑马鱼条纹再生的研究”, 中国激光，45(2), 0207024 (2018).

103. 孔腾飞，梁朋辉，刘宏德，郑大怀，刘士国，陈绍林，孔勇发，许京军, “三元同成分掺镁铌酸锂晶体的生长与抗光损伤性能研究”, 人工晶体学报 47(8), 1507-1511 (2018).

104. 商继芳，孙军，李清连，吴婧，张玲，窦飞飞，董潮涌，许京军. “高重复频率铌酸锂电光调 Q Nd:YVO_4 激光器（英文）”, 光子学报，47(5), 0514001 (2018).

105. 董潮涌，商继芳，孙军，窦飞飞，张玲. “50Hz 铌酸锂电光调 Q 开关”, 人工晶体学报，47(3), 539-543 (2018).

106. 张旭光，王卫民，鲁燕华，许夏飞，张雷，任怀瑾，刘芳，孙军，阮旭，闫雪静，孙舒娟. “基于单块周期极化铌酸锂晶体级联三倍频的 440 nm”, 强激光与粒子束, 30(4), 041005 (2018).

合作文章：

非第一单位

107. Lei Xu, Mohsen Rahmani, Khosro Zangeneh Kamali, Aristeidis Lamprianidis, Lavinia Ghirardini, Jurgen Sautter, Rocio Camacho-Morales, Haitao Chen, Matthew Parry, Isabelle Staude, Guoquan Zhang, Dragomir Neshev, and Andrey Miroshnichenko, “Boosting third-harmonic generation by a mirror-enhanced anapole resonator”, Light: Science & Applications 7, 44 (2018).

108. Biao Yang, Qinghua Guo*, Ben Tremain*, Rongjuan Liu*, Lauren E. Barr, Qinghui Yan, Wenlong Gao, Hongchao Liu, Yuanjiang Xiang, Jing Chen, Chen Fang, Alastair Hibbins, Ling Lu, and Shuang Zhang1, “Ideal Weyl points and helicoid surface states in artificial photonic crystal structures”, Science, 6379,1013-1016 (2018).

109. Nickolai Kukhtarev*, Tatiana Kukhtareva, Juan Geng, Xinzheng Zhang*,Yanzi Zhai and Jingjun Xu, "Photogalvanic/pyroelectric power conversion and self-pulsing of electro-wetting of LC droplet on lithium niobate (LN)-crystal", Journal of Molecular Liquids 267, 187-191 (2018).

110. Yunxiu Ma, Xiushan Zhu*, Luyun Yang*, Xinzheng Zhang, R. A. Norwood, and N. Peyghambarian, "Wavelength Tunable Ho^{3+}-doped ZBLAN Fiber Lasers in the 1.2 μm Wavelength Region", IEEE Photon. Tech. Lett. 30(16) 1483-1486 (2018).

111. Raluca-Sorina Penciu, Yujie Qiu, Michael Goutsoulas, Xiaopei Sun, Yi Hu, Jingjun Xu, Zhigang Chen, and Nikolaos K. Efremidis, “Observation of microscale nonparaxial optical bottle beams”, Opt. Lett. 43(16), 3878-3881 (2018).

112. Yong Sun, Daniel Leykam, Stephen Nenni, Daohong Song, Hong Chen, Y. D. Chong, and Zhigang Chen, “Observation of Valley Landau-Zener-Bloch Oscillations and Pseudospin Imbalance in Photonic Graphene”, Phys. Rev. Lett. 121, 033904 (2018).

113. Fanfan Lu, Wending Zhang*, Ligang Huang, Shuhai Liang, Dong Mao, Feng Gao, Ting Mei, and Jianlin Zhao, "Mode evolution and nanofocusing of grating-coupled surface plasmon polaritons on the metallic tip," Opto-Electronic Advances 1, 180010 (2018).

114. Xuecheng Zhang, Wending Zhang*, Chenyang Li, Dong Mao, Feng Gao, Ligang Huang, Dexing Yang, Ting Mei, and Jianlin Zhao, "All-fiber cylindrical vector beams laser based on an acoustically-induced fiber grating," J. Opt. 20, 075608 (2018).

115. Wending Zhang*, Cheng Li, Kun Gao, Fanfan Lu, Min Liu, Xin Li, Lu Zhang, Dong Mao, Feng Gao, Ligang Huang, Ting Mei, and Jianlin Zhao, "Surface-enhanced Raman spectroscopy with Au-nanoparticles substrates fabricated by using femtosecond pulse," Nanotechnology 29 205301 (2018).

116. Ligang Huang, Wending Zhang, Yujia Li, Haonan Han, Xiaoting Li, Pengfa Chang, Feng Gao, Guoquan Zhang, Lei Gao, and Tao Zhu, "Acousto-optic tunable bandpass filter based on acoustic-flexural-wave-induced fiber birefringence," Opt. Lett., 43(21), 5431-5434 (2018).

117. Ligang Huang,* Pengfa Chang, Xiaoting Li, Wending Zhang, Yujia Li, 1 Feng Gao,* Fang Bo, Lei Gao, Wei Huang, Min Liu, And Tao Zhu, "All-fiber narrow-linewidth ring laser with continuous and large tuning range based on microsphere resonator and fiber Bragg grating" Opt. Express. Vol 26, 32652-32661(2018).

专利/Patents

申请专利/ Patents Applied

[1] CN108627465A；一种基于压缩感知高光谱成像的快速无损监测装置；发明；周文远，金森林，惠王伟，田建国。南开大学（2017.3.22）

[2] 201810044280.4；一种二维材料光热效应的测定方法和装置；发明；刘智波，高晓光，田建国。南开大学（2018.1.12）

[3] 2018100464451；一种便携溶解氧检测器；发明；王斌，徐晓轩，黄津辉，李强，车颖，梁菁，徐阳阳，文虹镜，时金蒙，马雨霏。南开大学（2018.1.17）

[4] 2018100460198；一种水质检测设备光学窗口自动清洗装置；发明；王斌，徐晓轩，黄津辉，李强，车颖，梁菁，徐阳阳，文虹镜，时金蒙，马雨霏。南开大学（2018.1.17）

[5] 2018100464466；一种水质检测用采样装置；发明；王斌，徐晓轩，黄津辉，李强，车颖，梁菁，徐阳阳，文虹镜，时金蒙，马雨霏。南开大学（2018.1.17）

[6] 2018100464625；一种水质污染源分析方法；发明；王斌，徐晓轩，黄津辉，李强，徐阳阳，车颖，梁菁，文虹镜，时金蒙，张文杰。南开大学（2018.1.17）

[7] 2018100464659；一种基于 PH 测定的样品清洗系统；发明；王斌，徐晓轩，黄津辉，李强，徐阳阳，车颖，梁菁，文虹镜，时金蒙，张文杰。南开大学（2018.1.17）

[8] 2018100464610；一种拖拽式水质检测装置；发明；王斌，徐晓轩，黄津辉，李强，徐阳阳，车颖，梁菁，文虹镜，时金蒙，张文杰。南开大学（2018.1.17）

[9] 2018100460427；一种水质监测预警系统；发明；王斌，徐晓轩，黄津辉，李强，徐阳阳，车颖，梁菁，文虹镜，时金蒙，张文杰。南开大学（2018.1.17）

[10] 2018100461082；一种烟管内检测装置；发明；徐晓轩，王斌，杨江涛，文虹镜，徐阳阳，车颖，梁菁，时金蒙，张卓。南开大学（2018.1.17）

[11] 2018100461078；一种烟气监测管路中光学窗口自动吹扫装置；发明；徐晓轩，王斌，杨江涛，文虹镜，徐阳阳，车颖，梁菁，时金蒙，张卓。南开大学（2018.1.17）

[12] 2018100464771；一种二氧化硫检测装置；发明；徐晓轩，王斌，杨江涛，文虹镜，徐阳阳，车颖，梁菁，时金蒙，张卓。南开大学（2018.1.17）

[13] 2018100461063；一种无人值守烟气检测系统；发明；张卓，徐晓轩，王斌，杨江涛，文虹镜，徐阳阳，车颖，梁菁，时金蒙，张卓。南开大学（2018.1.17）

[14] 201810046128X；一种增强拉曼光谱信号的装置；发明；徐晓轩，王斌，文虹镜，时金蒙，车颖，梁菁，徐阳阳，杨江涛，。南开大学（2018.1.17）

[15] 2018100461487；一种拉曼光谱检测仪校准方法；发明；徐晓轩，王斌，文虹镜，时金蒙，车颖，梁菁，徐阳阳，杨江涛，。南开大学（2018.1.17）

[16] 2018100461472；一种食品安全快速检测的增强拉曼光谱方法；发明；徐晓轩，王斌，文虹镜，时金蒙，车颖，梁菁，徐阳阳，杨江涛，。南开大学（2018.1.17）

[17] 2018100461805；一种紫外线固化装置；发明；徐晓轩，王斌，梁菁，车颖，徐阳阳，时金蒙，文虹镜，杨江涛，林宝志。南开大学（2018.1.17）

[18] 2018100464841；一种紫外光固化纳米压印的方法；发明；徐晓轩，王斌，梁菁，车颖，徐阳阳，时金蒙，文虹镜，杨江涛，林宝志。南开大学（2018.1.17）

[19] 201810046199X；一种固化纳米压印装置；发明；徐晓轩，王斌，梁菁，车颖，徐阳阳，时金蒙，文虹镜，杨江涛，林宝志。南开大学（2018.1.17）

[20] 201811226681.8；一种基于掩模曝光法的大面积液晶区域定向方法及其系统；发明；张心正，宋筱，高少华，张玉娇，许京军。南开大学（2018.10.22）

[21] 201811263959.9；一种基于金膜光热效应的溶液检测方法和装置 ；发明；刘智波，许恩泽，田建国。南开大学（2018.11.21）

[22] 201811272361.6；一种低维材料各向异性显微的成像方法和装置；发明；刘智波，黄凯旋，田建国。南开大学（2018.11.26）

[23] CN108484413A；一种由甲胺碘铅和甲胺碘构成的红色荧光粉的制备方法和应用；发明；刘磊，武莉，张毅，邢志雪。南开大学（2018.3.23）

[24] CN107966824A；一种分光器以及采用该分光器的光通讯系统和显示装置；发明；张迪，任梦昕，兀伟，高宁慧，禹宣伊，蔡卫，张心正，许京军。南开大学（2018.4.27）

[25] CN108760593A；一种振荡天平测量 PM2.5 的放射性补偿装置；发明；梅剑春，叶青，田建国。南开大学（2018.5.14）

[26] CN108061936A；一种分光器以及采用该分光器的分光方法；发明；张迪，任梦昕，兀伟，高宁慧，禹宣伊，蔡卫，张心正，许京军。南开大学（2018.5.22）

[27] 201810536490.5；基于 Pt 衬底的外延取向铌酸锂薄膜及其生长方法 ；发明 ；郑大怀，宋晓鹏，孔勇发，李文灿，贾龙飞，王烁琳，刘宏德，许京军。南开大学（2018.5.31）

[28] 201810727906.1；一种激光清洗的在线监测方法；实用新型；宋峰，蔺诗洁。南开大学（2018.7.5）

[29] 201810999804.5；一种应力可调光纤声光器件支架及安装方法；发明；高峰，张国权，许京军，薄方。南开大学（2018.8.30）

[30] 201811053887.5；一种制备亚微米周期任意极化图案铌酸锂微盘腔的方法；发明；薄方，张莉，郝振中，高峰，张国权，许京军。南开大学（2018.9.25）

授权专利/ Patents Approved

[1] US10,036,102, B2; Bismuth and magnesium co-doped lithium niobate crystal, preparation method thereof and application; 国际发明专利; Yongfa Kong, Dahuai Zheng, Shiguo Liu, Jingjun Xu, Peiming Xu, Zhiyong Bian, Shaolin Chen, Ling Zhang, Hongde Liu. Nankai University, Taishan Sprots Industry Group Co., Ltd.（2018.7.31）

[2] 2977815；A method and system for liquid crystal alignment in micro/nano region based on

laser direct writing；欧洲发明专利；张心正，许京军，李威，Irena Drevensek-Olenik，崔伟，石彬，王振华，吴强，孔勇发。南开大学（2018.9.5）

[3] ZL201510860470.X；一种基于动态调控的焦场轨迹制作微结构的装置；发明；涂成厚，蔡孟强，李萍萍，潘岳，李勇男，王慧田。南开大学（2018.1.30）

[4] ZL201510245720.9；一种测量电光晶体电光系数的方法及装置；发明；孙军，许京军，张玲，商继芳，李清连。南开大学（2018.2.2）

[5] CN201510801683.5；偏振成像系统以及采用该偏振成像系统成像的方法；发明；任梦昕，兀伟，皮彪，蔡卫，张心正，许京军。南开大学（2018.3.20）

[6] CN201510801179.5；光学非线性偏振调控元件以及调控入射光波偏振的方法；发明；任梦昕，兀伟，皮彪，蔡卫，张心正，许京军。南开大学（2018.3.20）

[7] ZL201310444659.1；微型转动扫描傅里叶变换光谱仪；发明；徐晓轩，李昊宇，王斌。南开大学（2018.3.30）

[8] ZL201710127413.X；一种表面过饱和掺杂光电探测器的钝化方法；发明；吴强，曾强，张春玲，姚江宏，刘丹，齐继伟，许京军。南开大学（2018.5.11）

[9] CN103334158B；空间频率生物芯片；发明；周文远，门双仁，惠王伟，叶青，田建国。南开大学（2018.5.22）

[10] ZL201410850183.6；一种同时采用 MEMS 平动和扭转微镜的微型傅里叶红外光谱仪；发明；徐晓轩，李昊宇，王斌，叶坤涛，郭振龙。南开大学、江西理工大学（2018.6.15）

[11] ZL201410289213；扭曲角度可控的多层石墨烯结构制备方法；发明；刘智波，陈旭东，田建国。南开大学（2018.6.19）

[12] CN106283194B；一种铌酸锂晶体纳米畴机构的制备装置及方法；发明；张国权，王晓杰，薄方，陈璟，陈绍林，孔勇发，许京军。南开大学（2018.7.17）

国际合作与交流/International Cooperation and Exchange

来访人员名单/Visitors List

序号	姓名	国家或地区	单位	技术职称	报告题目	来访时间	来访目的
1	Andrii Ilyin	乌克兰	乌克兰科学院物理所	研究员	A view on LC's prospects for holography applications	2018.10.19-11.30	合作交流
2	Claudio Conti	意大利	罗马大学物理系	教授	Topological lasers	2018.4.22-26	工作访问 学术交流
3	Daniel Leykam	韩国	Institute for Basic Science	教授	Probing topological physics using photonic lattices	2018.10.11-18	工作访问 学术交流
4	Dennis Couwenberg	荷兰	《Nanophotonics》杂志社	编辑	A publishing editor's view and insights on how to get your research published in the journal Nanophotonics	2018.10.8	工作访问
5	Georgios A. Siviloglou	荷兰	阿姆斯特丹大学	博士后	From optical Airy beams to quantum gases of strontium	2018.4.7-11	工作访问 学术交流
6	Hrvoje Buljan	克罗地亚	萨格勒布大学物理系	教授	Engineering Weyl fermions and anyons; engineering synthetic magnetic fields and dimensions in photonic lattices	2018.9.5-11	工作访问 学术交流
7	Irena Olenik-Drevensek	斯洛文尼亚	斯特藩研究所	教授	Magnetically tunable diffractive optical elements based on ferromagnetic liquid crystals	2018.11.6-15	合作交流

8	Luka Cmok	斯洛文尼亚	斯特藩研究所	讲师		2018.11.6-15	合作交流
9	Macello Ferrera	英国	英国赫瑞瓦特大学	助理教授	Advancing in Science	2018.7.1-30	暑期小学期英文课程
10	Marko Loncar	美国	哈佛大学	教授	Towards a Quantum Cloud	2018.5.16-17	工作访问讲学
11	Nickolai Kukhtareva	美国	美国阿拉巴马农工大学	教授		2018.7.3-8.1	合作交流
12	Nikos Efremidis	希腊	克里特大学数学与应用数学系	教授		2018.5.29-6.6	工作访问讲学
13	Ping Yu	美国	美国密苏里大学	教授		2018.1.3-10	科研合作
14	Ping Yu	美国	美国密苏里大学	教授		2018.12.13-2019.1.16	科研合作
15	Romano Rupp	奥地利	维也纳大学	教授	Physics Training with YPT Problem	2018.6.27-7.27 2018.10.12-11.15	小学期授课、合作交流
16	Tatiana Kukhtareva	美国	美国阿拉巴马农工大学	教授		2018.7.2-8.1	合作交流
17	Wang Qiang	美国	Colorado State University	教授	嵌段共聚物界面的涨落对其在纳米刻蚀应用中的影响	2018.6.19-22 2018.7.2-5	工作访问讲学
18	金辰皓	美国	康奈尔大学卡佛里纳米研究中心	研究员	Generation, transport and detection of pure valley currents in two-dimensional	2018.7.5	交流访问

					heterostructures		
19	李毅	英国	帝国理工大学	博士后	纳米光子学的非线性研究以及单分子检测应用	2018.1.1-3	工作访问

出访人员名单/Personnel Exchange Researchers List

序号	姓名	国家或地区	单位	职称或职位	出访时间	出访目的
1	薄　方	巴基斯坦	Pakistan Institute of Engineering and Applied Science	教授	2018.11.12-14	参加会议
2	薄　方	俄罗斯	Institute of Laser Physics, Siberian Branch of Russian Academy of Science	教授	2018.8.25-31	参加会议
3	宋　峰	俄罗斯	喀山国立大学、莫斯科大学等	教授	2018.10.11-14	参加会议 访问交流
4	宋　峰	英国	剑桥大学等	教授	2018.10.14-17	访问交流
5	宋　峰	澳门	澳门大学	教授	2018.6.6-8	访问
6	宋　峰	俄罗斯	俄罗斯科学院激光物理所	教授	2018.8.25-9.1	参加会议 访问交流
7	宋　峰	香港	香港科技大学	教授	2018.9.10-15	访问
8	孙同庆	美国	休斯顿大学	副教授	2017.10.14 -2018.10.16	访问学者
9	张国权	美国	SPIE PhotonicsWest 2018	教授	2018.1.28-2.1	参加会议
10	张国权	香港	香港中文大学	教授	2018.11.21-22	访问交流
11	张心正	奥地利	维也纳大学	教授	2018.2.12-18	合作研究

研究生交流情况/Personnel Exchange Students List

序号	姓名	国家或地区	单位	博士生/硕士生	出访时间	出访目的
1	Adnan Khan	俄罗斯	新西伯利亚大学	博士生	2018.8.23-9.1	会议
2	Adnan Khan	巴基斯坦	PIEAS	博士生	2018.11.11 -12.25	会议、交流
3	黄凯旋	中国	浙江大学	博士生	2018.9-2019.9	联合培养
4	刘汉雄	俄罗斯	新西伯利亚大学	博士生	2018.8.23-9.1	会议
5	张　路	美国	参加 FIO 会议	博士生	2018.9.16-20	学术交流

序号	姓名	国家或地区	单位	博士生/硕士生	出访时间	出访目的
6	宋　筱	斯洛文尼亚	斯特藩研究所	硕士生	2018.10.15-28	合作研究

国内、国际会议报告/Talks at Conferences

1 Zhigang Chen, “Tunable nonlinearity in biological suspesnions”, Photonic Vitality - Workshop on Nonlinear and Quantum Photonics, Canberra, Australia, Dec. 7-8, 2018. (**Keynote talk**)

2 Zhigang Chen, “Valley phenomena in photonic lattices”, The 7th Conference on Advances in Optoelectronics and Micro/nano-optics (AOM 2018), Xi’an, China, Oct 9-12, 2018. (**Keynote talk**)

3 Zhigang Chen, “Valley-mediated Phenomena in Photonic Graphene”, International Conference on Metamaterials and Nanophotonics (METANANO), Sochi, Russia, Sep. 17-21, 2018. (**Keynote talk**)

4 Zhigang Chen, “Photonic Graphene: Novel topological phenomena”, The 1st International Conference on Optics, Photonics and Lasers (OPAL' 2018), Barcelona, Spain, May 9-11, 2018. (**Keynote talk**)

5 Feng Song, “Plasmonic core-shell nanostructures tuning the luminescence properties of lanthanide Eu^{3+} ions for fluorescence multiplexing applications”, 2018 China-Russia Series Workshop on Laser and Photonics, Kazan, Russia, Oct. 11-15, 2018. (**Plenary talk**)

6 S. Chen, “Metasurface empowered wide-angle fourier transform”, The 8th International Multidisciplinary Conference on Optofluidics (IMCO-2018), Shanghai, China, Aug. 5-8, 2018. (**Invited talk**)

7 Fang Bo*, Zhenzhong Hao, Li Zhang, Ang Gao, Guoquan Zhang and Jingjun Xu, “Periodically poled lithium niobate whispering gallery mode microcavities on a chip”, The 8th International Multidisciplinary Conference on Optofluidics (IMCO 2018), Shanghai, China, Aug. 5-8, 2018. (**Invited talk**)

8 Shuqi Chen, “Metasurface enabled wide-angle Fourier lens” , The 7th Conference on Advances in Optoelectronics and Micro/nano-optics (AOM 2018), Xi’an, China, Oct. 9-12, 2018. (**Invited talk**)

9 Xinzheng Zhang, Wei Cai, Xiaodan Xu, Bin Shi, Weiwei Luo, Zenghong Ma, Lei Wang, Jingjun Xu, “Surface Plasmons in Various Graphene Structures”, Highlights in Functional Materials Research, Vienna, Austria, Feb. 15-16 (2018). (**Invited talk**)

10 Mengxin Ren. “Functional Metasurfaces for Linear and Nonlinear Control of Light”, METANANO2018, Sochi, Sep.17-21, 2018. (**Invited talk**)

11 Mengxin Ren. “Controlling Light in Nanoscales using Metasurfaces”, IMCO2018, Shanghai, China, Aug. 5-8, 2018. (**Invited talk**)

12 Mengxin Ren. “Controlling Light by Metasurfaces in the Linear and Nonlinear Regimes”, MEAT2018, Paris, France, Jun. 24-Jul. 1, 2018. (**Invited talk**)

13 Qiang Wu, Jianghong Yao, Chunling Zhang, Jiwei Qi, Chongpei Pan and Jingjun Xu, “Femtosecond laser modification of crystal materials”, Ultrafast Laser Modifications of Materials 2018 (ULMM2018), Colorado, USA, Jun. 13-16, 2018. (**Invited talk**)

14 Qiang Wu, Jianghong Yao, Chunling Zhang, Jiwei Qi, Chongpei Pan and Jingjun Xu, “Femtosecond laser modification of crystal materials from semiconductor to dielectric”, The 10^{th} International Conference on Information Optics and Photonics (CIOP 2018), Beijing, China, Jul. 8-11, 2018. (**Invited talk**)

15 Huitian Wang, “Structured light: manipulation and application”, The 7th Conference on Advances in Optoelectronics and Micro/nano-optics (AOM 2018), Xi’an, China, Oct. 9-12, 2018. (**Invited talk**)

16 Yi Hu, Yumiao Pei, Ping Zhang, Chunmei Zhang, Cibo Lou, Christian E. Rüter, Detlef Kip, Demetrios Christodoulides, Zhigang Chen, Jingjun Xu, "Novel nonlinear dynamics mediated by negative-mass fields", The 7th Conference on Advances in Optoelectronics and Micro/nano-optics (AOM 2018), Xi'an, China, Oct. 9-12, 2018. (**Invited talk**)

17 Daohong Song, Jingjun Xu and Zhigang Chen, "Pseudospin and topological phenomena in photonic graphene", The 7th Conference on Advances in Optoelectronics and Micro/nano-optics (AOM 2018), Xi'an, China, Oct. 9-12, 2018. (**Invited talk**)

18 Fang Bo*, Li Zhang, Zhenzhong Hao, Feng Gao, Guoquan Zhang, and Jingjun Xu, "On-chip periodically poled lithium niobate microdisk resonators", The 7th Conference on Advances in Optoelectronics and Micro/nano-optics (AOM 2018), Xi'an, China, Oct. 9-12, 2018. (**Invited talk**)

19 Guoquan Zhang*, Xiaojie Wang, Yuejian Jiao, Fang Bo, Yongfa Kong, and Jingjun Xu, "Engineering conductive nano-domain structures in lithum niobite crystals", The 7th Conference on Advances in Optoelectronics and Micro/nano-optics (AOM 2018), Xi'an, China, Oct. 9-12, 2018. (**Invited talk**)

20 Yi Hu, "Negative-mass propulsion in an optical analog", EMN Meeting on Photonics 2018, Taiwan, China, Oct. 21-24, 2018. (**Invited talk**)

21 Zhigang Chen, "Valley-dependent vortex generation and Landau-Zener-Bloch oscillations in photonic graphene", Active Photonic Platforms X conference, SPIE Optics and Photonics Congress, San Diego, CA, Aug. 19-23, 2018. (**Invited talk**)

22 Zhigang Chen, "Valley-mediated Phenomena in Photonic Lattices", The International Conference on "Nonlinear Localization in Lattices", Spetses, Greece, Jun. 18-22, 2018. (**Invited talk**)

23 Zhigang Chen, "Synthetic Optical Properties of Nonlinear Soft-Matter", Collaborative Conference on Nonlinear Optics 2018, Amsterdam, Netherlands, Apr. 16-20, 2018. (**Invited talk**)

24 Zhigang Chen, "Synthetic optical nonlinearity in plasmonic nanosuspensions", The 23rd Australian Institute of Physics Congress, Perth, West Australia, Dec. 9-13, 2018. (**Invited talk**)

25 Fang Bo,* Zhenzhong Hao, Li Zhang, Ang Gao, Guoquan Zhang and Jingjun Xu, Fabrication and Nonlinear Optical Effects of On-chip Periodically Poled Lithium Niobate Microdisk Resonators, The 2nd International Workshop on Asymmetric Microcavity and Wave Chaos, Fuzhou, China, May 18-20, 2018 (**Invited talk**)

26 Fang Bo, Li Zhang, Zhenzhong Hao, Guoquan Zhang, and Jingjun Xu, "On-chip periodically poled lithium niobate whispering gallery mode microcavities", International workshop on 2D materials and quantum effect devices, Islamabad, Pakistan, Nov. 12-14, 2018. (**Invited talk**)

27 Guoquan Zhang, "Optical signal processing via light pulse storage in electromagnetically induced transparency media", SPIE Photonics West, San Francisco, California, United States, Jan. 27-Feb. 1, 2018. (**Invited talk**)

28 Qingxiao Li, Baohui Li "Self-assembly of Giant Amphiphiles Based on Polymer-Tethered Nanoparticle in Selective Solvents: A Brownian Dynamics Study", International Symposium on Polymer Physics, Xi'an China, Jun 11-15, 2018. (**Invited talk**)

29 Li Wu, Huan Yi, Liwei Wu, Yuxing Bai, Yi Zhang, Yongfa Kong, Jingjun Xu, "New strategies for improving the thermal stability of phosphors", The 4th International Workshop on Persistent and Photostimulable Phosphors, Beijing, China, Apr. 4-8, 2018. (**Invited talk**)

30 Feng Song, "Principle and applications of Laser cleaning", The 8th International Conference of Modern Problem on Laser Physics, Novosbirisk, Russia, Aug. 25-Sept.1, 2018. (**Invited talk**)

31 Feng Song, “Fabrication of Plasmonic core-shell nanostructures and its tuning of the luminescence properties”, The International Symposium on 2D Material Fabrication and Optical Performance, Islambad, Pakistan, Nov. 11-15, 2018. (**Invited talk**)

32 Shaohua Gao, Wenhua Li, Yanzi Zhai, Yujiao Zhang, Jiayi Wang, Xiao Song, Irena Drevenšek-Olenik, Xinzheng Zhang, and Jingjun Xu, “Compartmentalized Liquid crystal alignment by out-of-plane surface relief gratings and its applications”, The 7th symposium on liquid crystal photonics, Nanjing, China, Apr. 13-16 (2018). (**Oral talk**, Best Paper Award)

33 Zhi-Bo Liu, Xiaoguang Gao, “Photothermal Detection in Two-Dimensional Materials”, The 7th Conference on Advances in Optoelectronics and Micro/nano-optics (AOM2018), Xi’an, China, Sep. 9-12, 2018. (**Oral talk**)

34 Leiting Pan, “Spatiotemporal Characteristics of Intercellular Calcium Wave Communication in Micropatterned Assemblies of Single Cells”, The 12th International Symposium on Calcium Signaling in China, Shenyang, China, Jul. 18-22, 2018 (**Oral talk**)

35 Feng Gao, Xiaofang Han, Caifen Li, Ligang Huang, Wending Zhang, Guoquan Zhang and Jingjun Xu, “Configurable Two Wavelength Laser Based on In-fiber Acousto-optic Mach-Zehnder Interferometer,” The 7th Conference on Advances in Optoelectronics and Micro/nano-optics (AOM 2018), Xi’an, China, Oct. 9-12, 2018. (**Oral talk**)

36 Gao Xiaoguang, Chen Guoxing, Li Dekang, Zhi-Bo Liu*, “Modulation of photothermal anisotropy using black phosphorus/rhenium diselenide heterostructures”, The 7th edition of the largest European Conference & Exhibition in Graphene and 2D materials (Graphene 2018), Dresden, Germany, Jun. 26-29, 2018.

37 Xiuying Liu, Daohong Song, Shiqi Xia, Zhixuan Dai, Liqin Tang, Jingjun Xu and Zhigang Chen, “Demonstration of pseudospin-to-orbital angular momentum conversion in photonic graphene”, Conference on Lasers and Electro-Optics, San Jose, California, United States, May 13-18, 2018.

38 Shiqi Xia, Ajith Ramachandran, Shiqiang Xia, Denghui Li, Xiuying Liu, Liqin Tang, Daohong Song, Sergej Flach, and Zhigang Chen “Observation of Unconventionally Extended Flat-band States in Photonic Lieb Lattices”, Conference on Lasers and Electro-Optics, San Jose, California, United States, May 13-18, 2018.

39 Daohong Song，Xiuying Liu, Shiqi Xia, Zhixuan Dai, Liqin Tang, Jingjun Xu and Zhigang Chen, “Demonstration of pseudospin dependent topological charge transformation in photonic graphene”, CLEO Pacific Rim, Hong Kong , China, Jul. 29-Aug. 3, 2018

40 Fang Bo, Zhenzhong Hao, Li Zhang, Ang Gao, Wenbo Mao, Feng Gao, Guoquan Zhang, Jingjun Xu, “On-chip periodically-poled lithium niobate microdisk resonators”, SPIE Photonics Asia, Beijing, China, Oct. 11-13, 2018.

41 Shaohua Gao, Wenhua Li, Xinzheng Zhang and Andrey Iljin, “Random lasing in chiral nematic liquid crystals”, The 7th International Symposium on Liquid Crystal Photonics, Nanjing, China, Apr. 13-16 (2018). (**Poster**, Best Poster Award)

42 Wenbo Mao, Fang Bo*, Guoquan Zhang, Jingjun Xu, “Directional Emission in X-cut Calcite Whispering Gallery Mode Microcavities”, The 2nd International Workshop on Asymmetric Microcavity and Wave Chaos, Fuzhou, China, May 18-20, 2018. (**Poster**)

43 Fang Bo, Zhenzhong Hao, Li Zhang, Jie Wang, Feng Gao, Guoquan Zhang, and Jingjun Xu, “Lithium niobate microdisk resonators on a chip”, the 8th International Symposium on "Modern Problems of Laser Physics", Novosibirsk, Russia, Aug. 25- 31, 2018. (**Poster**)

44 Pengfa Chang, Xiaoting Li, Ligang Huang, Feng Gao*, Wending Zhang, Fang Bo, Guoquan Zhang, and Jingjun Xu*, “Fast light in the generation configuration of stimulated Brillouin scattering based on high-Q micro-cavites,” Photonics Asia 2018, Beijing, China, Oct. 11-13 2018. (**Poster**)

45 Lu Zhang, Yiping Lu, Liming Li and Guoquan Zhang*, “Superbunching Effect of Light with

Digitally Designed Wavefront", Frontiers in Optics / Laser Science, OSA Technical Digest (Optical Society of America, 2018), Washington, District of Columbia, United States, Sep. 16-20, 2018. (**Poster**)

46 Dan Wang, Yue Pan, Jia-Qi Lv, Ping-Ping Li, Gui-Geng Liu, Meng-Qiang Cai, Yong-Nan Li, Cheng-Hou Tu, and Hui-Tian Wang, "Collapsing dynamics of elliptic-symmetry vector optical fields with hybrid states of polarization", CLEO , San Jose, USA, May 13-19, 2018. (**Poster**)

47 任梦昕，许京军，"超构材料:纳微尺度光调控及其应用"，第十九届全国凝聚态光学性质学术研讨会，西宁（2018.7.25-28）。（**大会报告**）

48 高少华，张心正，张玉娇，李文华，翟艳子，宋筱，王佳艺，冀志超，Irena Drevenšek-Olenik，Romano A. Rupp，许京军，"新型区域液晶面外定向技术及其在光场调控中的应用"，第十九届全国凝聚态光学性质学术研讨会，西宁（2018.7.25-28）（**邀请报告**）

49 武莉，易欢，武丽伟，白宇星，张毅，孔勇发，许京军，"New strategies for improving the thermal stability of phosphors"，第十九届全国凝聚态光学性质学术会议，西宁（2018.7.25-28）（**邀请报告**）

50 郑大怀，王烁琳，曲达，刘士国，刘宏德，陈绍林，张玲，孔勇发，许京军，"掺铋铌酸锂晶体的动态全息显示研究"，第十九届全国凝聚态光学性质学术会议，西宁（2018.7.25-28）（**邀请报告**）

51 张心正，高少华，翟艳子，张玉娇，冀志超，Irena Drevenšek-Olenik，许京军，"新型区域液晶面外定向技术及其在光场调控中的应用"，第二届京津冀青年物理学术论坛，石家庄（2018.11.2-4）（**邀请报告**）

52 潘雷霆，"基于超分辨成像技术的人红细胞骨架结构特性的研究"，2018 中国生物医学工程学会天津青年论坛，天津（2018.8.3-5）（**邀请报告**）

53 潘雷霆，"基于随机光学重构成像技术的人红细胞骨架结构的研究"，第二届全国纤毛生物学会议暨首届发育与疾病的细胞骨架基础研讨会，济南（2018.5.18-20）（**邀请报告**）

54 吴强、姚江宏、张春玲、齐继伟、潘崇佩、杨富华、许京军，"飞秒激光改性（过饱和掺杂）晶体材料及其器件"，第十三届全国激光技术与光电子学学术会议（LTO2018），上海（20018.3.11-14）（**邀请报告**）

55 吴强、姚江宏、张春玲、齐继伟、潘崇佩、杨富华、许京军，"飞秒激光与晶体相互作用—从过饱和掺杂器件到太赫兹集成芯片"，2018 光电工程春季论坛，成都（2018.3.17-19）**(邀请报告、优秀大会报告奖)**

56 吴强、姚江宏、张春玲、齐继伟、潘崇佩、杨富华、许京军，"飞秒激光与晶体的瞬态相互作用"，第二十三届全国激光学术会议，宁波（2018.7.11-13）（**邀请报告**）

57 胡毅，"负质量光场引起的新颖非线性动力学"，第二十三届全国激光学术会议，宁波（2018.7.11-13）（**邀请报告**）

58 薄方，"铌酸锂晶体回音廊模式光学微腔"，全国第 18 次光纤通信暨第 19 届集成光学学术大会，长春（2018.7.13-16）（**邀请报告**）

59 薄方*，张莉，郝振中，高昂，毛文博，高峰，张国权，许京军，"周期极化铌酸锂晶体微盘腔"，2018 年微腔光子学学术研讨会，大连（2018.820-23）（**邀请报告**）

60 薄方，"周期极化铌酸锂回音廊模式光学微腔"，中国物理学会 2018 年秋季学术会议，大连（2018.09.12-16）（**邀请报告**）

61 董校，"高压下的新型碳酸盐"，中国化学学会 2018 年第一届高压化学学术讨论会北京怀柔，（2018.11.09-11.11）（**邀请报告**）

62 李宝会，"聚合物接枝纳米粒子巨分子在溶液中的自组装行为的模拟研究"，2018 软物质非平衡统计动力学研究，温州（2018. .4-6）（**邀请报告**）。

63 李宝会，"巨分子在选择性溶剂中自组装行为的模拟研究",中国化学会 2018 年软物质理

论、模拟与计算，上海（2018.8.26-29）（**邀请报告**）

64 孙军，“熔体提拉法生长晶体的热场设计与控制策略”，第十八届全国晶体生长与材料学术会议，西安（2018.7.22-27）（**邀请报告**）

65 杨帆，陈俊锋，“超快闪烁材料的研究现状与探索”，第十八届全国晶体生长与材料学术会议，西安（2018.7.22-27）（**邀请报告**）

66 孙军，“Nd:YAG 晶体生长控制策略的探讨”，2018 稀土科技成果推介会暨学术交流会，北京（2018.7.17-19）（**邀请报告**）

67 武莉，武丽伟，白宇星，张毅，孔勇发，许京军，“五配位晶场环境下二价锰离子的发光”，第七届全国掺杂纳米材料发光性质学术会议，大连（2018.7.21-24）（**邀请报告**）

68 武莉，武丽伟，白宇星，张毅，孔勇发，许京军，“特殊晶场环境下二价锰离子的非常规获得及反常发光”，第十三届全国 X-射线衍射学术大会暨国际衍射数据中心（ICDD）研讨会，兰州（2018.7.28-8.1）。（**邀请报告**）

69 高晓光，陈国行，李德康，刘智波*，“二维材料的光热信号探测及其应用研究”，2018“科教结合”第四届全国物理学科博士生论坛，北京中国科学院物理研究所（2018.12.14-16）（**口头报告**）

70 涂成厚等，第五届光与物质相互作用国际会议，长沙（2018.11.11-13）（**口头报告**）

71 吕家琪，李萍萍，王丹，涂成厚，李勇男，王慧田，“非线性介质 CS_2 中螺旋型光丝的操控”，中国物理学会 2018 年秋季学术会议，大连（2018.09.12-16）（**口头报告**）

72 董海阳， 井志平，黄双印，涂成厚， 李勇男，王慧田，“铌酸锂纳米耦合光栅研究”，中国物理学会 2018 年秋季学术会议，大连（2018.09.12-16）（**口头报告**）

73 张冠林，“赝拓扑 Julia 分形矢量光场”，中国物理学会 2018 年秋季学术会议，大连（2018.09.12-16）（**口头报告**）

74 何新玲，董校，周向锋，王慧田，“硼及其化合物的结构预测”，高压学术研讨会，秦皇岛（2018.7.21）（**口头报告**）

75 潘雷霆，“基于光刻细胞图案化技术的细胞间钙波通讯特性研究”，第十六次中国暨国际生物物理大会，成都（2018.8.24-27）（**口头报告**）

76 高峰，“全光纤声光滤波器件及可调谐激光器”，2018 年光纤激光前沿论坛，天津（2018.10.20）（**口头报告**）

77 李宝会，“Conformation transitions of a single polyelectrolyte chain in a poor solvent: a replica-exchange lattice Monte-Carlo study”, 第十届全国软物质与生命物质物理学术会议，重庆（2018.11.9-12）（**口头报告**）

78 郑大怀，王烁琳，曲达，刘士国，刘宏德，陈绍林，张玲，孔勇发，许京军，“掺铋铌酸锂晶体的动态全息显示研究”，第十八届全国晶体生长与材料学术会议，西安（2018.7.22-27）（**口头报告**）

79 王维维，钟阳，郑大怀，刘宏德，张立新，孔勇发，“掺氮铌酸锂缺陷结构及其 p 型导电微观机理的第一性原理研究”，第十八届全国晶体生长与材料学术会议，西安（2018.7.22-27）（**口头报告**）

80 贾龙飞，宋晓鹏，郑大怀，李文灿，刘宏德，孔勇发，许京军，“La-Co 双掺铁酸铋薄膜的制备和性能研究”，第十八届全国晶体生长与材料学术会议，西安（2018.7.22-27）（**口头报告**）

81 Shahzad Saeed, Hongde Liu, Dahuai Zheng, Liyun Xue, Shiguo Liu, Shaolin Chen, Yongfa Kong, Romano Rupp, Jingjun Xu, “Enhanced photorefractive properties of vanadium co-doped lithium niobate crystals in visible region”，第十八届全国晶体生长与材料学术会议，西安（2018.7.22-27）（**口头报告**）

82 郭丽英，余华，刘锦锦，武兵，赵丽娟，“Yb^{3+}双光子合作发光物理机制的研究”，第十

九届全国凝聚态光学性质学术会议，西宁（2018.7.25-28）（**口头报告**）

83 王维维，钟阳，郑大怀，刘宏德，张立新，孔勇发，“掺氮铌酸锂缺陷结构及其 p 型导电微观机理的第一性原理研究”，第十九届全国凝聚态光学性质学术会议，西宁（2018.7.25-28）（**口头报告**）

84 Shahzad Saeed, Hongde Liu, Dahuai Zheng, Liyun Xue, Shiguo Liu, Shaolin Chen, Yongfa Kong, Romano Rupp, Jingjun Xu, “Enhanced photorefractive properties of vanadium co-doped lithium niobate crystals in visible region”, 第十九届全国凝聚态光学性质学术会议，西宁（2018.7.25-28）（**口头报告**）

85 范友静，刘宏德，郑大怀，张玲，刘士国，陈绍林，孙军，孔勇发，许京军，“不同光场条件下的铌酸锂畴反转研究”，第十九届全国凝聚态光学性质学术会议，西宁（2018.7.25-28）（**口头报告**）

86 叶青，第二届微流控技术应用创新论坛，西安（2018.12.7-10）

87 刘建基，刘甲琛，张国权，“基于电磁感应透明效应的相干光场操控和光学信息处理”，第十届全国光学青年学术论坛，南京（2018.11.16-18）（**张贴报告，优秀张贴报告奖**）

88 刘磊，邢志雪，董瑞，武莉，蔡宏琨，张毅，“碘甲胺（CH_3NH_3I）与甲胺铅碘（$CH_3NH_3PbI_3$）粉体发光增强的研究”，中国晶体学会第七届学术年会，天津（2018.9.25-28）。（**张贴报告、优秀墙报**）

89 高峰，“回音廊模微腔阵列的位置传感应用”，第八届全国原子分子光物理青年科学家论坛，北京（2018.10.19-20）（**张贴报告**）

90 常朋发、李晓婷、黄礼刚、高峰*、张文定、薄方、张国权、许京军，“利用微腔的自激发受激布里渊散射产生快光”，中国物理学会 2018 年秋季学术会议，大连（2018.09.12-16）（**张贴报告**）

91 张路，陆一平，张国权*，“基于数字化波前设计的超聚束效应”，第十八届全国基础光学与光物理学术讨论会，青岛（2018.8.27-30）（**张贴报告**）

92 Lu Zhang, Dongxu Zhou, Yiping Lu, and Guoquan Zhang*, “Realization of superbunching effect with classical light”, 第十八届全国量子光学学术会议，张家界市（2018.10.26-29）（**张贴报告**）

93 李利明，洪佩龙，张国权，“Experimental realization of Heisenberg-resolution imaging with classical light”, 第十八届全国量子光学学术会议，张家界市（2018.10.26-29）（**张贴报告**）

94 Fang Liu, Xin Zhao, Xiao-Qing Yan, Xiufeng Xin, Zhi-Bo Liu, and Jian-Guo Tian, "Ultrafast saturation absorption of CVD-grown ReS_2 and $ReSe_2$ films," 第十八届全国基础光学与光物理会议，青岛（2018.8.27-8.30）（**张贴报告**）

95 Junfang Xie, Di zhang, Xiaoqing Yan, Mengxin Ren, Zhibo Liu, Jianguo Tian "Effective refractive index and extinction coefficient of chemical vapor deposition-grown $PtSe_2$ characterized by Spectroscopic ellipsometry" 中国物理学会 2018 年秋季学术会议，大连（2018.09.12-16）（**张贴报告**）

96 Xiufeng Xin, Fang Liu, Xiao-Qing Yan, Wangwei Hui, Xin Zhao, Xiaoguang Gao, Zhi-Bo Liu, and Jian-Guo Tian, "Two-photon absorption and non-resonant electronic nonlinearilities of quai-two-dimensional layered semiconductor $TlGaS_2$," 中国物理学会 2018 年秋季会议，大连（2018.9.12-16）（**张贴报告**）

97 黄凯旋，李德康，郭浩炜，霍唱福，“Anisotropic Microscopy for Low-Dimensional Materials”，中国物理学会 2018 秋季学术会议，大连（2018.9.12-16）（**张贴报告**）

98 Dan Wang, Lu-Lu Huang, Jia-Qi Lv, Ping-Ping Li, Meng-Dan Zhao, Guan-Lin Zhang , Yong-Nan Li, Cheng-Hou Tu, and Hui-Tian Wang, “Nonlinear helical collapsing behavior of uniformly elliptically-polarized vector optical fields”，中国物理学会 2018 年秋季学术会议，大连（2018.09.12-16）（**张贴报告**）

99 赵梦丹，张冠林，王珂，王丹，涂成厚，李勇男，王慧田，“The breaking and information

recovery of multifractal vector optical field”，中国物理学会 2018 年秋季学术会议，大连（2018.09.12-16）（**张贴报告**）

100 井志平，涂成厚，李勇男，王慧田，“矢量光场与金属材料菲涅尔波带片相互作用特性研究”，中国物理学会 2018 年秋季学术会议，大连（2018.09.12-16）（**张贴报告**）

101 朱梦红，翁晓基，周向锋，“新型二维磁性硼的性质研究”，中国物理学会 2018 年秋季学术会议，大连（2018.09.12-16）（**张贴报告**）

102 吕家琪，李萍萍，王丹，涂成厚，李勇男，王慧田，“Phase-modulation nested structure optical field for extending optical filament”，第十八届全国基础光学与光物理学术讨论会，青岛（2018.8.27-30）（**张贴报告**）

103 王丹，黄露露，吕家琪，李萍萍，赵梦丹，涂成厚，李勇男，王慧田，“均匀椭偏率矢量光场的非线性螺旋坍缩行为的研究”，第十八届全国基础光学与光物理学术讨论会，青岛（2018.8.27-30）（**张贴报告**）

104 赵梦丹，张冠林，王珂，王丹，涂成厚，李勇男，王慧田，“多重分形矢量光场的破缺与信息恢复”，第十八届全国基础光学与光物理学术讨论会，青岛（2018.8.27-30）（**张贴报告**）

105 王强，李勇男，涂成厚，王慧田，“基于焦场轨迹控制的飞秒激光动态加工”，第十八届全国基础光学与光物理学术讨论会，青岛（2018.8.27-30）（**张贴报告**）

106 董海阳，黄双印，涂成厚，李勇男，王慧田，“铌酸锂纳米波导倍频研究”，第十八届全国基础光学与光物理学术讨论会，青岛（2018.8.27-30）（**张贴报告**）

107 范友静，刘宏德，郑大怀，张玲，刘士国，陈绍林，孙军，孔勇发，许京军，“不同光场约束条件下的铌酸锂畴结构研究”，第十八届全国晶体生长与材料学术会议，西安（2018.7.22-27）（**张贴报告**）

108 薛丽云，孔勇发，刘宏德，郑大怀，田甜，Shahzad Saeed，诸玲，刘士国，陈绍林，许京军，“高价钼掺杂铌酸锂晶体的研究”，第十八届全国晶体生长与材料学术会议，西安（2018.7.22-27）（**张贴报告**）

109 李文灿，崔娇，郑大怀，贾龙飞，宋晓鹏，刘宏德，刘士国，张玲，Rumano Rupp，孔勇发，许京军，“Fabrication of p-type conductivity Nitrogen-doped $LiNbO_3$ films”，第十八届全国晶体生长与材料学术会议，西安（2018.7.22-27）（**张贴报告**）

110 钟阳，单排，孙同庆，孔勇发，张立新，许京军，“具有深紫外透过性的 β-$CsBa_2(PO_3)_5$ 非线性光学晶体的生长及其光学性质的理论研究”，第十八届全国晶体生长与材料学术会议，西安（2018.7.22-27）（**张贴报告**）

111 Liyun Xue, Dahuai Zheng, Hongde Liu, Shahzad Saeed, Shiguo Liu, Shaolin Chen, Ling Zhang, Yongfa Kong, Romano Rupp, Jingjun Xu, “Fast photorefractive response of lithium niobate crystals using nanosecond pulsed lasers”, 第十九届全国凝聚态光学性质学术会议，西宁（2018.7.25-28）（**张贴报告**）

112 贾龙飞，宋晓鹏，郑大怀，李文灿，刘宏德，孔勇发，许京军，“La-Co 双掺铁酸铋薄膜的制备和性能研究”，第十九届全国凝聚态光学性质学术会议，西宁（2018.7.25-28）（**张贴报告**）

113 李文灿，崔娇，郑大怀，贾龙飞，宋晓鹏，刘宏德，刘士国，张玲，Rumano Rupp，孔勇发，许京军，“Fabrication of p-type conductivity Nitrogen-doped $LiNbO_3$ films”，第十九届全国凝聚态光学性质学术会议，西宁（2018.7.25-28）（**张贴报告**）

主办国内、国际会议/Conferences Sponsored by the Laboratory

材料设计暨第十四届 USPEX 国际会议 2018（2018.6.24-6.26；天津）

2018 年 6 月 24 日至 26 日，材料设计暨第十四届 USPEX 国际会议(International Symposium on Material Design & 14th USPEX Workshop) 在天津南开大学举行。会议由南开大学物理科学学院主办，南开大学弱光非线性光子学教育部重点实验室、西北工业大学、俄罗斯 Skoltech 大学，美国内华达大学拉斯维加斯分校承办。

本次会议邀请国内外凝聚态物理和材料科学领域的知名科学家和青年才俊，共同探讨学术前沿和技术难题，旨在促进国内外材料设计与计算，以及晶体结构预测软件 USPEX 的发展和应用等学术交流和科研合作，同时积极推动南开大学凝聚态物理及相关学科的发展，促进人才队伍的建设。

本次会议共有 100 余名会议代表参会。会议共安排了 18 个邀请报告和 2.5 小时的上机操作。在会议过程中，与会代表就晶体结构预测软件 USPEX 的功能与使用、晶体结构拓扑性质研究、极端条件下的材料设计与物性预测等主题与报告人积极交流讨论，现场气氛十分活跃。

南开大学弱光非线性光子学教育部重点实验室/ The Key laboratory of Weak Light Nonlinear Photonics (Nankai University, Tianjin 300457), Ministry of Education, China

2018 年微腔光频率梳研讨会（2018.9.28-9.29；天津）

微腔光频率梳成功地将诺贝尔奖成果——光学频率梳——引入了集成光学领域，并因其体积小、功耗低等特点，具有非常广泛的应用前景。

为了促进微腔光频率梳相关的学术交流，探讨其未来发展，物理科学学院薄方教授于 2018 年 9 月 28 日至 9 月 29 日期间组织举办了“2018 年微腔光频率梳研讨会”。本次会议共有来自北京大学、加州理工学院、南京大学、南开大学、清华大学、天津大学、西安光机所、中国科学技术大学等单位的 11 位专家、学者就微腔频率梳的产生、控制和应用等方面内容作了精彩报告，50 余名校内外师生参加会议,聆听报告并进行了热烈的学术讨论。

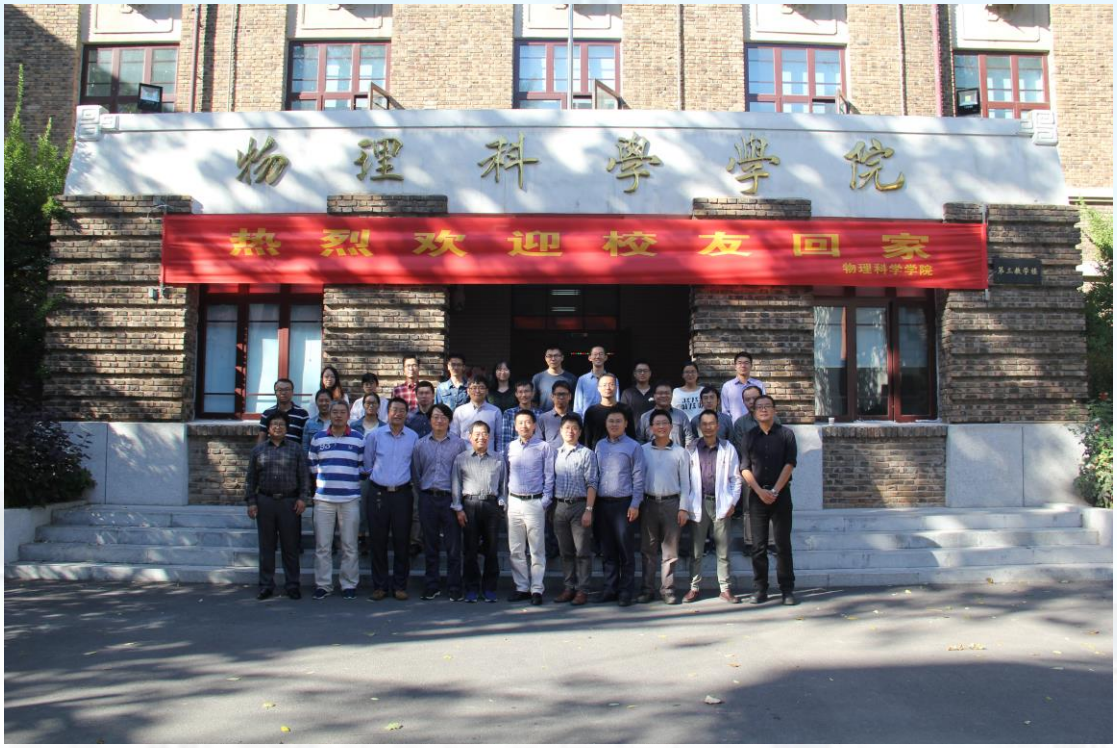

南开大学弱光非线性光子学教育部重点实验室/ The Key laboratory of Weak Light Nonlinear Photonics (Nankai University, Tianjin 300457), Ministry of Education, China

学术组织与期刊任职/Academic Service

国内外学术组织任职/Service to the Professional Societies

序号	姓名	任职机构	职位	任期
1	许京军	天津市光学学会	副理事长	2010-
2	许京军	天津市激光技术学会	副理事长	2010-
3	许京军	应用光学国家重点实验室	主任	2009-
4	许京军	中国高校知识产权研究会	副理事长	2008-
5	许京军	中国光学学会	理事	2006-
6	陈志刚	American Physical Society	Fellow	
7	陈志刚	The Optical Soceity (OSA)	Fellow Member	
8	田建国	天津市光学学会	常务理事	
9	张国权	美国光学学会	高级会员	2013-
10	张国权	中国光学学会	理事	2017-
11	孔勇发	中国硅酸盐学会晶体生长与材料分会	理事	2012-
12	宋　峰	全国中学生物理竞赛委员会	常委	2010.4-
13	宋　峰	天津市激光技术学会	副理事长	2009-
14	宋　峰	天津市物理学会	常务理事兼秘书长	2008.7-
15	宋　峰	中国光学学会激光技术专业委员会	委员	
16	宋　峰	中国仪器仪表学会光机电技术与系统成分会	常务理事	2007.6-
17	宋　峰	固体激光技术重点实验室学术委员会	委员	
18	孙　骞	教育部实验室建设专家委员会	委员	2013-2017
19	孙　骞	天津市光电子学会	常务理事	
20	孙　骞	中国光学学会光电技术委员会	委员	2006-
21	张心正	天津市光学学会	常务理事	2015-2020
22	张心正	天津市激光技术学会	理事	2015-2020
23	张天浩	天津市照明学会	常务理事	2008-
24	吴　强	天津市物理学会	副秘书长 常务理事 光学与光电子委员会主任	2017-
25	武　莉	国际粉末衍射数据中心	会员	2010.03-
26	武　莉	中国材料研究会青年工作委员会	理事	2014.12-
27	孙　军	国家标准化管理委员会	委员	2012.9—
28	孙　军	人工晶体标准化技术委员会	委员	2012.9—
29	孙　军	无机非金属材料河南工程实验室学术委员会	委员	2018.4-
30	孙　军	中国兵工学会激光技术专业委员会	委员	2018.9-

序号	姓名	任职机构	职位	任期
31	孙　军	中国材料与试验团体标准委员会光电材料及产品领域委员会	委员	2018.11-
32	孙　军	中国材料与试验团体标准委员会光学晶体标委会	副主任委员	2018.12
33	孙　军	中国材料与试验团体标准委员会建筑材料领域人工晶体技术标委会	委员	2018.8-
34	孙　军	中国硅酸盐学会晶体生长与材料分会	理事	2018.7-
35	陈树琪	天津市优秀创新创业导师人才库	创新导师	2018-
36	徐晓轩	中国仪器仪表学会近红外光谱专业分委员会	委员	2013-2019
37	徐晓轩	中国仪器仪表学会物理光学仪器专业委员会	委员	2013-2019
38	潘雷霆	中国光学学会生物医学光子学专业委员会	青年委员	2015.12-2020.12
39	潘雷霆	中国生物物理学会自由基生物学与自由基医学学会	青年委员	
40	潘雷霆	中国微循环学会微循环与血液治疗专业委员会	常委	2017.12-2021.12
41	杨　帆	IEEE	会员	2012-
42	杨　帆	中国材料研究会青年工作委员会	理事	2017.10-
43	王　斌	天津市物联网开发与应用协会	副理事长	2018-2019

国内外期刊任职/Service to the Journals

序号	姓名	任职机构	职位	任期
1	许京军	Chinese Physics Letters	编委	2009-
2	许京军	Journal of Optics	Topic Editor	
3	许京军	光学学报	副主编	2008-
4	许京军	红外与毫米波学报	编委	
5	许京军	中国光学与应用光学	编委	2008-
6	陈志刚	Advances in Physics: X, (Taylor & Francis Group)	Editor	2015-
7	陈志刚	Optics Letters	Topical Editor	2014-
8	陈志刚	Science Bulletin	Editorial Board Member	2014-
9	陈志刚	Scientific Reports	Editorial Board Member	2015-
10	田建国	Scientific Reports	Editorial Board member	
11	王慧田	Chinese Optics Letters	Topic Editor	
12	王慧田	Chinese Physics Letter	Editorial Board	

序号	姓名	任职机构	职位	任期
			Member	
13	张国权	激光技术	编委	2006-
14	张国权	激光与光电子学进展	编委	2010-
15	李宝会	Europhysics Letters	Co-Editor	2015-2018
16	李宝会	Scientific Reports	Editorial Board Member	2014-
17	孔勇发	激光技术	编委	2015-2018
18	宋　峰	大学物理	副主编	2009.5-
19	宋　峰	清洗世界	编委	2011-
20	宋　峰	激光杂志	编委	
21	宋　峰	光电技术应用	编委	
22	张心正	激光技术	编委	2015-2022
23	吴　强	Scientific Reports	Editorial Board Member	2013-
24	吴　强	中国激光杂志社	青年编委	2017-
25	薄　方	Scientific Reports	Editorial Board Member	2018.5-
26	陈树琪	American Journal of Optics and Photonics	Editorial Board Member	2017-
27	陈树琪	Scientific reports	Editorial Board Member	2018-
28	陈树琪	光学学报	Topic Editor	2017-
29	陈树琪	光学学报	编委	2019-2021
30	陈树琪	中国激光杂志社	青年编委常务委员	2017-
31	孙　军	现代电子技术	编委	2017.7-
32	胡　毅	Institute of Physics	Invited editor	

博士后情况

序号	姓名	性别	年龄	合作导师	在站时间
1	刘伯飞	男	31	许京军	2014.6-2018.1
2	王　烁	男	33	田建国	2015.11-2018.7
3	石　玥	女	33	宋　峰	2015.12-2018.4
4	董繁龙	男	33	宋　峰	2016.10-2018.9
5	陈东学	男	31	王慧田	2016.11-2018.12
6	李清连	女	30	胡　毅	2017.7-
7	武丽伟	女	29	张心正	2017.7-
8	朱俊达	男	27	薄　方	2018.7-
9	李占成	男	28	陈树琪	2018.7-

获奖情况/Awards & Honors

获奖教师/Award for excellent teachers

国家自然科学奖二等奖：
项目名称：面向能源转化与存储的有机和碳纳米材料研究
获奖日期：2018.12.12
完 成 人：陈永胜，万相见，黄毅，田建国，王成扬

中国光学科技奖二等奖：
项目名称：光束传播的线性与非线性智能调控
获奖日期：2018.12
完 成 人：陈志刚，宋道红，胡毅，唐莉勤，许京军

天津市创新人才推进计划青年科技优秀人才：蔡　卫　　胡　毅

南开大学 2018 年“知行南开”师生同行暑期社会实践先进指导教师：郑大怀

获奖学生/Award for excellent students

全国光学优秀博士毕业论文提名奖：李建雄

第十四届王大珩光学奖高校学生奖：李占成

天津市优秀学生：高晓光
天津市优秀学生干部：胡梦媛

研究生国家奖学金：　博士生　高晓光　李　智　邢福临
　　硕士生　李晓婷　高宁慧　张　迪

南开大学奖学金：
特定奖学金：　高晓光
一等奖学金：　王　超　杨　渤　杜成林　王丹阳　郝振中　巨丹丹
二等奖学金：　王烁琳　王　丹　黄露露　赵晓敏
光华奖学金：　郭丽英　周爱华
三星奖学金：　张　平
优秀新生奖学金：张　利
留学生优秀奖一等奖：Saeed Shahzad

2017-2018 年度“南开十杰”称号：高晓光
2017-2018 年度“南开大学学生年度人物”：高晓光
2017-2018 年度“南开大学校级三好学生”：高晓光　王　丹
南开大学优秀学生干部：胡梦媛　张冠林　张海涵　王日德　王丹阳　杨鹏真
南开大学优秀党员：赵梦丹　杨鹏真
南开大学优秀硕士论文：王艳娥　闫　娜

学位论文/Dissertations

1. 博士学位论文 Dissertation for Doctoral Degree

[1] 高旭珍，几种新型矢量光场的设计、性质与应用；导师：王慧田

[2] 韩迎东，稀土基微纳荧光材料的发光调控与应用；导师：宋峰、黄维

[3] 韩中兴，氧化铈和二氧化钛基催化剂的结构、性质及其还原 CO_2 生成 CH_4 的活性研究，导师：曹亚安

[4] 蒋鹏翀，小胶质细胞间钙波通讯机制的实验及数值模拟研究；导师：张心正

[5] 孔腾飞，高掺镁铌酸锂晶体的若干问题研究；导师：孔勇发

[6] 李青霄，聚合物接枝纳米粒子巨分子在溶液中自组装行为的模拟研究；导师：李宝会

[7] 李占成，超表面光场单维度与多维度调控研究；导师：田建国

[8] 刘旭，自加速光束与回音廊模式谐振腔的耦合研究；导师：胡毅

[9] 刘继宗，基于全息光镊的微流通道设计与实验研究；导师：陈志刚

[10] 刘文玮，人工微结构光场调控物理及应用；导师：田建国

[11] 刘秀英，光子石墨烯中赝自旋与轨道角动量的转化；导师：陈志刚

[12] 马增红，石墨烯等离激元调控研究；导师：RomanoA.Rupp、蔡卫

[13] 邱文娟，接枝线形和环形聚合物在溶液中自组装行为的自洽场理论研究；导师：李宝会

[14] 商继芳，基于铌酸锂/钽酸锂晶体的高性能电光调 Q 开关及其应用研究；导师：黄存新、孙军

[15] 王聪，二维材料的应变效应及其范德瓦尔斯 p-n 结电学特性研究；导师：刘前、张心正

[16] 张明偲，若干非对称导电连接结构纳米光子学器件；导师：孙骞

[17] 诸玲，掺钼系列铌酸锂晶体的生长与光折变性能研究；导师：孔勇发

2. 硕士学位论文 DissertationforMasterDegree

[1] 安炳旭，基于二维材料的新型折射率传感器的设计及应用；导师：刘智波

[2] 白江波，高均匀性高掺镁铌酸锂晶体的生长研究；导师：孙军

[3] 冯源，接枝聚合物和受限两嵌段共聚物在溶液中自组装行为的模拟退火研究；导师：李宝会

[4] 耿娟，基于铌酸锂薄膜的摩擦纳米发电机及其机理研究；导师：张心正

[5] 郭埠，三磷酸腺苷诱发的小胶质细胞迁移及相关机制的研究；导师：潘雷霆

[6] 韩小芳，基于声光效应的全光纤移频器研究；导师：张国权

[7] 黄少蕾，$PbSbO_2Cl$ 和 CeO_2 的制备及其光催化性质的研究，导师：曹亚安

[8] 回振海，成骨细胞分化过程中 TRVP4 通道介导的信号通路及细胞骨架变化的研究；导师：李任植

[9] 靳建宁，无序晶体局部结构的晶体学和光谱学解析；导师：余华

[10] 李珊，先进放电等离子体烧结技术在制备高性能热电材料领域内的应用；导师：武

莉

[11] 栗星星，基于 MIM 波导耦合谐振腔宽带滤波结构的研究；导师：孙骞

[12] 梁朋辉，钛铁双掺铌酸锂系列晶体的生长及非挥发全息存储性能的研究；导师：刘士国

[13] 刘冬雪，嵌段共聚物在半球受限下自组装行为的模拟研究；导师：李宝会

[14] 栾敏，基于克尔透镜的无背景时间分辨光谱技术及应用；导师：RomanoA.Rupp

[15] 马姝琼，微盘辐轮腔中光力学效应研究；导师：薄方

[16] 曲达，铋镁双掺铌酸锂晶体动态全息显示性能研究；导师：孔勇发

[17] 时金蒙，STED 显微镜分辨率提高及纳米材料超分辨成像研究；导师：徐晓轩

[18] 宋晓鹏，镧锰双掺铁酸铋薄膜和铌酸锂薄膜的制备及其性能研究；导师：孔勇发

[19] 王欢，大功率激光清洗实验和理论的研究；导师：宋峰

[20] 王艳娥，金属纳米新月结构超赝手性研究；导师：吴强、齐继伟

[21] 荀爽，基于微流控系统的人红细胞变形性表征的研究；导师：潘雷霆

[22] 闫娜，全光纤声光滤波器件与可调谐双波长光纤激光器的研究；导师：高峰

[23] 颜森，周期性背电极的研究及其在超薄 CIGS 薄膜太阳电池中的应用；导师：武莉

[24] 杨超，氧化石墨烯快速还原和应用；导师：刘智波

[25] 杨慧梅，基于铌酸锂波导的窄带 THz 波的产生和性质研究；导师：吴强

[26] 杨江涛，大气污染气体的紫外差分吸收光谱研究；导师：徐晓轩

[27] 杨鹏宇，微型光谱仪及光束质量分析系统的设计与实现；导师：叶青

[28] 姚森，三偏磷酸钾镁和六偏磷酸四钠锌晶体的制备、结构与性质；导师：孙同庆

[29] 周超，碘酸锌晶体的制备与性质；导师：孙同庆